OPTIMIZATION OF NONHOMOGENEOUS FACESHEETS IN COMPOSITE SANDWICH PLATES

by

Mário Kataoka Filho

A thesis submitted in conformity with the requirements
for the degree of Doctor of Philosophy
Graduate Department of Aerospace Science and Engineering
University of Toronto

Abstract

Minimum weight design is an important criterion in aircraft and spacecraft because it allows either an increased pay-load or higher performance. As a result, the use of composite sandwich panels has grown due to their light weight and high rigidity. In order to further increase the efficiency of these structures, designers have used different materials in different shapes in the facesheets and in the core. One of the most recent innovations has been the use of a uniform net of carbon fibre/epoxy as the facesheets.

In the present study, the optimal design of sandwich plates with heterogeneous facesheets is treated. The plate mass is minimized, considering the first natural frequency and certain failure loads as constraints. Weight reduction is obtained by defining a nonuniform distribution of composite material in the facesheets. Initially, the facesheets are assumed to be constructed of composite strips in a regular pattern. During the optimization process, both the widths of the strips and the spacing between them are varied to decrease the amount of material used. Such a design is conceptually straightforward to manufacture and, therefore, would lead to improved performance with little cost penalty.

In order to solve this problem, it is first necessary to develop a computer code to determine the natural frequencies and the stresses in these plates. The bending and vibration problems for sandwich plates with heterogeneous facesheets are solved using the Ritz Method in conjunction with the assumptions formulated by Reissner for sandwich plates. Since the sandwich plate considered in this study has facesheets constructed of nets and the computer code was developed to analyse laminates with heterogeneous continuous layers, it was necessary to use a procedure to approximate the nonuniform net as a smoothed orthotropic heterogeneous continuum. The smoothing process is accomplished using the theory of homogenisation and the material coefficients were calculated using the Finite Element Method. Two approaches were considered to define the design variables of the problem: an independent design approach, in which the facesheets are discretized into regions with uniform design parameters; and a reduced basis formulation, in which the design is specified by a linear combination of orthogonal basis functions.

This study solved the problem proposed. It has been demonstrated that variation in density is important and can lead to significant design improvement. Across of the face of the optimally designed plate, the density varies by a factor of 9. Also, the problems solved showed that the mass of the facesheets can be reduced up to 50%.

Acknowledgements

I would like to thank my supervisor Prof. J. S. Hansen for his guidance, advice, encouragement and friendship throughout the development of this research. I would also like to thank the other members of my committee, Prof. J. D. DeLaurier and Prof. G. M. T. D'Eleuterio, for reviewing my work and offering very useful suggestions.

I would like to thank all the UTIAS staff, for their kind assistance whenever I needed them. I am specially thankful to Ms. N. Burnett, for provinding all the help I needed to find the necessary books, journals and articles, and to Mr. G. Elliott, for the computational support during the development of my dissertation, including the time I was in Brazil. I would also like to thank Mr. M. M. Domb and Mr. F. Wong for the friendship and companionship that made my stay at UTIAS very enjoyable.

I am grateful for the financial support received from many sources. My stay in Canada during my doctoral program was only possible because of the support received from CAPES - Coordenação de Aperfeiçoamento de Ensino Superior and INPE - Instituto Nacional de Pesquisas Espaciais. I am also thankful to the CNPQ - Conselho Nacional de Desenvolvimento Científico e Tecnológico and to the School of Graduate Studies of the University of Toronto.

I want to express my thankfulness to Prof. Sérgio F. M. de Almeida for his valuable suggestions and to my very good friend Mr. Walter K. Takahashi for helping me throughout the development of my research in every possible manner, even taking over my duties at INPE during these last few months.

Finally, I am specially thankful to my parents, my wife Heloneida and my son Mário for their love and support throughout the development of my doctoral program. I dedicate this dissertation to them.

Contents

List of Figures

List of Tables

Nomenclature

Roman

a	Length of the plate in the x-direction.
a'	Exponent of r'_p: extended penalty method.
a_c	Acceleration.
A	Area of the plate.
$\overline{\mathbf{A}}$	Shear stiffness matrix.
A_{al}	Augmented Lagrangian.
ALM	Augmented Lagrange Multiplier Method.
A_o	Centre of the hypersphere: method of centres.
b	Length of the plate in y-direction.
$\mathbf{B}$	Body force vector.
$\mathbf{B}_h$	Approximation to the Hessian: sequential quadratic programming method.
$\mathbf{c}$	Unknown coefficient vector: Rayleigh-Ritz method.
C	Positive constant: extended penalty method.
$\mathbf{d}$	Unknown coefficient vector: Rayleigh-Ritz method.
$\mathbf{D}$	Bending stiffness matrix.
DOF	Degrees of freedom.
$\mathbf{e}$	Unknown coefficient vector: Rayleigh-Ritz method.
E_c	Compressive Young's modulus of the core.
E_{11}	Young's modulus in the fibre direction.
E_{22}	Young's modulus in the direction normal to the fibre.
f	Preselected orthogonal basic function.
F	Objective function.
$\mathbf{F}$	Force vector.
FDX	Material density in x-direction.
FDY	Material density in y-direction.
F_{ib}	Critical buckling stress.
F_{wc}	Critical wrinkling stress.
$\overline{FS}$	Specified failure stress.

F_{wc}	Facesheet wrinkling strength.
g	Inequality constraints.
$\overline{g}$	Penalty function: extended penalty method.
g_e	Energy function: simulated annealing method.
G_{12}	Shear modulus.
h	Equality constraints.
h'	Given step: tabu method.
$\mathbf{H}$	Metric matrix that approximates the inverse of the Hessian.
$\mathbf{H}_t$	Set of steps: tabu method.
h_c	Core thickness.
h_f	Facesheet thickness.
h_j	Distance from the centre of the hypersphere to the j^{th} linearised constrain.
h_o	Distance from the centre of the hypersphere to the linearised objective function.
$\mathbf{K}$	Stiffness matrix.
l	Number of equality constraints.
	Length of the basic cell.
L	Lagrangian.
	Length of the fibre-strip net model.
m	Number of inequality constraints.
$\mathbf{M}$	Mass matrix.
M_{sf}	Mass of the facesheets.
$\mathbf{N}$	Matrix of the active constraint gradients.
N_{bc}	Number of nodes on the boundary of the basic cell.
NDV	Number of design variables.
NFM	Number of failure modes.
NT	Number of terms in the series expansion.
n_1	Number of nodes on Side 1 of the basic cell.
n_2	Number of nodes on Side 2 of the basic cell.
n_3	Number of nodes on Side 3 of the basic cell.
n_4	Number of nodes on Side 4 of the basic cell.
p	Index used during unconstrained minimization.
P	Imposed penalty function.

$\mathbf{P}$	Orthogonal projection operator.
P_s	Probability to be selected: genetic algorithm.
r_p	Scalar factor: exterior penalty method.
r'_p	Scalar factor: interior penalty method.
$\mathbf{q}$	Generalised coordinates.
$\mathbf{Q}$	Hessian matrix.
$\overline{\mathbf{Q}}$	Transformed reduced stiffness.
$\mathbf{s}$	Search direction.
$\mathbf{S}$	Matrix that relates displacements with stresses.
S_1	Part of the boundary with prescribed forces.
S_2	Part of the boundary with prescribed displacements.
T	Kinetic energy.
$\mathbf{T}$	Surface traction vector.
T'	Tabu list: tabu method.
T_e	Temperature: simulated annealing method.
u	Displacement in x-direction.
$\mathbf{u}$	Displacement vector.
U	Strain energy.
U_m^x	Strain energy in the FEM model due to an unitary displacement in x-direction.
U_h^x	Strain energy in the homogenised cell due to an unitary displ. in x-direction.
U_m^y	Strain energy in the FEM model due to an unitary displacement in y-direction.
U_h^y	Strain energy in the homogenised cell due to an unitary displ. in y-direction.
U_m^{xy}	Strain energy in the FEM model due to an unitary shear deformation.
U_h^{xy}	Strain energy in the homogenised cell due to an unitary shear deformation.
v	Displacement in y-direction.
w	Displacement in z-direction.
W	External work.
W_{ij}	Weight coefficients: neural network.
We	Spacing of the strip.
Ws	Width of the strip.
$\mathbf{x}$	Design variables vector.
X	Internal nodal force in the x-direction.

$\overline{\mathbf{x}}$	New design variables vector.
$\mathbf{x}^*$	Optimal design variables vector.
X_c	Compression allowable stress.
X_{ij}	Neuron inputs: neural network.
$\mathbf{x}^l$	Lower limit for design variables vector.
$\mathbf{x}_o$	Initial design variables vector.
$\mathbf{x}_q$	Design variables vector at the q^{th} iteration.
X_t	Tension allowable stress.
$\mathbf{x}^u$	Upper limit for design variables vector.
Y	Internal nodal force in the y-direction.
Y_{ij}	Neuron output: neural network.
z	Slack variable: augmented Lagrange multiplier method.

Greek

α	Distance to be travelled in a given direction.
β_p	Probability of a new design to be accepted: simulated annealing method.
γ	Transverse shear strain.
ε	Transition point: extended penalty method.
ϵ	Strain vector.
ζ	Rotation in y-direction.
θ	Push-off factor: method of feasible directions.
κ	Middle-surface curvature.
κ_b	Boltzmann constant.
λ	Lagrange multiplier.
λ^*	Optimal Lagrange multiplier.
ν_{12}	Poisson's ratio.
ν_{21}	Poisson's ratio.
ξ	Rotation in x-direction.
Π	Total potential energy.
ρ	Density.
σ	Stress vector.

τ	Shear stress.
$\varphi_{cm}(x)$	Basis functions for displacement w.
$\varphi_{cn}(y)$	Basis functions for displacement w.
$\varphi_{dm}(x)$	Basis functions for rotation ζ.
$\varphi_{dn}(y)$	Basis functions for rotation ζ.
$\varphi_{em}(x)$	Basis functions for rotation ξ.
$\varphi_{en}(y)$	Basis functions for rotation ξ.
ψ	Equivalent equality constraint: augmented Lagrange method.
Ψ	Mode shape.
Δ_x^x	Cell extension in x-direction due to an unitary displacement in x-direction.
Δ_x^y	Cell compression in x-direction due to an unitary displacement in y-direction.
Δ_y^x	Cell compression in y-direction due to an unitary displacement in x-direction.
Δ_y^y	Cell extension in y-direction due to an unitary displacement in y-direction.
Ω	Frequency of vibration.
Ω_1	The first natural frequency.
$\overline{\Omega_1}$	Specified first natural frequency.

Subscript

c	Compression.
	Core.
f	Facesheet.
h	Homogenised.
l	Lower limit.
m	Finite Element Model.
o	Initial.
q	q^{th} iteration.
t	Tension.
u	Upper limit.
x	x-direction.
y	y-direction.
z	z-direction.

1	1-direction.
2	2-direction.

Superscript

h	Homogenised.
l	Lower limit.
u	Upper limit.
x	x-direction.
y	y-direction.
$*$	optimal value.

Chapter 1

Introduction

1.1 Motivation

Minimum weight is an important criterion in aircraft and spacecraft design as it allows either an increased pay-load or higher performance. As a result, the use of composite sandwich panels has grown due to their light weight and high rigidity. These panels are manufactured as a three layer structure. The external layers, the facesheets, usually consist of thin laminates of high-stiffness material. The central layer, the core, is a slab of low stiffness and density. This type of panel has an efficient structural geometry, because it places the stiff material away from the neutral plane thereby increasing the flexural rigidity. In order to further increase the efficiency of these structures, designers have used different materials in different shapes in the facesheets and in the core. One of the most recent innovations has been the use of a uniform net of carbon fibre/epoxy as the facesheets.

The idea for this work came from a satellite project called CBERS (China-Brazil Earth Resource Satellite), Figure 1.1. This is a remote sensing satellite developed in a joint program between the Brazilian and Chinese governments. This satellite has an appendage composed of three sandwich panels; these panels covered with solar cells which generate power during operation in space. The sandwich panels have facesheets composed of carbon fibre/epoxy nets and a core of aluminium honeycomb. The goal of this thesis is to undertake an optimization study related to these panels where the objective is to obtain a minimum weight design.

In the next section, a brief history and status of structural optimization will be presented. Then a literature review related to the analysis and optimization of sandwich panels

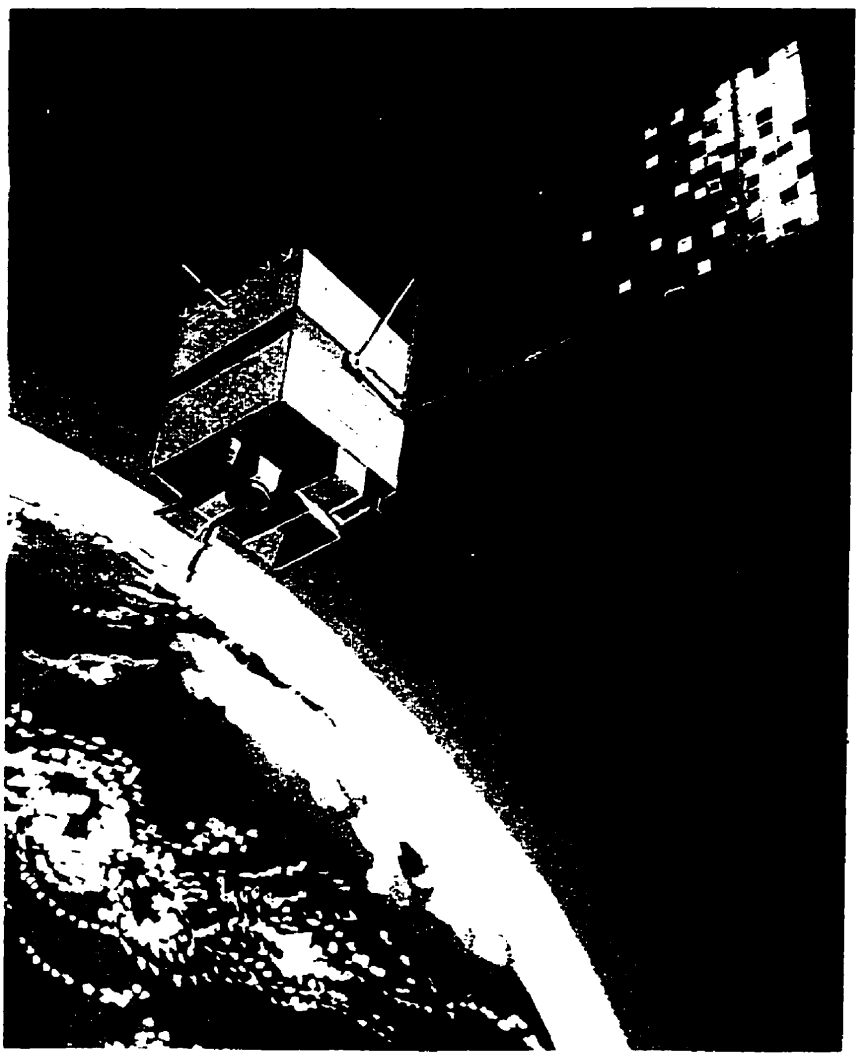

Figure 1.1: China-Brazil Earth Resources Satellite.

will be completed. Following this, the objectives of this dissertation are explained and then the outline of the thesis is given.

1.2 History and Status of Structural Optimization

This section presents a brief overview of structural optimization. A more complete presentation may be found in the paper published by Venkayya [110] or in any number of publications dealing with structural optimization [8, 49, 71].

Research in the area of structural optimization goes back as far as Galileo Galilei, 1638. His strongest cantilever beam in bending and constant shear formulation can be considered an optimal design for minimum weight under a uniform stress constraint [65]. However, the development of mathematical optimization started only after the introduction of calculus by Newton and/or Leibniz at the end of the 17th century. This was followed by the development of the calculus of variations in the 17th and 18th centuries.

The development of high-speed digital computers in the 1950s and the subsequent computer revolution have had an immeasurable impact in the field of engineering. Increased computational power has resulted in calculation capabilities never seen before for the solution of complex mathematical and engineering problems. The computer has led to the development of powerful numerical methods such as the finite element and finite difference techniques; these techniques have as their main feature the characteristic that they reduce the differential field equations of solid and fluid mechanics to algebraic form. Algebraic equations of almost any order are easily solvable by modern digital computers.

Also during the 1950s, the simplex method was introduced by Dantzig [19]. It is a simple and versatile method which is very attractive for solving linearized constrained optimization problems. This work also led to the development of many nonlinear programming methods known today, such as: gradient projection, feasible directions, and penalty functions, as examples. In 1960, Schmit [93] developed an idea that was critical in bringing these techniques to the attention of the researchers in the area of structural mechanics.

The cost and lack of robustness when numerical search techniques are applied to large-scale problems, revived discrete optimality research during the 1960s and 1970s. In the 1980s, Vanderplaats [107] implemented the feasible direction methods (CONMIN); currently these are probably the most widely used techniques in structural optimization. It was also

at this time that structural optimization started to become accepted as one of the design tools in practical structural design. This happened not only because designers had gained confidence, but also because large-scale software tools for production applications started appearing in the latter half of the 1980s. Duysinx & Fleury [24] and Johnson [43] present a broad survey of structural optimization tools that have been developing in Europe and North America, respectively.

Some topics in structural optimization which have recently received the attention of researchers include: sensitivity analysis, multidisciplinary design, heuristic methods, optimization by decomposition and shape optimization. *Sensitivity analysis* is being increasingly investigated because of the recognition of the power and broad range of applicability of sensitivity derivatives. These ideas have been applied to approximate analysis, analytical model improvement, and assessment of design trends. Haber *et. al.* [35], Choi [18] and Arora & Lee [4] have recently presented a comprehensive review of the latest publications in this topic.

Although there has been considerable progress in the field of *multidisciplinary design* [83], there remains a great deal to be done. The principal difficulty is that the combination of individually complicated disciplines leads to even more complex discipline interactions; these complex interactions are serious impediments to further developments. On the other hand, practical applications of optimization algorithms to multidisciplinary design problems are expected to advance with the increasingly more powerful computers.

Heuristic search methods have been developed to solve complex combinatoric problems. They are powerful tools for locating optimal solutions for difficult problems, since they do not require gradient calculations. Among these methods, four are most commonly used: genetic algorithms [41] and neural networks [15,48] have the biological sciences as their background; simulated annealing is inspired by the second law of thermodynamics; while tabu search results from attractive procedures for problem solving.

Large optimization problems considered intractable due to their large number of design variables and constraints can be treated through *optimization by decomposition* [100]. In this case, a large problem is transformed in a set of coordinated smaller subproblems. This approach is well-suited to an engineering team, where each member concentrates on different parts of a project.

One important area of structural optimization explored recently is *shape optimiza-*

tion [8,66] (geometry and topology of a structural layout). The reason for focusing on this problem is that it has a great impact on the performance of the structures. The standard approach to shape optimization is to introduce boundary variations for a given topology of the structure. This methodology can now be considered mature for planar structures; however, there is still developments remaining regarding boundary shape optimization for three-dimensional solids. This results from the complexity of geometrical representations and the associated automatic finite element mesh generation methods in these structures. Recently a *homogenisation method* [6] for generating optimal topologies of structural elements has appeared in the literature. This method predicts grid- and truss-like structures for planar structures.

1.3 Structural Analysis of Sandwich Plate

A considerable number of papers have been published concerning the analysis of sandwich plates. These papers can be divided in three main categories: analytical, numerical and experimental. This work is now discussed.

- Analytical Work

One of the earliest analytical papers concerning sandwich plates was due to Reissner [87]. He presented the basic differential equations for finite transverse deflections of sandwich plates under the assumptions that in-plane stresses in the core and variation of the stress over the thickness of the facesheets are negligible. After that, Yu [113] published several papers treating one-dimensional flexural vibration of sandwich plates. In the early 1960s, Habip [36] presented a survey of the analysis of sandwich structures. Liaw & Little [54] developed the governing equations for bending of multi layered sandwich plates; in their model the plate is considered to be a multi layer sandwich with n membranes and (n-1) orthotropic cores. In 1970, Pagano [69] published a three-dimensional elasticity solution for rectangular laminates with pinned edges. Since then, this paper has been used as a reference for verifying numerical methods to solve sandwich plate problems. Pearce & Webber [73] presented a method to determine the overall buckling and local wrinkling loads of sandwich panels with honeycomb cores and laminated angle-ply faces; their work was based on the assumption that the facesheets have a sufficient number of layers so as they may be considered to be orthotropic sheets. Using generalised harmonic analysis, Kulkarni

et. al. [52] have investigated the displacement response of orthotropic sandwich plates subjected to ideal white noise. Frostig & Baruch [29] present a high-order theory for the bending behaviour of a sandwich panel with flexible core to study localised load effects. Their theory uses classical thin-plate theory to model the skin and a three-dimensional elasticity representation of the core material. They used this model to study the effect of the plate aspect ratio on the deformations, internal resultants, and stresses at skin-core interfaces.

- Numerical Work

Among papers published concerning numerical methods applied to sandwich plate analysis, one of the first was written by Bacon & Bert [5]. They used the Rayleigh-Ritz technique to determine both the axisymmetric and unsymmetric vibrational characteristics of arbitrary open-ended sandwich shells of revolution. The facing and core materials can be either orthotropic or isotropic. Chan & Cheung [16] used the finite element strip method to solve bending and vibration problems of multi-layered sandwich plates. Khatua & Cheung [47] formulated beam and plate elements of the displacement type for bending and vibration analysis of multi layer sandwich beams and plates. In the formulation of these elements the bending stiffness of the face layers and independent shear deformation of the core and facesheets were considered. Monforton & Ibrahim [63] studied the effect of coupling in the static structural response of sandwich plates constructed with an orthotropic core and laminated faces. They considered simply supported sandwich plates under lateral loads in which the faces are antisymmetric cross-ply laminated plates. Using an accurate hybrid-stress finite element, Rao & Mayer-Piening [84] performed bending analyses of thick angle-ply composite sandwich plates and concluded that these plates are very sensitive to various inherent parameters such as the relative thicknesses of face and core, fibre orientation of the facesheets and boundary conditions. Argyris & Tenek [3] developed a three-node layered triangular element based on the natural mode method for bending analysis of isotropic, anisotropic and hybrid plates. This element is free of shear locking, has zero strains under rigid body motion and converges to the true state of deformation.

- Experimental Work

Most of the papers in the literature reporting experimental results for sandwich plates deal with stability experiments. However, Raville & Ueng [86] described vibration tests of a simply-supported sandwich plate. Sullins *et. al.* [102] presented an extended study on

stability of sandwich plates, including some experimental results. Later, Pearce & Webber [74] conducted experiments to determine overall buckling and facesheet wrinkling loads for sandwich plates with carbon fibre composite facesheets and honeycomb cores. These experimental results are compared with the analytical results they presented in [73].

1.4 Optimization of Sandwich Structures

In the past sixty years many studies have been completed investigating sandwich-structure optimization problems. Vinson [111] discussed these studies up to 1964. Here, the more recent research in this area is discussed. The sandwich-structure optimization problems described below are divided in three groups, according to the type of structure being optimized: beams, plates or shells.

- Optimization of Sandwich Beams

Paydar & Park [72] studied the minimum weight design of sandwich beams that have variable facing and core thicknesses. They presented a small deflection theory that determines the stresses and deformations for this type of beam. The design variables are the parameters that define the thicknesses of the facesheets and the core. The constraints are the upper limits on the maximum stresses in the facesheet and core and the displacement at the end of the beam. In order to solve the optimization problem, the Recursive Quadratic Programming Algorithm was used.

- Optimization of Sandwich Plates

Vinson [111] presented closed-form solutions for the analysis and design of minimum weight sandwich plates with hex-cell and square cell cores. He considered overstressing, overall buckling, core shear instability, face wrinkling, and monocell buckling as constraints. Later, Vinson [112] developed analytical solutions to determine optimal stacking sequences of minimal weight design of sandwich panels subjected to various in-plane loads (compressive and shear).

Ueng & Liu [105] investigated the least-weight problem of a sandwich panel with lightweight core made from a superplastic sheet. The modified Fletcher-Powell method in conjunction with the golden section searching technique was used to solve the sequence of unconstrained minimization problems.

Kodiyalam *et. al.* [50] used the genetic search method for tailoring composite material

structures, including a satellite solar array substrate. In this problem the objective function was the weight of the panel with constraints on the fundamental frequency, ply strength, and sandwich local buckling failure margins of safety. The design variables used were the ply thicknesses and ply angle orientation. Using a linear least-squares approximation procedure, they concluded that the genetic search method they implemented required too many function evaluations.

Malott *et. al.* [57] compared the performance of three genetic algorithm topologies when used to determine the optimal layup (orientation and number of plies in the top and bottom facesheets) of a cantilever sandwich plate (an idealisation of an airfoil). They minimized the weight of the structure while maximising the twist in the direction opposite to the one caused by the loading. Stiffness, strength and ply clustering were considered as constraints.

- Optimization of Sandwich Shells

Min & de Charentenay [62] developed a code to determine the minimum weight of a sandwich cylinders with orthotropic facings and core. The design variables were the facesheet ply-fibre angles and the facesheet and core thicknesses. The constraints are quite general and relate to local buckling (dimpling and wrinkling) and the strength of the composite material under the combined action of axial compression, bending moment and transverse shear. The variable metric method for constrained optimization was used to find the optimal design; multiple starting points were used.

Ding [22] optimized the weight of sandwich construction by viewing thicknesses of the face and the core as design variables. The constraints were different failure modes: facesheet tension failure, core shear failure, general buckling, facesheet wrinkling, shear crimping, and facesheet dimpling. the stresses in the face and in the core were determined using a six-node triangular sandwich shell element. Later, Ding [23] extended this work by considering cell wall thickness and the diameter of an inscribed circle in a honeycomb cell as additional design variables.

Ostwald [68] solved the problem of minimum weight design for sandwich cylindrical shells under axial compression and external pressure. The shell facesheets were constructed of aluminium alloy and the core was a foamed plastic; the thickness of the layers were the design variables. He considered stability and material strength as constraints. The stability problem is solved using the Bubnov-Galerkin method.

1.5 Objective

Lightweight composite sandwich panels have been designed for space applications such as satellite solar panels. In these structures, the fibre reinforced composite material of the facesheets are arranged in a net configuration composed of fibre strips interwoven in a perpendicular fashion. This facesheet configuration has been used in the CBERS solar array support (Figure 1.2), as well as in other satellite sandwich panels. A typical detail illustrating the CBERS design is shown in Figure 1.3. In the present study, the optimal design of this type of structure is treated. The mass of the sandwich plates with orthotropic facesheets and core is minimized, considering the first natural frequency and certain failure loads as constraints. Weight reduction is obtained by permitting a nonuniform distribution of composite material in the facesheets. Initially, the facesheets are assumed to be constructed of strips in a regular pattern. During the optimization process, both the widths of the strips and the spacing between them are varied to decrease the amount of material used. Such a design is conceptually straightforward to manufacture and therefore could lead to improved performance with little cost penalty.

In order to solve this problem, it is first necessary to develop a computer code to determine the natural frequencies and the stresses of these plates when they are subjected to a specified load condition. The bending and vibration problems for anisotropic sandwich plates was solved using the Ritz Method; the assumptions formulated by Reissner for sandwich plates were adopted, [87].

Since the sandwich plate considered in this study has facesheets constituted of nets and the computer code was developed to analyse laminates with heterogeneous continuous layers, it was necessary to use a procedure to approximate the nonuniform net as a smoothed orthotropic heterogeneous continuum. The smoothing process was accomplished using the theory of homogenisation and the material coefficients are calculated using the Finite Element Method.

The next step is to define the design variables of the problem. Two approaches were considered: an independent design approach, in which the facesheets are discretized into regions with uniform design parameters; and a reduced basis formulation, in which the design is specified by a linear combination of orthogonal and complete basis functions.

The last step was to determine from among all the numerical optimization methods

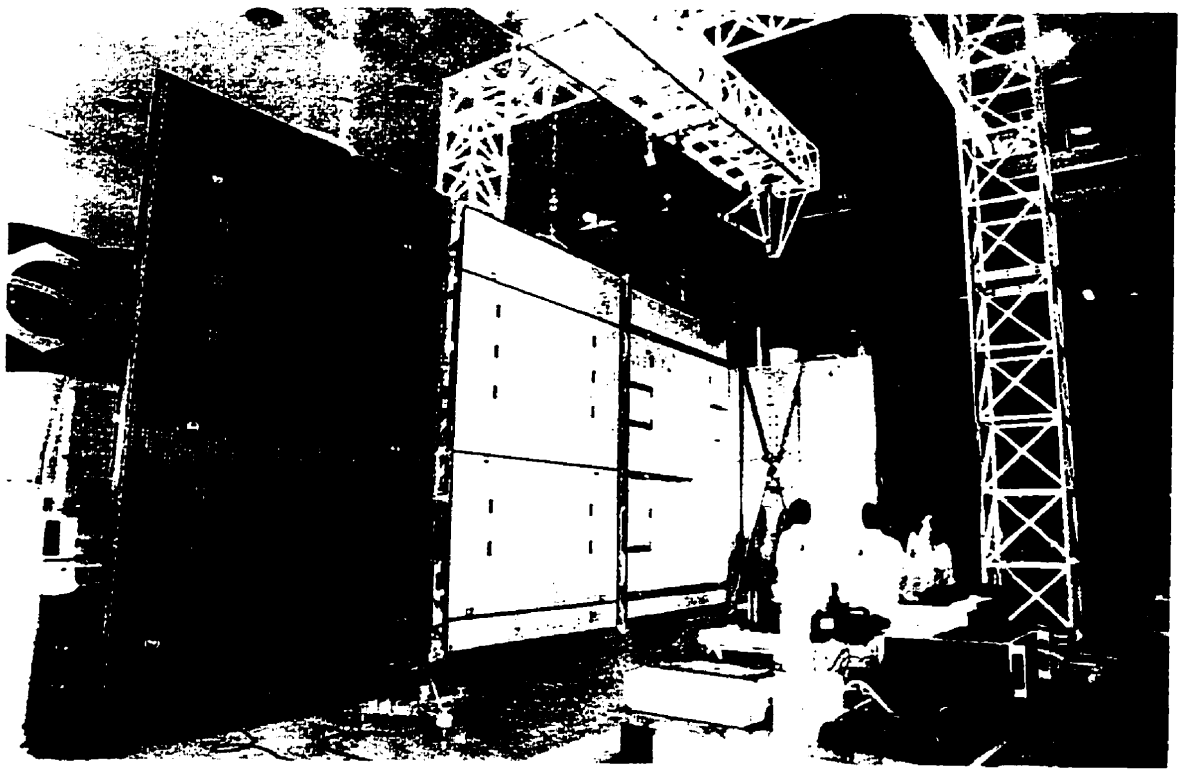

Figure 1.2: The Solar Array Support of CBERS.

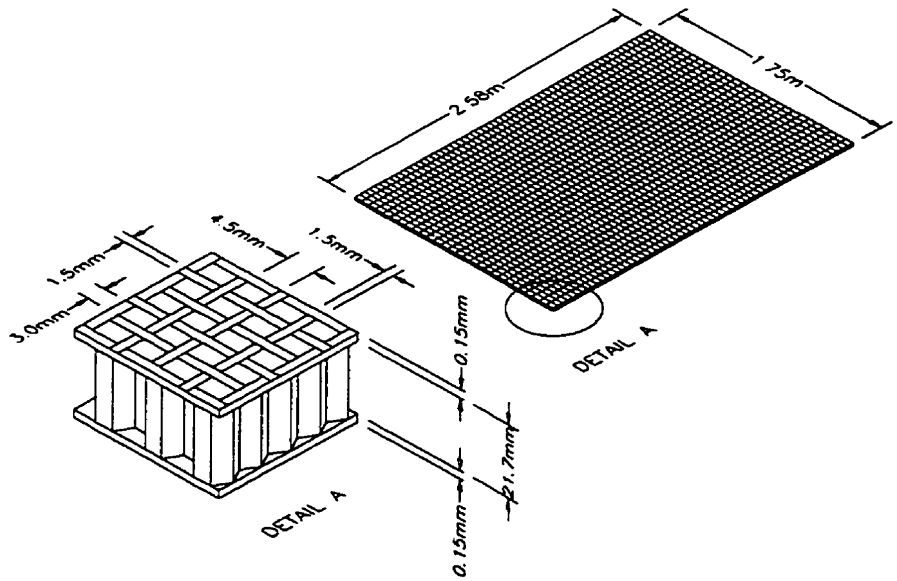

Figure 1.3: Dimensions of the CBERS Solar Array Support.

which one functions best for the solution of this problem. A computer package was created based on a range of numerical methods which have been used in structural optimization problems. These methods were evaluated by solving example sandwich plate problems and then the most efficient algorithm was chosen.

1.6 Thesis Outline

Chapter 2 presents a description of the most common numerical optimization methods used to solve structural optimization problems. This chapter reports on a computer package which was developed using some of these methods.

A comprehensive description of the numerical models developed in this study to determine stresses and natural frequencies of composite sandwich plates is presented in Chapter 3. Two numerical models were generated: one for a simply-supported and another for a free-free composite sandwich plate. These models were verified by comparing their results with results available in the literature or with results from a commercial Finite Element code (MSC/NASTRAN).

Chapter 4 describes the procedure used to determine the homogenised engineering constants of an anisotropic layer that models the composite net. These properties were calculated using the Finite Element Method and the boundary conditions of the finite element model used are specified in this chapter as well. At the end of the chapter the verification of the procedure adopted is presented, in which a sandwich plate with facesheets formed from a net was built, and tested; the experimental results were compared with numerical results obtained using these homogenised engineering constants.

Two approaches were developed to define the design variables in these optimization problems. These approaches are described in Chapter 5. In addition, the failure modes considered and the sensitivity analysis are described. The final part of this chapter outlines the process of choosing the optimization algorithm.

Chapter 6 presents optimal solutions for composite sandwich plates with facesheets of carbon fibre/epoxy nets. In these problems, the effect of the approach used to define the design variable, the plate aspect ratio and failure modes are presented.

Finally, in Chapter 7, the conclusion of this work are presented as well as some recommendations for future work.

Chapter 2

Numerical Methods for Structural Optimization

Before describing some of the numerical methods used in structural optimization, it is necessary to define the terminology utilized in this area. The property of the structure to be minimised or maximised (weight, cost, stiffness, strength, etc.) is called the *objective function*. In this study, only the minimization problem is considered, since the maximization problem can be obtained simply by multiplying the objective function by minus one. The objective function depends on a number of parameters called *design variables*, such as dimensional parameters and material properties; each design variable is defined within a particular range. All these ranges delimit a region of all possible designs, the *design space*. The structure to be optimized is typically subjected to some *constraints*, such as maximum weight, minimum stiffness, etc. The constraints set boundaries to the design space, thus specifying the *feasible space*; a space of all possible designs which do not violate the constraints.

A typical procedure in the search for the optimal design begins with the selection of an *initial design*; this is arbitrary but must be within the design space. A *search direction*, is then specified starting from this design and the minimum of the objective function in this direction is sought; such a minimizing point is called an *intermediate design*. This process is repeated until a minimum of the objective function is found. Such a design represents a *global minimum* or *optimal design* if the feasible space is convex. Figure 2.1 illustrates schematically all the aforementioned nomenclature.

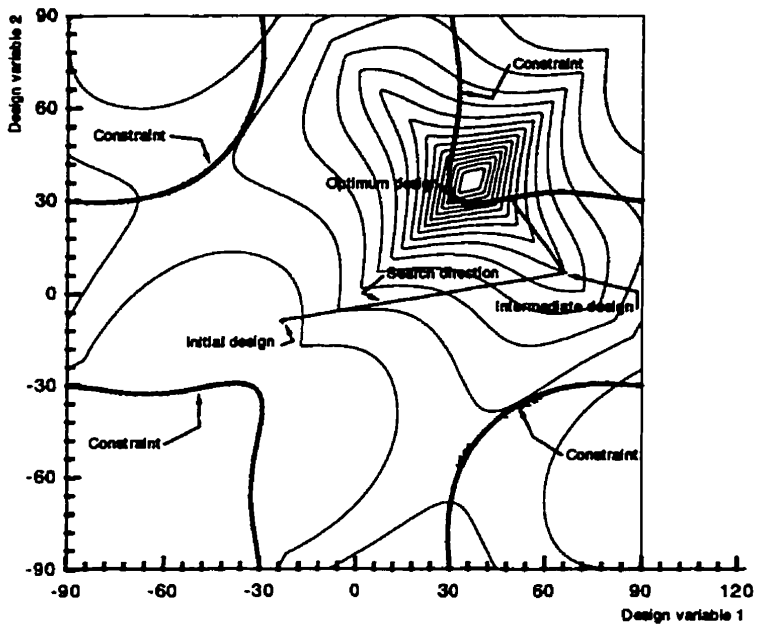

Figure 2.1: Nomenclature of Structural Optimization

In general, a structural optimization problem can be formulated as follows:

$$\begin{aligned} \text{Minimize} \quad &: \quad F(\mathbf{x}) \\ \text{Subject to} \quad &: \quad g_j(\mathbf{x}) \leq O \qquad \text{j = 1,m} \\ &\qquad h_k(\mathbf{x}) = O \qquad \text{k = 1,l} \\ &\qquad x_i^l \leq x_i \leq x_i^u \quad \text{i = 1,n} \end{aligned} \tag{2.1}$$

where

$\mathbf{x}$ – vector of design variables

x_i – design variables

$F(\mathbf{x})$ – objective function

$g_j(\mathbf{x})$ – inequality constraints

$h_k(\mathbf{x})$ – equality constraints

x_i^l and x_i^u – side constraints (design space)

There are many possible approaches to solve this problem and they can be divided in two basic groups. The first group uses only function evaluations (that is, the value of the objective function and constraints) to search for the optimum and includes methods such

as:

- Random search method
- Grid search technique
- Heuristic method

The second group uses gradient information of both the objective function and constraints as well as function evaluations to seek the minimum. In this case the optimization procedure involves three steps. In the first, a strategy is defined to deal with the constraints. This is done using any of the following, among others:

- Exterior Penalty Function
- Interior Penalty Function
- Extended Interior Penalty Function
- Augmented Lagrange Multiplier Method
- Sequential Linear Programming
- The Method of Centres
- Sequential Quadratic Programming

In the second step, a search direction is determined using one of the algorithms below:

- Steepest Descent
- Conjugate Direction Method
- Variable Metric Methods
  - Davidon-Fletcher-Powell Method (DFP)
  - Broydon-Fletcher-Goldfarb-Shanno Method (BFGS)
- Newton's Method
- The Method of Feasible Directions

- Gradient Projection Method

and finally in the third step, the minimum is determined in the search direction using one of the following:

- The Bracketing Method
- The Golden Section Method
- Polynomial approximation

These are not all the possible methods applied in structural optimization, but are the most frequently used. A brief description of these techniques is presented below.

2.1 Random Search Technique

As an example of a random search method, consider the procedure presented by Luus and Jaakola [55]. This is a direct search using random numbers combined with an interval reduction algorithm. It has four steps: 1 - an initial point and region around this point are defined in the design space; 2 - a certain number of points (usually 100) are chosen randomly in this region; 3 - among these points the one which gives the best design is selected; 4 - a new region around the chosen point is defined. The size of this new region is smaller than the previous one by pre-defined factor (5 %) and the process is repeated a certain number of times (usually 200 iterations). This procedure has been shown to be effective in solving nonlinear programming problems.

2.2 Grid Search Technique

A special grid search program is described here. Instead of looking at all possible combinations of design variables, the program uses a technique to save function evaluations. In order to explain this technique, consider the two dimensional problem shown in Figure 2.2.

The grid search starts by using a coarse mesh. In this mesh, the point in the grid which gives the minimum value for the objective function and does not violate the constraints is sought. Once this point is found, the grid is subdivided locally and a new search region is defined. The mesh is refined in this area and the search starts again seeking the point

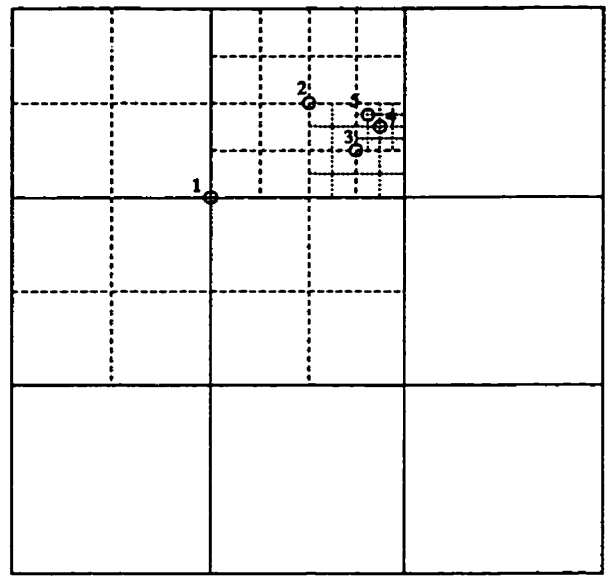

Figure 2.2: The Grid Search Technique

in this finer grid which minimizes the objective function without violating the constraints. This process is repeated until the size of the mesh in the region around the last point found is smaller than a specified value.

To verify if the final point gives the global minimum, the process is restarted, but this time the size of the initial mesh is decreased by a half. The same procedure is followed and at the end the final result is compared with the one from the previous iteration. If the difference between these two points is smaller than a specified value the search is terminated. Otherwise, the process is repeated again.

2.3 Heuristic Search

Heuristic search methods have been developed to solve complex combinatorial problems. Among these methods, four are worth mentioning: genetic algorithms and neural networks have the biological sciences as their background; simulated annealing is inspired by the second law of thermodynamics; the remaining one, tabu search, derives from good procedures of problem solving.

2.3.1 Genetic Algorithms

According to Holland's original work [41], genetic algorithms are based on the idea of creating new solutions from parent ones. During the biological reproduction process the information stored in chromosomal strings changes so that new generations can adapt favourably to the environment. This notion is presented in genetic algorithms through three fundamental processes: selection, crossover and mutation. *Selection* uses a ranking technique. The designs are first evaluated and sorted in a decreasing order of fitness. The probability of a particular design to be selected is P_s and is a function of its rank. *Crossover* allows the parents to transmit some of their characteristics to their offspring. It can be accomplished by breaking the chromosomes in one point chosen randomly and exchanging parts of strings. There is also a probability associated with crossover (usually between 60% and 100%). *Mutation* is a stochastic operator, usually applied with a low probability. Its purpose is to protect against a complete loss of genetic material. Indeed, under the action of selection, the variety of alleles for any given gene in the population diminishes and the chromossomes all tend toward the best known chromosomes. Alleles associated with lower fitness individuals are usually not transmitted to the next generation. Once the population is mainly uniform, crossover loses its ability to create new designs and the search stalls. Thus, by keeping some genetic diversity in the population, mutation preserves the ability of the crossover to find new good designs.

2.3.2 Neural Networks

Based upon the works of McCulloch and Pitts [59] and Rosenblatt [91], the idea of a neural network is a model of stimulus/response in which the importance of structural links and rules for transmitting signals across these links are emphasized. The cornerstone of the neural network is that it can be artificially trained to recognize specific patterns and extrapolate from these patterns when new information is presented. The network is composed of neurons (single computational elements) which are connected to others by non-linear functions. One of the functions most frequently used to represent the numerical behaviour of a single link is the sigmoid function:

$$Y_j = \frac{1}{1 + \epsilon^{\beta_j}} \tag{2.2}$$

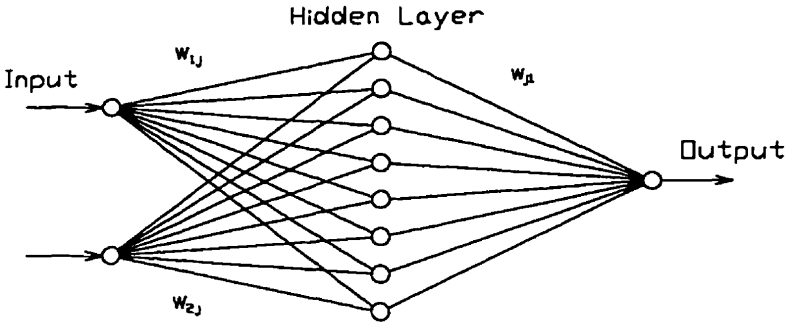

Figure 2.3: Neural Network

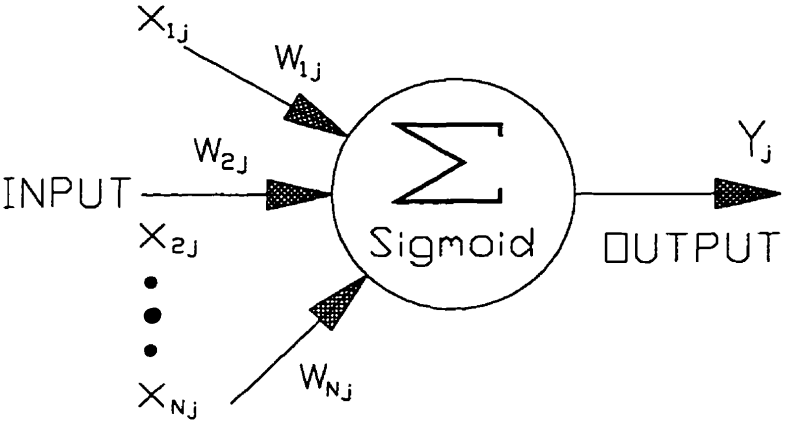

Figure 2.4: Typical Neuron

where

$$\beta_j = \sum_{i=1}^{N} (W_{ij} X_{ij} - \Theta_j) \tag{2.3}$$

where Y_j is the neuron output and the X_{ij} the inputs.

Figure 2.3 shows a simple neural network configuration. In this example, there is a "two-element" input layer, a hidden layer of 8 neurons, and an output layer with a single output neuron.

A typical neuron is presented in Figure 2.4. The w_{ij} coefficients are called weights, and a coefficient unique to each neuron is termed the bias. The computational characteristics of a neuron are defined by the values of these coefficients.

The number of inputs and outputs of a neural network depends on the design problem at hand. The inputs are the design variables and the outputs are the objective function and constraints. Usually, hidden layers are required. Determining the number of the hidden lay-

ers is an issue that is currently being addressed in the literature. The hidden layer geometry is a function of the design space complexity to be mapped. When the number of hidden layers increases, the design space is better represented, but the cost of this is to increase the training time of the network. This training is the determination of neuron coefficient values which is accomplished by using sets of information whose functional relationship is to be represented by the neural network.

2.3.3 Simulated Annealing

Introduced by Cerny [15] and by Kirkpatrick, Gelatt and Vecchi [48], simulated annealing has been heralded as a new and powerful methodology for combinatorial problems, with implications for the field of artificial intelligence. The name *simulated annealing* derives from the intent to pattern the approach after the physical process of annealing, which is a heat-treatment process which usually involves a relatively slow cooling after holding the material for some time at the annealing temperature. The purpose is to produce a definite microstructure with minimum energy or ground state.

In the annealing process, the temperature of the heat bath is increased above the re-crystalization temperature. Then, the temperature is decreased until the particles arrange themselves in the ground state of the solid. The ground state is only obtained if the maximum temperature is sufficiently high and the cooling is done sufficiently slowly, allowing molecules to reach the lowest energy state. The key to the process is that the thermal energy allows molecules to temporarily move to higher energy states, thus avoiding being trapped in local minima. The probability of getting higher energy states decreases with the bath temperature, and tends to zero at the minimum temperature allowed.

In simulated annealing, designs are generated at random in the neighbourhood of a current design. Better designs are always accepted, and poorer designs are accepted with a probability that depends on an artificial temperature which is gradually reduced during the optimization process. At the beginning, when the temperature is high, poorer designs are readily accepted. Later on, the probability of accepting poorer designs is reduced. This mechanism enables the algorithm to escape local minima and eventually reach the global optimum.

The algorithm *Metropolis* [61] can be used to describe this process: let S be the set of all possible states of the system, while s is a current state of the system and let $g_e : S \rightarrow \mathbf{R}$

describe an energy function, which is to be minimized. A small perturbation is applied to s, producing a new state $\overline{s}$, having energy $g_e(\overline{s})$. If $g_e(\overline{s}) < g_e(s)$, then the state $\overline{s}$ is a better estimate of the ground state, and $\overline{s}$ becomes the current state. If, however, $g_e(\overline{s}) \geq g_e(s)$, then $\overline{s}$ can be accepted as the current state with probability

$$P(s, \overline{s}, T_e) = e^{\frac{-[g_e(\overline{s}) - g_e(s)]}{\kappa_b T_e}} \tag{2.4}$$

where T_e is the temperature, e is the base of the natural logarithm and κ_b is the Boltzmann constant. This acceptance value is called the Metropolis criterion. Typically a number $\beta_p \in [0, 1)$ is chosen randomly, using a uniform distribution, to which

$$e^{\frac{-[g_e(\overline{s}) - g_e(s)]}{\kappa_b T_e}} \tag{2.5}$$

is compared. If $\beta_p < P(s, \overline{s}, T_e)$ then $\overline{s}$ becomes the current state, otherwise the current state remains s.

2.3.4 Tabu Search

Introduced by Glover [31, 32], this method constitutes a meta-procedure that can be combined with other heuristic procedures to prevent them from being trapped at locally optimal solutions. Instead of terminating upon reaching a point of local optimality, tabu search ensures that the search operation continues. This is accomplished by forbidding moves with certain attributes (making them tabu), and choosing moves from the remaining that an embedded heuristic has assigned the highest priority.

In the Tabu search with random moves, two concepts are involved, the neighbour of a given point and a random move in the neighbour. For a given point x and a given step h', its neighbour $N(x, h')$ is defined as $N(x, h') = y : |x - y| < h'$. When a point y is generated randomly in a given neighbour $N(x, h')$, it is called a random move in the neighbour $N(x, h')$. If a random move in a neighbour satisfies all constraints, it is called a feasible random move.

In the tabu search method with random moves, a set of steps h'_i, $H_t = \{h'_1, h'_2, ..., h'_t\}$ is given. For an initial feasible solution x, the search moves are made over a set of active neighbours $N(x, h'_i)$, where $h'_i \in H_t - T'$ and T' is the tabu list, which is initially empty. For each active neighbour one feasible random move is generated. Suppose, for a feasible

random move y in the neighbour $N(x, h_i')$, the cost is less than that of current solution x, then y is saved as the current solution x, and the corresponding h_{ij}' is added to T'. When $H_t - T'$ is empty, T' empty is updated; otherwise the procedure is repeated.

2.4 Strategy for Considering the Constraints

In this step a strategy is defined for dealing with the constraints.

2.4.1 Penalty Methods

The objective of all penalty methods is to convert the original constrained minimization problem into an unconstrained one by creating a pseudo-objective function of the form [108]:

$$\Phi(\mathbf{x}, r_p) = F(\mathbf{x}) + r_p P(\mathbf{x}) \tag{2.6}$$

where

$F(\mathbf{x})$: original objective function

$P(\mathbf{x})$: imposed penalty function

r_p : scalar that decides the magnitude of the penalty

p : index used during unconstrained minimization

The pseudo-objective function is often a source of numerical ill-conditioning; therefore penalty methods are chosen mainly for convenience instead of efficiency. One way to deal with ill-conditioned problems is to start the optimization process with a moderate penalty ($r_p P(\mathbf{x})$), and solve the unconstrained minimization problems several times. In each solution the value of the scalar r is changed (increased for the Exterior Penalty Method and decreased for the Interior Penalty Method).

Exterior Penalty Method

For the exterior penalty function method the penalty function, $P(\mathbf{x})$, is defined as (Figure 2.5):

$$P(\mathbf{x}) = \sum_{j=1}^{m} \{\text{MAX}[0, g_j(\mathbf{x})]\}^2 + \sum_{k=1}^{l} [h_k(\mathbf{x})]^2 \tag{2.7}$$

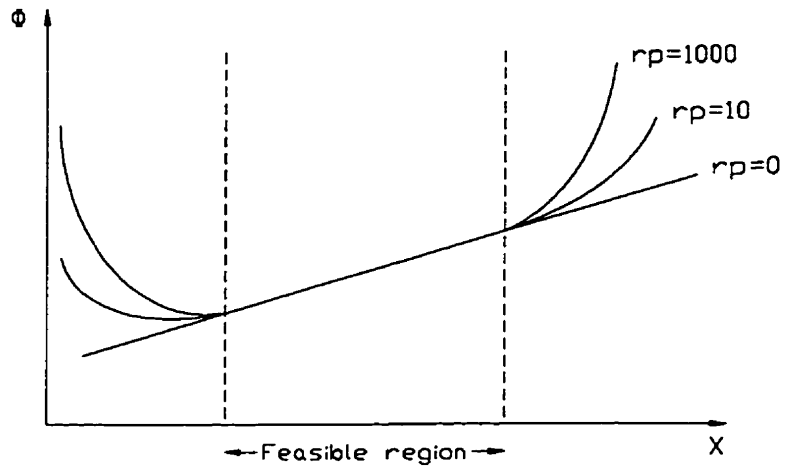

Figure 2.5: The Exterior Penalty Method

It should be noted that the first derivative of the penalty function is continuous at the constraint boundary, which makes this method suitable for use with any other method based on gradient information for unconstrained minimization. However, since the second derivative is not continuous at the constraint boundary, this method is not recommended to be used with second-order methods for unconstrained minimization. In this method r_p is initially given a small value and after each unconstrained minimization its value is increased.

One disadvantage of this method is that the optimum is approached from an infeasible region; therefore all intermediate designs are not usable.

Interior Penalty Method

For the interior penalty method the penalty function, $P(\mathbf{x})$, is defined as:

$$P(\mathbf{x}) = r'_p \sum_{j=1}^{m} \frac{-1}{g_j(\mathbf{x})} + r_p \sum_{k=1}^{l} [h_k(\mathbf{x})]^2 \tag{2.8}$$

Here, r'_p is initially a large positive number and after each unconstrained minimization its value is decreased (Figure 2.6). The factor r_p is the same as in the exterior penalty function method.

The advantage of the interior over the exterior penalty function method is that the optimum is approached from the feasible region; all intermediate designs are therefore usable.

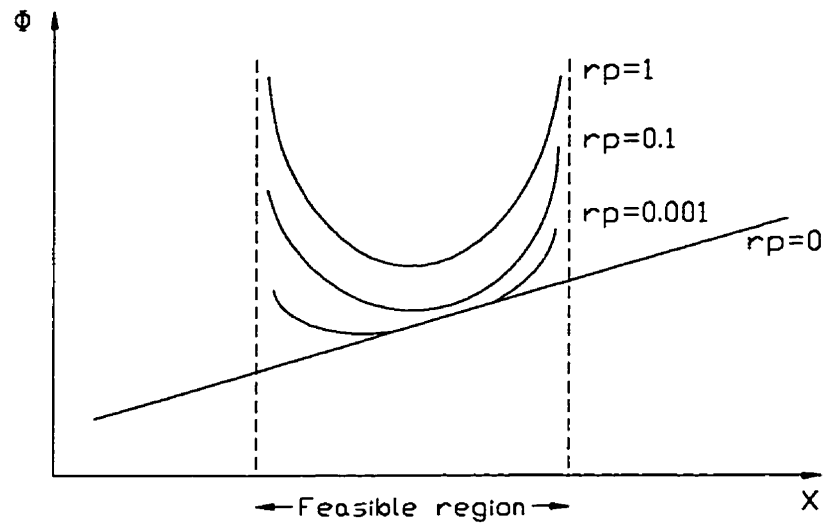

Figure 2.6: The Interior Penalty Method

However, this brings two restrictions: first, the initial design must be feasible and sometimes it is difficult to obtain a feasible design; second, all points must be in the feasible domain. The last requirement is difficult to satisfy, since approximate analysis methods often cause constraint violation [39].

Extended Penalty Method

The extended interior penalty function was developed as a solution for problems related to infeasible designs in the interior penalty function method. It attempts to incorporate the best features of the interior and exterior methods. Further, it provides a mechanism to recover from violations caused by approximate analyses and permits a infeasible initial design.

Kavlie and Moe [45] presented the first application of this method in engineering design. They proposed a linear extended interior penalty function in which the penalty function is expressed as:

$$P(\mathbf{x}) = \sum_{j=1}^{m} \overline{g}_j(\mathbf{x}) \tag{2.9}$$

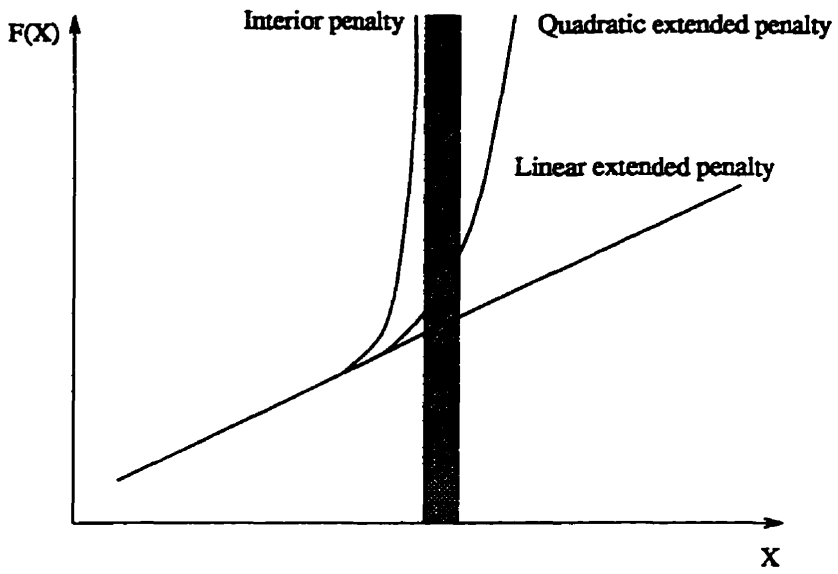

Figure 2.7: The Extended Penalty Method

where

$$\overline{g}_j(\mathbf{x}) = -\frac{1}{g_j(\mathbf{x})} \quad if \quad g_j(\mathbf{x}) \leq \varepsilon$$
$$\overline{g}_j(\mathbf{x}) = -\frac{2\varepsilon - g_j(\mathbf{x})}{\varepsilon^2} \quad if \quad g_j(\mathbf{x}) > \varepsilon$$

Here, ε is a transition point between the two constraint functions.

The linear extended interior penalty function has discontinuous second derivatives at the transition point. Because of this a second-order method cannot be used to define the search direction. In order to overcome this problem, Haftka and Starnes [39] created a quadratic extended penalty function of the type (Figure 2.7):

$$P(\mathbf{x}) = \sum_{j=1}^{m} \overline{g}_j(\mathbf{x}) \tag{2.10}$$

where

$$\overline{g}_j(\mathbf{x}) = -\frac{1}{g_j(\mathbf{x})} \quad if \quad g_j(\mathbf{x}) \leq \varepsilon$$
$$\overline{g}_j(\mathbf{x}) = -\frac{1}{\varepsilon}\left\{\left[\frac{g_j(\mathbf{x})}{\varepsilon}\right]^2 - 3\left[\frac{g_j(\mathbf{x})}{\varepsilon} + 3\right]\right\} \quad if \quad g_j(\mathbf{x}) > \varepsilon$$

and

$$\varepsilon = -C(r_p')^{a'} \qquad \frac{1}{3} \leq a' \leq \frac{1}{2}$$

with C a positive constant.

The limits on a' guarantee that the penalty function increases when constraints are violated, as r_p' goes to zero. It also guarantees that the minimum of the pseudo-objective function is in the quadratic range of the penalty function, where $P(\mathbf{x})$ has smoother behaviour than $1/g_j(\mathbf{x})$.

Haftka and Starnes [39] chose r_p' so that the penalty function had the same value as the objective function at the beginning of the process.

Augmented Lagrange Multiplier Method

Powell [81] suggested that penalty function methods should include Lagrange multipliers as a practical optimization tool. In the augmented Lagrange multiplier method (ALM) conditions for optimality are incorporated which use Lagrange multipliers. With this method, efficiency and reliability are improved, and dependence on the choice and updating of penalty parameters is decreased.

First consider a problem with equality constraints:

$$\begin{aligned} &\text{Minimize:} \quad F(\mathbf{x}) \\ &\text{Subject to:} \quad h_k(\mathbf{x}) = 0, \quad k = 1, \ldots, l \end{aligned} \tag{2.11}$$

There are three conditions for constrained optimality of a general optimization problem, and they are referred to as the Kuhn-Tucker necessary conditions [51]. If $\mathbf{x}^*$ is an optimal design, these conditions are satisfied when:

$$\mathbf{x}^* \text{ is feasible} \tag{2.12}$$

$$\lambda_j g_j(\mathbf{x}^*) = 0 \qquad j = 1, m \qquad \lambda_j \geq 0 \tag{2.13}$$

$$\nabla F(\mathbf{x}^*) + \sum_{j=1}^{m} \lambda_j \nabla g_j(\mathbf{x}^*) + \sum_{k=1}^{l} \lambda_{k+m} \nabla h_k(\mathbf{x}^*) = 0 \tag{2.14}$$

where $\lambda_j \geq 0$ and λ_{k+m} is unrestricted in sign.

So, defining the Lagrangian as

$$L(\mathbf{x}, \lambda) = F(\mathbf{x}) + \sum_{k=1}^{l} \lambda_k h_k(\mathbf{x}) \tag{2.15}$$

then the stationary conditions of $L(\mathbf{x}, \lambda)$ with the equality constraints give the necessary conditions for optimality.

If an exterior penalty function is added to the Lagrangian, this creates a pseudo objective function called *the augmented Lagrangian*:

$$A_{al}(\mathbf{x}, \lambda, r_p) = F(\mathbf{x}) + \sum_{k=1}^{l} \{\lambda_k h_k(\mathbf{x}) + r_p [h_k(\mathbf{x})]^2\} \tag{2.16}$$

This pseudo objective function has some interesting features. First, if all the Lagrange multipliers are set to zero, the usual exterior penalty function is recovered. On the other hand, if the optimal values of the multipliers, λ^*, are specified the correct minimum for the constrained problem, for any positive value of r_p, is obtained. Therefore, with this method precise constraint satisfaction can be achieved, whereas with the exterior penalty function approach it cannot.

The optimal values λ^* are not known in advance. So at the beginning λ is given an arbitrary value (usually zero or unity). Then it is updated after each iteration using

$$\lambda_k^{p+1} = \lambda_k^p + 2 r_p h_k(\mathbf{x}^p) \qquad\qquad k = 1, \ldots, l \tag{2.17}$$

where r_p is increased using the same approach as in the exterior penalty function method.

Now, consider a problem with inequality constraints:

$$\begin{aligned} &\text{Minimize:} \quad F(\mathbf{x}) \\ &\text{Subject to:} \quad g_j(\mathbf{x}) \leq 0, \quad j = 1, \ldots, m \end{aligned} \tag{2.18}$$

The first step in solving this problem using the ALM is to convert the constraint to equivalent equality constraints, by adding slack variables. Doing so, the constraint equations become:

$$g_j(\mathbf{x}) + z_j^2 = 0 \qquad\qquad j = 1, \ldots, m \tag{2.19}$$

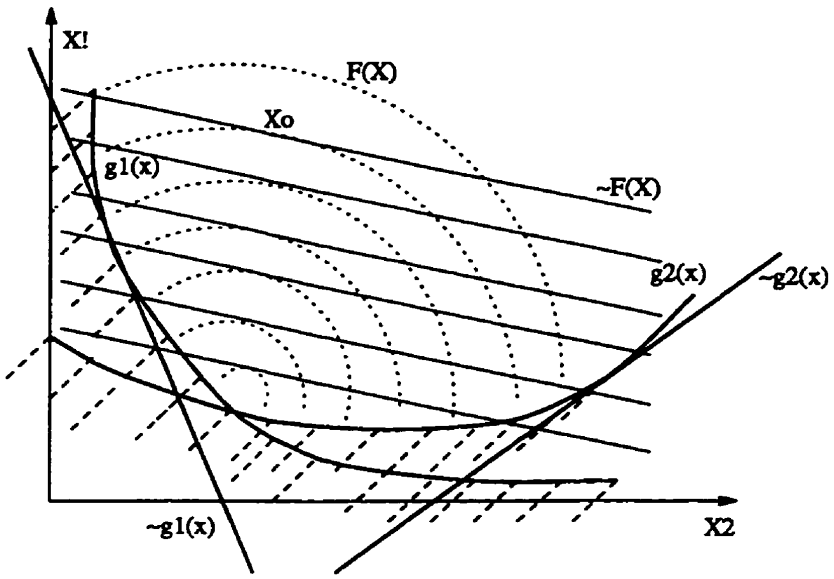

Figure 2.8: The Linear Programming Method

and the augmented Lagrangian is:

$$A(\mathbf{x}, \lambda, \mathbf{z}, r_p) = F(\mathbf{x}) + \sum_{k=1}^{l} \{\lambda_k (g_j(\mathbf{x}) + z_j^2) + r_p [g_j(\mathbf{x}) + z_j^2]^2\} \tag{2.20}$$

Rockafellar [90] proved that this expression is mathematically equivalent to:

$$A(\mathbf{x}, \lambda, r_p) = F(\mathbf{x}) + \sum_{j=1}^{l} \{\lambda_j \Psi_j + r_p \Psi_j^2\} \tag{2.21}$$

where

$$\Psi_j = MAX \left[g_j(\mathbf{x}), -\frac{\lambda_j}{2r_p} \right] \tag{2.22}$$

This process yields a pseudo objective function just as in the case of equality constraint problems.

2.4.2 Sequential Linear Programming Method (SLP)

The idea of this method, also called Kelly's cutting plane method [46], is to linearize the optimization problem and solve it by using the linear programming (LP) (Figure 2.8). Having this solution, the problem is linearized at this new point and the process is repeated, until the solution converges to specified tolerance.

The problem statement is:

$$\begin{aligned} \text{Minimize:} \quad & F(\mathbf{x}) \\ \text{Subject to:} \quad & g_j(\mathbf{x}) \leq 0, \quad j = 1, \ldots, m \\ & h_k(\mathbf{x}) = 0, \quad k = 1, \ldots, l \\ & x_i^l \leq x_i \leq x_i^u \end{aligned} \tag{2.23}$$

This can be linearized using a first-order Taylor series expansion as:

$$\begin{aligned} \text{Minimize:} \quad & F(\mathbf{x}) \simeq F(\mathbf{x}_o) + \nabla F(\mathbf{x}_o).\delta\mathbf{x} \\ \text{Subject to:} \quad & g_j(\mathbf{x}) \simeq g_j(\mathbf{x}_o) + \nabla g_j(\mathbf{x}_o).\delta\mathbf{x} \leq 0, \quad j = 1, \ldots, m \\ & h_k(\mathbf{x}) \simeq h_k(\mathbf{x}_o) + \nabla h_k(\mathbf{x}_o).\delta\mathbf{x} = 0, \quad k = 1, \ldots, l \\ & x_i^l \leq x_i + \delta x_i \leq x_i^u \end{aligned} \tag{2.24}$$

where, $\delta\mathbf{x} = \mathbf{x} - \mathbf{x}_o$

The Simplex method [19] is used to solve the linear approximation. The advantage of this method is the existence of several reliable LP packages. However, it has three main disadvantages. First, it increases the computational cost of the optimization operations, since they are repeated several times. This makes using this method reasonable only when the cost of analysis is small compared to the cost of optimization. Second, limits must be set for design change in each iteration; without this the process usually does not converge. Choosing these limits is the most difficult part of the method. Haftka et al. [38] suggested that at the beginning the move limits should be ten percent of a typical value of design variable and be shrunk by ten to fifty percent of their previous values after each linear programming problem. Third, the solution of the linearized problem can give an infeasible design.

The Simplex Method

This is a standard solution technique to solve linear programming (LP), posed as

$$\text{Minimize:} \quad F(\mathbf{x}) = \sum_{j=1}^{n} c_j x_j \tag{2.25}$$

$$\text{Subject to:} \quad \sum_{j=1}^{n} a_{ij}x_j \leq b_i, \quad i = 1, \cdots, m_1$$
$$\sum_{j=1}^{n} a_{ij}x_j \geq b_i, \quad i = m_1 + 1, \cdots, m_2$$
$$\sum_{j=1}^{n} a_{ij}x_j = b_i, \quad i = m_2 + 1, \cdots, m$$
$$x_j \geq 0 \qquad j = 1, \cdots, n$$

The first step is to put the problem in canonical form by defining artificial variables as

$$\begin{array}{ccccccccccc} a_{11}x_1 & + & \cdots & + & a_{1n}x_n & + & x_{n+1} & + & \cdots & + & 0 & = & b_1 \\ \vdots & & & & \vdots & & \vdots & & & & \vdots & = & \vdots \\ a_{m1}x_1 & + & \cdots & + & a_{mn}x_n & + & 0 & + & \cdots & + & x_{n+m} & = & b_m \end{array}$$

x_i for $i = n + 1, \cdots, m + n$ are the artificial variables.

The next step is to find a *basic feasible solution* using pivot operations; this is a feasible solution (all constraints are satisfied) in which at least $n - m$ of the variables are zero. The variables that are not equal to zero in this solution are called *basic variables.* Through additional pivot operations a new set of basic variables can be found, generating another basic feasible solution.

Gass [30] proved that some optimal solution of a linear programming problem is also a basic feasible solution of the problem. In other words, the minimum of the problem can be found by going from one basic feasible solution to another.

In 1948, Dantzig [19] published an iterative method, called the *simplex method*, that is a stepwise procedure that goes from one basic feasible solution to another in such a way that the objective function always decreases. This is done by appending the objective function equation to the canonical form, creating the *the simplex tableau*, and then eliminating all the basic variables from this last equation. The criterion for improving the solution is to bring into the basis a variable that has a negative coefficient in the objective function equation after it has been cleared of all the basic variables.

2.4.3 The Method of Centres

This method, also known as the method of inscribed hyperspheres, is a SLP technique that produces *a sequence of improving designs following a path down the centre of the design space* [7]. The main idea of this method is to linearize the objective function and

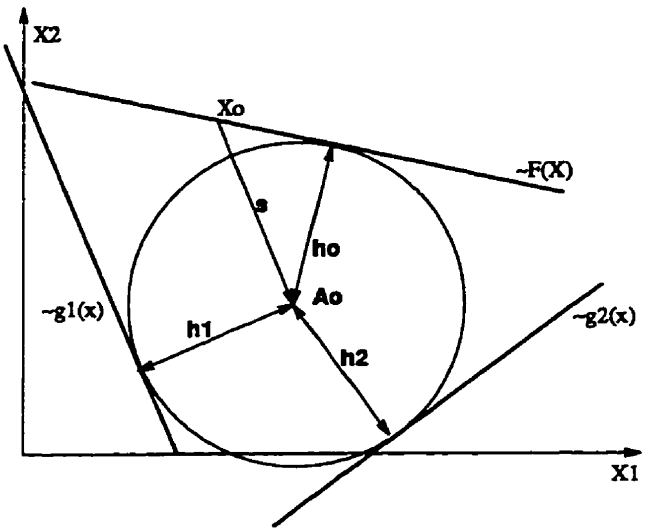

Figure 2.9: The Method of Centers

its constraints, then to try to find the largest hypersphere that fits inside the space defined by the linearized functions (hyperplane). After this, the design variables are moved to the centre of this hypersphere. The process is repeated until the solution has converged to a specified tolerance. If the initial design is infeasible, the linearized objective is not considered in the first iteration so that the next hypersphere will be inside the feasible region.

Consider the point A_o, (Figure 2.9), as the centre of the largest hypersphere completely inscribed inside the feasible region. The distance from that point to any hyperplane is given by:

$$h_f = -\frac{\nabla F(\mathbf{x}_o).\mathbf{s}}{|\nabla F(\mathbf{x}_o)|} \tag{2.26}$$

$$h_j = -\frac{g_j(\mathbf{x}_o) + \nabla g_j(\mathbf{x}_o).\mathbf{s}}{|\nabla g_j(\mathbf{x}_o)|} \tag{2.27}$$

Now let r be a radius of this hypersphere. The following linear problem is created:

$$\begin{aligned} &\text{Maximise:} && r \\ &\text{Subject to:} && \nabla F(\mathbf{x}_o).\mathbf{s} + |\nabla F(\mathbf{x}_o)|r \leq 0 \\ & && \nabla g_j(\mathbf{x}_o).\mathbf{s} + |\nabla g_j(\mathbf{x}_o)|r \leq 0 \end{aligned} \tag{2.28}$$

$$x_j \geq -g_j \qquad\qquad j = 1, \cdots, m$$

This problem can be solved by the Simplex method.

2.4.4 Sequential Quadratic Programming Method

This method is also known as the Projected Lagrangian Method. In this method the search direction is determined by solving a quadratic programming problem which is a quadratic approximation to the Lagrangian of the objective function and a linear approximation to the inequality constraints:

$$\begin{aligned} \text{Minimize:} \quad & Q(\mathbf{s}) = F(\mathbf{x}) + \nabla F(\mathbf{x}).\mathbf{s} + \tfrac{1}{2}\mathbf{s}^T.\mathbf{B}_k.\mathbf{s} \\ \text{Subject to:} \quad & \nabla g_j(\mathbf{x}).\mathbf{s} + g_j(\mathbf{x}) \leq 0, \qquad j = 1, \ldots, m \end{aligned} \tag{2.29}$$

where $\mathbf{B}_k$ is a positive definite approximation to the Hessian of the Lagrangian function. Initially $\mathbf{B}_k$ is taken as the identity matrix and it is updated at every iteration; Powell [80] recommends the BFSG variable metric formula (Section 2.5.4) as an update procedure.

Having defined the search direction s, the optimum design in this direction is found by using the exterior penalty method with another approximate Lagrangian function:

$$\text{Minimize:} \quad \Phi = F(\mathbf{x}) + \sum_{j=1}^{m} u_j \ \text{MAX}[0, g_j(\mathbf{x})] \tag{2.30}$$

where

$$\begin{aligned} \mathbf{x}_q &= \mathbf{x}_{q-1} + \alpha \mathbf{s} \\ u_j &= |\lambda_j| \qquad\qquad j = 1, \ldots, m \quad \text{first iteration} \\ u_j &= \text{MAX}\left[|\lambda_j|, \tfrac{1}{2}\left(u'_j + |\lambda_j|\right)\right] \qquad j = 1, \ldots, m \quad \text{subsequent iteration} \end{aligned}$$

and $u'_j = u_j$ from the previous iteration. Here, λ_j are the Lagrange multipliers calculated in the quadratic programming problem.

2.5 Definition of the Search Direction

Once the strategy for applying the constraints has been chosen the next step is to determine the search direction. In this step a search direction, s, is calculated along which the minimum

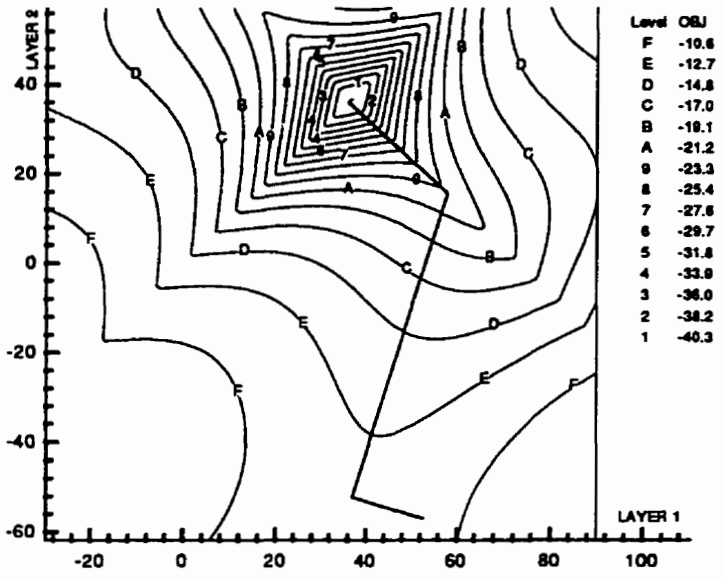

Figure 2.10: The Steepest Descent Method

of the objective function is sought. When this direction is defined, the optimization problem of N variables becomes a one variable problem, *a one-dimensional line search*:

$$\mathbf{x}_{min} = \mathbf{x}_o + \alpha^* \mathbf{s} \tag{2.31}$$

where α is a variable of the new problem.

2.5.1 The Steepest Descent Method

This approach was first proposed by Cauchy [14] for solving a system of linear equations. This method uses the negative gradient of the function as the search direction, $\mathbf{s} = -\nabla F$. This method was very popular in the mid 1950s. However, since then, it has lost favour as it can be very slow for functions with large differences in slopes, (Figure 2.10).

2.5.2 The Conjugate Direction Method

The convergence rate of the optimization process can be improved considerably with a simple modification to the steepest descent method (Figure 2.11). The conjugate direction method picks directions that are **Q**-conjugate to the previous ones, where **Q** is the Hessian of the function [27]. Its algorithm begins by first minimizing F along the steepest descent direction, $s_o = -\nabla F$. Then, the next directions are chosen to be **Q**-conjugates.

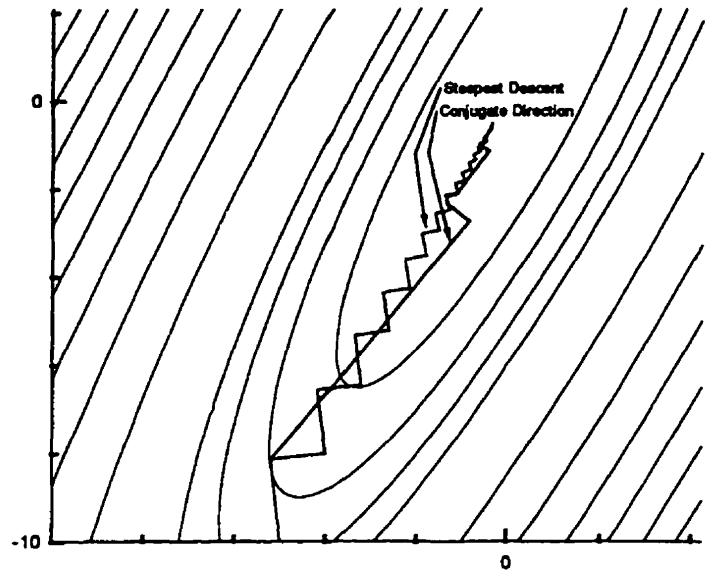

Figure 2.11: Steepest Descent and Conjugate Direction Comparison.

$$\mathbf{s}_{q+1} = -\nabla F_{q+1} + \beta \mathbf{s}_q \tag{2.32}$$

where

$$\beta = \frac{|\nabla F_{q+1}|^2}{|\nabla F_q|^2}$$

Powell's theorem on conjugate direction for quadratic functions says that this method will converge in N or fewer iterations, where N is the order of the function. For non quadratic functions the Hessian is not a constant matrix and the conjugacy of the direction loses its meaning. So the method is not guaranteed to converge in N iterations and it is necessary to restart the process after every N steps. The method has two main advantages: it is easy to implement and requires little computer storage.

2.5.3 Newton's Method

This method makes explicit use of the second derivatives; therefore it is refered to as a second-order method. It is based on a second-order Taylor's series expansion of the objective function. That is, consider the expansion of F up to the quadratic terms about some

reference state $\mathbf{x}_q$:

$$F(\mathbf{x}) \simeq F(\mathbf{x}_q) + \nabla F(\mathbf{x}_q).\delta\mathbf{x} + \frac{1}{2}\delta\mathbf{x}^t\mathbf{Q}\delta\mathbf{x} \tag{2.33}$$

where

$$\delta\mathbf{x} = \mathbf{x}_{q+1} - \mathbf{x}_q$$

A stationary value of this expansion, is obtained from the requirement:

$$\delta\mathbf{x} = -\mathbf{Q}^{-1}(\delta\mathbf{x}_q)\nabla F(\mathbf{x}_q) \tag{2.34}$$

or

$$\mathbf{x}_{q+1} = \mathbf{x}_q - \mathbf{Q}^{-1}(\mathbf{x}_q)\nabla F(\mathbf{x}_q) \tag{2.35}$$

The advantage of Newton's method is the fact that it has a quadratic rate of convergence. However, it presents two serious disadvantages: the need to evaluate the Hessian matrix, $\mathbf{Q}$, and to invert it. Both calculations are very numerically intensive.

2.5.4 Variable Metric Methods

In these methods the search direction is defined by: $\mathbf{s}_q = -\mathbf{H}\nabla F(\mathbf{x}_q)$. $\mathbf{H}$ is a metric matrix that approximates the inverse of the Hessian matrix during the optimization process. Therefore these methods have characteristics of convergence similar to Newton's method. During this process $\mathbf{H}$ must maintain its symmetric and positive definiteness properties and satisfy the following equation [38]:

$$\mathbf{H}_{q+1}\mathbf{y}_q = \mathbf{p}_q \tag{2.36}$$

where

$$\mathbf{p}_q = \mathbf{x}_q - \mathbf{x}_{q-1}$$
$$\mathbf{y}_q = \nabla F(\mathbf{x}_q) - \nabla F(\mathbf{x}_{q-1})$$

Assuming at the beginning $\mathbf{H} = \mathbf{I}$, at the end of each iteration the new $\mathbf{H}$ can be calculated from [108]:

$$\mathbf{H}_{q+1} = \mathbf{H}_q + \mathbf{D}_q \tag{2.37}$$

where

$$\mathbf{D}_q = \frac{\sigma + \theta\tau}{\sigma^2}\mathbf{p}\mathbf{p}^t + \frac{\theta - 1}{\tau}\mathbf{H}_q\mathbf{y}(\mathbf{H}_q\mathbf{y})^t - \frac{\theta}{\sigma}[\mathbf{H}_q\mathbf{y}\mathbf{p}^t + \mathbf{p}(\mathbf{H}_q\mathbf{y})^t]$$

and

$$\sigma = \mathbf{p}.\mathbf{y}$$

$$\tau = \mathbf{y}^t\mathbf{H}_q\mathbf{y}$$

The two most used variable metric methods are Davidon-Fletcher-Powell (DFP) [20,26], $\theta = 0$, and Broydon-Fletcher-Goldfarb-Shanno (BFGS) [10,28,33,96], $\theta = 1$. Studies have shown that the DFP method works quite well, but its performance deteriorates when the accuracy of the line search decreases [67]. In a few cases it breaks down because $\mathbf{H}$ becomes singular [38]. Numerical experiments have showed that BFGS is the best among all known variable metric algorithms [21].

2.5.5 The Method of Feasible Directions

A feasible direction is a search direction such that at least a small step can be taken along it without leaving the feasible domain. In this method, a feasible direction, $\mathbf{s}$, that decreases the objective function is sought. That is $\mathbf{s}^t\nabla F < 0$.

To select this direction two criteria must be satisfied: first, the objective function should be reduced as quickly as possible; second, the constraint boundary should be avoided as much as possible. The problem can be specified as (Figure 2.12):

$$\begin{aligned} &\text{Maximise:} && \beta \\ &\text{Subject to:} && \nabla F(\mathbf{x}).\mathbf{s} + \beta \leq 0 \\ & && \nabla g_j(\mathbf{x}).\mathbf{s} + \theta_j\beta \leq 0 \quad j \in J \\ & && |\mathbf{s}| \leq 1 \end{aligned} \tag{2.38}$$

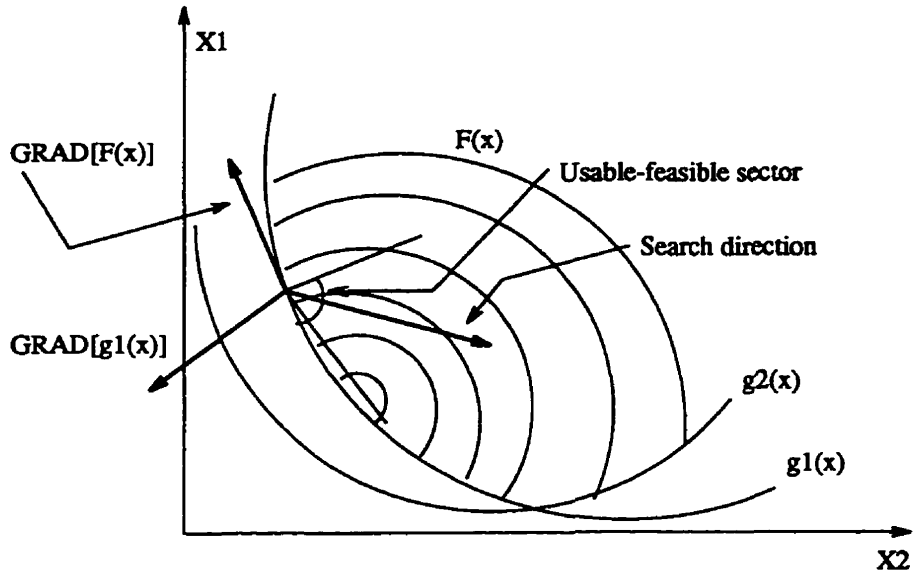

Figure 2.12: The Method of Feasible Directions

where

$\theta_j -$		*push-off factor*
	$\theta = 0,$ s	is tangent to the constraint boundary
	$\theta \to \infty,$ s	is tangent to the line of constant objective function
	$\theta = 1,$ s	roughly bisects the angle between the line of constant objective function and the constraint boundary
$J -$		set of active constraints

Vanderplaats and Moses [106] found that the best value for θ is given by:

$$\theta_j = \left[1 - \frac{g_j(\mathbf{x})}{\varepsilon}\right]^2 \theta_o \tag{2.39}$$

and usually $\theta_o = 1$.

One difficulty of this method is defining when a constraint is active. Vanderplaats [108] suggests that a constraint should be considered activated if $g_j(\bar{x}) \geq \varepsilon$, where $\varepsilon = -0.1$ at the beginning and is reduced to -0.001 near the end of the search process.

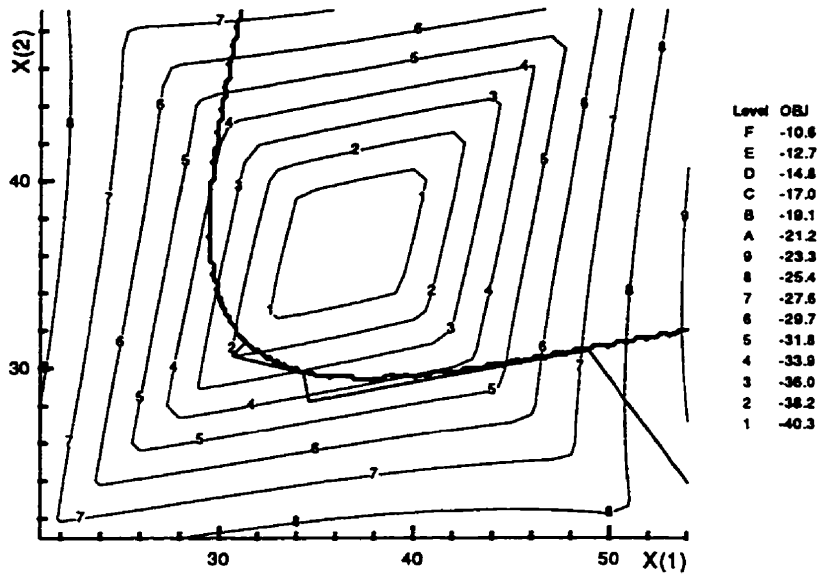

Figure 2.13: The Gradient Projection Method

2.5.6 The Gradient Projection Method

This method defines the search direction, $\mathbf{s}$, as the projection of $-\nabla F(\mathbf{x}_q)$ into the subspace tangent to the active constraints [92]. Let $\mathbf{N}$ denote the matrix composed of the gradients of active constraints at $\mathbf{x}_q$,

$$\mathbf{N} = [\nabla g_1(\mathbf{x}_q), ..., \nabla g_j(\mathbf{x}_q)] \tag{2.40}$$

where j is the number of active constraints. Then, $\mathbf{s}$ can be calculated as:

$$\mathbf{s} = -\mathbf{P}\nabla F \tag{2.41}$$

where $\mathbf{P}$ is the *orthogonal projection operator*, given by,

$$\mathbf{P} = \{\mathbf{I} - \mathbf{N}(\mathbf{N}^T\mathbf{N})^{-1}\mathbf{N}^T\} \tag{2.42}$$

If during the search for the minimum along $\mathbf{s}$, the design variable vector, $\mathbf{x}$, moves away from the constraint boundary, the process continues as the Steepest Descent Method, $\mathbf{s} = -\nabla F$, Figure 2.13.

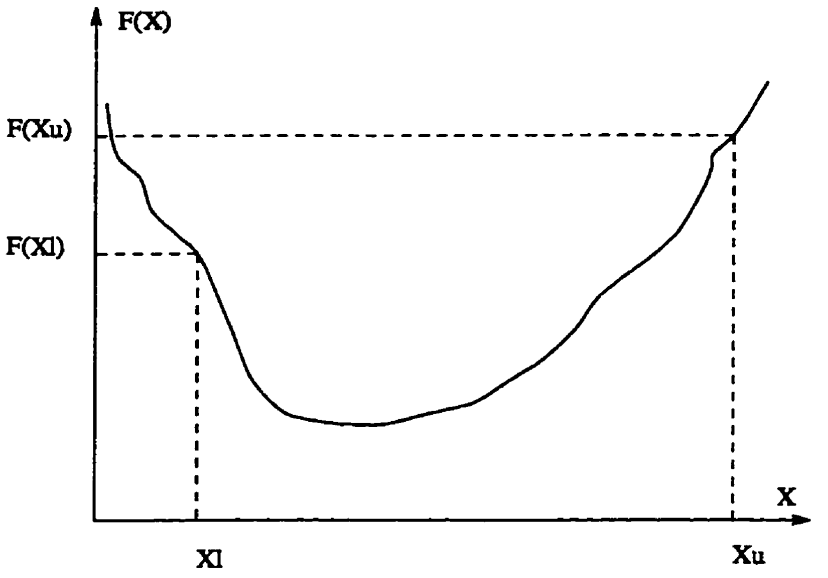

Figure 2.14: The Bracketing Method

2.6 One Directional Search

Once the search direction has been determined the minimum in that direction is found. In this step a one-dimensional line search is executed. It seeks the magnitude of a single scalar, α^*, which is the distance to be travelled in the given direction, s, from the initial design, $\mathbf{x}_o$, to the optimal design, $\mathbf{x}_{min}$, in that direction.

2.6.1 The Bracketing Method

In this method, two points (x_l, F_l) and (x_u, F_u) that bracket the minimum of the objective function, F (Figure 2.14) are sought. Consider F to be an unimodal function of the variable x. Then choose (x_l, F_l) and (x_1, F_1), so that x_l is the lower limit of the range in which the function is defined. If $F_1 \geq F_l$ and the function has a negative slope at x_l, then x_1 is an upper bound and the solution is complete. If not, choose another point x_2 greater than x_1. If $F_2 > F_1$ the solution is complete. Otherwise, x_1 is a new lower bound and the process is repeated. This process is continued until: F_{i+1} is large than F_i, which implies the solution is complete; or x_{i+1} is greater than upper limit of the range which means there is an unbound solution [108].

2.6.2 The Golden Section Method

This method is a popular line search technique for three main reasons. First, the objective function, F, does not need to have continuous derivatives. Second, if F is assumed to be unimodal, the rate of convergence is known. Third, it is easily programmed. However, this method requires many function evaluations.

In order to describe this algorithm, first consider F to be an unimodal function of the variable x, and choose (x_l, F_l) and (x_u, F_u) to bracket the minimum of F (Figure 2.15). Now, two other points (x_1, F_1) and (x_2, F_2) between x_l and x_u are chosen, such that $x_1 < x_2$. If it is assumed that F_1 is greater than F_2, then x_1 becomes the new lower bound and with x_u forms a new set of bounds. Again, choose another point (x_3, F_3) which is compared to F_2 and the process is repeat as before. This process is continued until the bounds are narrowed to a desired value.

The equations for choosing the interior points are:

$$x_1 = (1 - \tau)x_l + \tau x_u \tag{2.43}$$

$$x_2 = \tau x_l + (1 - \tau)x_u \tag{2.44}$$

where

$$\tau = \frac{3 - \sqrt{5}}{2}$$

2.6.3 Polynomial Approximation

This method consists of approximating the objective function with a polynomial whose minimum is easily determined. First, several values of the objective function are calculated. Then, a polynomial is fit to these values (Figure 2.16) and the minimum of the polynomial is determined. To check if this point is close to the true minimum, the values of the function and the polynomial at this point are compared. If the difference between this two values is not small the process is repeated by choosing other points around the point determined by the previous interpolation. This method requires few function evaluations, but the accuracy of the results cannot be guaranteed.

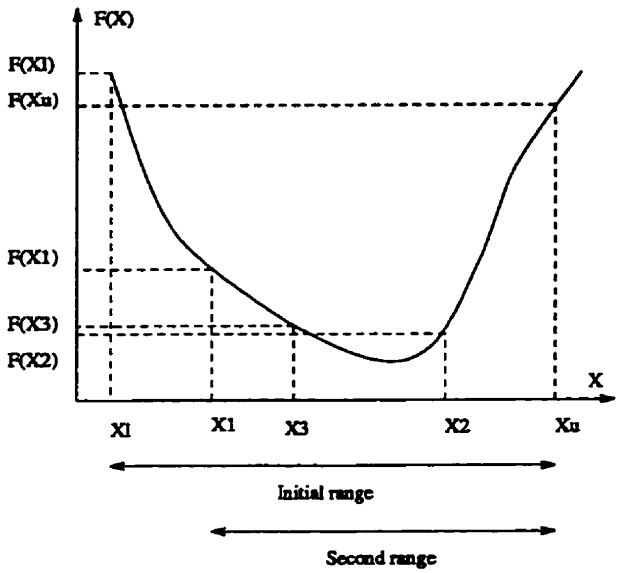

Figure 2.15: The Golden Section Method

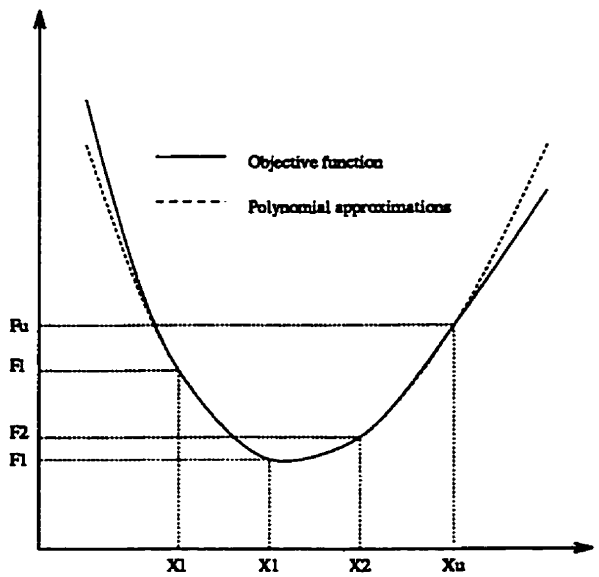

Figure 2.16: Polynomial Approximation

2.7 OPREDE

It is common knowledge that there is no single numerical method capable of solving all structural optimization problems. Because of this, OPREDE (Optimization PRogram for Engineering DEsign) was developed as part of this work. This is a general-purpose optimization program for engineering design. This program offers a wide variety of optimization algorithms for nonlinear constrained (or unconstrained) function minimization. It is based on ADS-1 (Automated Design Synthesis), a code developed by Vanderplaats [109]. It incorporates several optimization methods, so that one could decide which method works best for a particular class of problem, based on past experience or trial and error. This program includes the most frequently used numerical methods in structural optimization. The methods available in this package are:

- Strategy for considering the constraints
  - Exterior Penalty Function
  - Interior Penalty Function
  - Extended Interior Penalty Function
  - Augmented Lagrange Multiplier Method
  - Sequential Linear Programming
  - The Method of Centres
- Definition of the search direction
  - The Steepest Descent
  - The Conjugate Direction Method
  - Variable Metric Methods (DFP & BFGS)
  - The Method of Feasible Directions
  - The Gradient Projection Method
- One directional search
  - The Bracketing Method

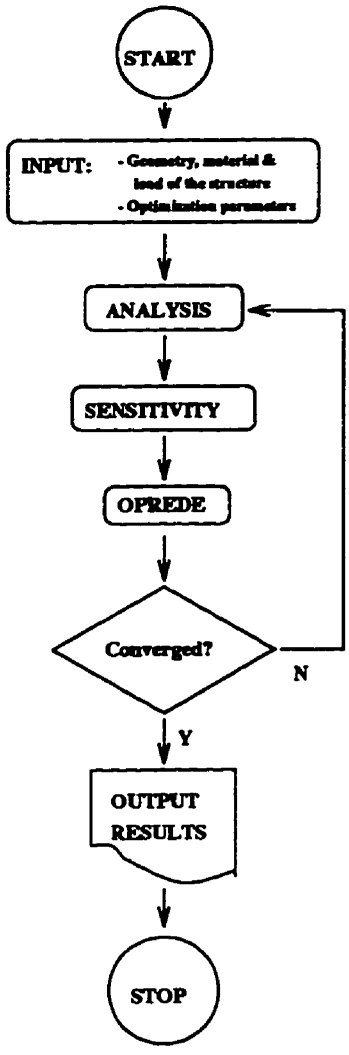

Figure 2.17: Optimization Code Flow Chart

- The Golden Section Method
- Polynomial approximation

Figure 2.17 is a schematic diagram of the coupling between both this optimization package and the analysis programs described in the next chapter.

Chapter 3

Equations of a Composite Sandwich Plate

The objective of this work is to study the optimization of heterogeneous facesheets in sandwich plates; the result of the analysis is the optimal distribution of the non-uniform material density in the facesheets. In order to do so, it is necessary to solve bending and vibration problems for these plates. Due to the fact that during the optimization process the structure is allowed to have spatially varying stiffness properties, it is not possible to obtain a closed form solution. Thus, numerical methods must be used.

Among the numerical methods available, two are most frequently applied in optimization solutions of composite structures: the Finite Element Method - FEM [13, 17, 22, 23, 50, 68, 85, 97, 98] and the Ritz Method [1, 64, 103, 104] . The Ritz Method was used in this work because it generates a solution that demands less computer time. This is important because in the optimization process the equilibrium and dynamic equations have to be solved many times. However, it is known that the FEM gives more flexibility to solve structures with different shapes and boundary conditions.

This chapter outlines the derivation of the equations to solve the bending and vibration problems for anisotropic sandwich plates, using the Ritz Method [95]. Reissner sandwich plate theory was adopted [87]. The following assumptions were used: the facesheets are identical anisotropic membranes that can have variable elastic properties and thickness; the core is a homogeneous orthotropic slab much thicker than the facesheets, and therefore it can be assumed that the in-plane stresses in the facesheets are uniform over the thickness

of the facesheet; the core resists only transverse shear stresses; the in-plane displacement varies linearly through the thickness; the normal displacement is constant with respect to the thickness coordinate; planes originally normal to the mid-plane remains straight on deformation (no warping), but not necessarily normal to the mid-plane after deformation (Reissner-Mindlin Plate Theory [88]); middle-surface stretching is neglected as the plate is assumed symmetric about the plate middle-surface; the materials are assumed to be linear elastic; and displacements are small compared to the dimensions of the plate.

3.1 Bending Equations

Considering a three-dimensional solid, the strain energy of deformation is expressed as follows:

$$U = \frac{1}{2}\int_V \sigma^T \epsilon \, dV \tag{3.1}$$

where σ is the stress vector; ϵ is the strain vector and V is the volume of the plate. The potential energy of the external load is given by

$$W = \int_V \mathbf{B}^T \mathbf{u} \, dV + \int_{S_1} \mathbf{T}^T \mathbf{u} \, dS \tag{3.2}$$

where $\mathbf{B}$ is the body force distribution throughout the volume; $\mathbf{u}$ is the displacement vector; and $\mathbf{T}$ are the surface tractions over part of the boundary, S_1, of the plate. Over the remaining part of the boundary, S_2, the displacement field is prescribed.

3.1.1 The Strain Energy

Based on the above assumptions for a sandwich plate with identical anisotropic facesheets, the displacement fields (functions of x, y and z) are assumed in the form (Reissner-Mindlin Plate Theory [88]):

$$\mathbf{u} = \begin{bmatrix} \overline{u}(x,y,z;t) \\ \overline{v}(x,y,z;t) \\ \overline{w}(x,y,z;t) \end{bmatrix} = \begin{bmatrix} z\,\zeta(x,y;t) \\ z\,\xi(x,y;t) \\ w(x,y;t) \end{bmatrix} \tag{3.3}$$

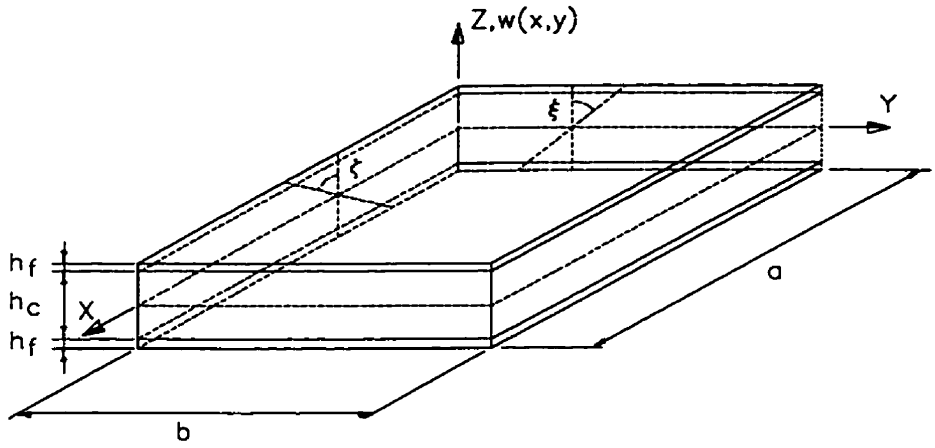

Figure 3.1: Displacements, Rotations and Dimensions of a Sandwich Plate.

In the above, w is the middle-surface displacement in the z direction, while ζ and ξ are rotation-like variables in the x and y directions, respectively. Figure 3.1 gives a graphical description of the plate and the variables used.

The strain field is derived directly from the displacements and is given by:

$$\begin{aligned}
\epsilon_x &= \frac{\partial \overline{u}}{\partial x} &&= z\frac{\partial \zeta}{\partial x} \\
\epsilon_y &= \frac{\partial \overline{v}}{\partial y} &&= z\frac{\partial \xi}{\partial y} \\
\gamma_{xy} &= \frac{\partial \overline{u}}{\partial y} + \frac{\partial \overline{v}}{\partial x} &&= z\left(\frac{\partial \zeta}{\partial y} + \frac{\partial \xi}{\partial x}\right) \\
\epsilon_z &= \frac{\partial \overline{w}}{\partial z} &&\equiv 0 \\
\gamma_{xz} &= \frac{\partial \overline{u}}{\partial z} + \frac{\partial \overline{w}}{\partial x} &&= \zeta + \frac{\partial w}{\partial x} \\
\gamma_{yz} &= \frac{\partial \overline{v}}{\partial z} + \frac{\partial \overline{w}}{\partial y} &&= \xi + \frac{\partial w}{\partial y}.
\end{aligned} \tag{3.4}$$

The strain energy is obtained by substituting Equations 3.4 into Equation 3.1 and using

the stress-strain relations [44]:

$$\begin{Bmatrix} \sigma_x \\ \sigma_y \\ \tau_{yz} \\ \tau_{zx} \\ \tau_{xy} \end{Bmatrix}_k = \begin{bmatrix} \overline{Q}_{11} & \overline{Q}_{12} & 0 & 0 & \overline{Q}_{16} \\ \overline{Q}_{12} & \overline{Q}_{22} & 0 & 0 & \overline{Q}_{26} \\ 0 & 0 & \overline{Q}_{44} & \overline{Q}_{45} & 0 \\ 0 & 0 & \overline{Q}_{45} & \overline{Q}_{55} & 0 \\ \overline{Q}_{16} & \overline{Q}_{26} & 0 & 0 & \overline{Q}_{66} \end{bmatrix}_k \begin{Bmatrix} \epsilon_x \\ \epsilon_y \\ \gamma_{yz} \\ \gamma_{zx} \\ \gamma_{xy} \end{Bmatrix}_k \tag{3.5}$$

where the subscript k denotes the k^{th} ply and $\overline{Q}_{ij}$ are the transformed reduced stiffnesses. After integrating through the thickness, the strain energy becomes

$$U = \int_A \frac{1}{2} \left[\begin{array}{c|c} \kappa^T & \gamma_z^T \end{array} \right] \left[\begin{array}{c|c} \mathbf{D} & \mathbf{0} \\ - + - & \\ \mathbf{0} & \overline{\mathbf{A}} \end{array} \right] \left\{ \begin{array}{c} \kappa \\ -- \\ \gamma_z \end{array} \right\} dA \tag{3.6}$$

where A is the area of the plate. The middle-surface curvature vector κ and the transverse shear strain vector γ are as follows:

$$\kappa^T = \left\{ \frac{\partial \zeta}{\partial x} \; ; \; \frac{\partial \xi}{\partial y} \; ; \; \frac{\partial \zeta}{\partial y} + \frac{\partial \xi}{\partial x} \right\}$$
$$\gamma_z^T = \left\{ \zeta + \frac{\partial w}{\partial x} \; ; \; \xi + \frac{\partial w}{\partial y} \right\}$$

The plate stiffness components are defined by

$$D_{ij} = \frac{1}{3} \sum_{k=1}^{N} (\overline{Q}_{ij})_k (z_k^3 - z_{k-1}^3); \quad i,j = 1,2,6$$
$$\overline{A}_{ij} = \sum_{k=1}^{N} (\overline{Q}_{ij})_k (z_k - z_{k-1}); \quad i,j = 4,5$$

where z_{k-1} and z_k are the lower and upper coordinates of the k^{th} layer relative to the plate middle-surface and N is the number of layers.

The calculation of the through–thickness shear stiffness of the sandwich beam based on Reissner–Mindlin theory must be done with care. The through–thickness shear stiffness of the facesheets is much greater than that of the core and the facesheets are much thinner than the core; thus the shear deformation is dominated by the shear of the core. However, within Reissner–Mindlin theory the through–thickness shear strain is constant and thus if the contribution of the stiffness from the facesheets is included in the calculation the

facesheet stiffness will dominate and the plate through–thickness shear stiffness will be too large. Thus the through–thickness shear stiffness is based only on the core stiffness. This effectively allows different shear strains in the facesheets and the core with the assumption that the facesheet shear stiffness is so large that the only contribution to the total shear strain comes from the core.

3.1.2 The Work

The only load considered here is a quasi-static load normal to the plate that represents the load generated on the structure when it is subjected to an acceleration in that direction (d'Alembert's principle [53, page 235]). It is assumed that the plate is being modelled during the launch of a satellite. Therefore, the work term W can be written as

$$W = \sum_{k=1}^{N} \int_V \rho_k a_{c_z} w dV \tag{3.7}$$

where ρ_k is the density of k^{th} layer and a_{c_z} is the acceleration in the z-direction, to which the structure is exposed during launch.

3.1.3 Solution Procedure

The displacement w and rotations ζ and ξ are approximated by:

$$\begin{aligned} w &= \sum_{m=1}^{NT}\sum_{n=1}^{NT} c_{mn}\varphi_{cm}(x)\varphi_{cn}(y) \\ \zeta &= \sum_{m=1}^{NT}\sum_{n=1}^{NT} d_{mn}\varphi_{dm}(x)\varphi_{dn}(y) \\ \xi &= \sum_{m=1}^{NT}\sum_{n=1}^{NT} e_{mn}\varphi_{em}(x)\varphi_{en}(y). \end{aligned} \tag{3.8}$$

where NT is the number of terms in each summation and c_{mn}, d_{mn} and e_{mn} are the unknown coefficients to be determined. Also, $\varphi_{cm}(x)$, $\varphi_{cn}(y)$, $\varphi_{dm}(x)$, $\varphi_{dn}(y)$, $\varphi_{em}(x)$ and $\varphi_{en}(y)$ are basis functions which are specified according to the problem being considered. Making use of these expressions, the strain energy becomes

$$U = \frac{1}{2}\int_A \left\{ \overline{A}_{55} \left[\sum_{m=1}^{NT}\sum_{n=1}^{NT} (d_{mn}\varphi_{dm}\varphi_{dn} + c_{mn}\varphi'_{cm}\varphi_{cn}) \right]^2 \right.$$

$$
\begin{aligned}
&+h_c\overline{A}_{44}\left[\sum_{m=1}^{NT}\sum_{n=1}^{NT}\left(e_{mn}\varphi_{em}\varphi_{en}+c_{mn}\varphi_{cm}\varphi'_{cn}\right)\right]^2 \\
&+D_{11}\left[\sum_{m=1}^{NT}\sum_{n=1}^{NT}d_{mn}\varphi'_{dm}\varphi_{dn}\right]^2+D_{22}\left[\sum_{m=1}^{NT}\sum_{n=1}^{NT}e_{mn}\varphi_{em}\varphi'_{en}\right]^2 \\
&+2D_{12}\left[\sum_{m=1}^{NT}\sum_{n=1}^{NT}d_{mn}\varphi'_{dm}\varphi_{dn}\right]\left[\sum_{m=1}^{NT}\sum_{n=1}^{NT}e_{mn}\varphi_{em}\varphi'_{en}\right] \\
&+2D_{16}\left[\sum_{m=1}^{NT}\sum_{n=1}^{NT}d_{mn}\varphi'_{dm}\varphi_{dn}\right]\left[\sum_{m=1}^{NT}\sum_{n=1}^{NT}\left(d_{mn}\varphi_{dm}\varphi'_{dn}+e_{mn}\varphi'_{em}\varphi_{en}\right)\right] \\
&+2D_{26}\left[\sum_{m=1}^{NT}\sum_{n=1}^{NT}\left(d_{mn}\varphi_{dm}\varphi'_{dn}+e_{mn}\varphi'_{em}\varphi_{en}\right)\right]\left[\sum_{m=1}^{NT}\sum_{n=1}^{NT}e_{mn}\varphi_{em}\varphi'_{en}\right] \\
&+D_{66}\left[\sum_{m=1}^{NT}\sum_{n=1}^{NT}\left(d_{mn}\varphi_{dm}\varphi'_{dn}+e_{mn}\varphi'_{em}\varphi_{en}\right)\right]^2\Bigg\}\,dA \qquad (3.9)
\end{aligned}
$$

$$
= \frac{1}{2}\left[\mathbf{c}^T\ \mathbf{d}^T\ \mathbf{e}^T\right]\mathbf{K}\begin{Bmatrix}\mathbf{c}\\ \mathbf{d}\\ \mathbf{e}\end{Bmatrix}
$$

where φ' indicates differentiation with respect to either x or y as is appropriate. Also, h_c is the core thickness and $\mathbf{K}$ is the stiffness matrix written as

$$
\mathbf{K} = \begin{bmatrix}\mathbf{U_{33}} & \mathbf{U_{34}} & \mathbf{U_{35}}\\ \mathbf{U_{34}}^T & \mathbf{U_{44}} & \mathbf{U_{45}}\\ \mathbf{U_{35}}^T & \mathbf{U_{45}}^T & \mathbf{U_{55}}\end{bmatrix} \qquad (3.10)
$$

and

$$
\begin{aligned}
U_{33}(i,j) &= h_c\int_A \left(\overline{A}_{55}\varphi'_{ck}\varphi_{cl}\varphi'_{cm}\varphi_{cn}\right.\\
&\qquad \left.+\overline{A}_{44}\varphi_{ck}\varphi'_{cl}\varphi_{cm}\varphi'_{cn}\right)dA\\
U_{34}(i,j) &= h_c\int_A \left(\overline{A}_{55}\varphi_{dk}\varphi_{dl}\varphi'_{cm}\varphi_{cn}\right)dA\\
U_{35}(i,j) &= h_c\int_A \left(\overline{A}_{44}\varphi_{ek}\varphi_{el}\varphi_{cm}\varphi'_{cn}\right)dA
\end{aligned}
$$

$$
\begin{aligned}
U_{44}(i,j) &= \int_A [h_c \overline{A}_{55} \varphi_{dk} \varphi_{dl} \varphi_{dm} \varphi_{dn} \\
&\quad + D_{11} \varphi'_{dk} \varphi_{dl} \varphi'_{dm} \varphi_{dn} \\
&\quad + D_{16} (\varphi_{dk} \varphi'_{dl} \varphi'_{dm} \varphi_{dn} \\
&\quad + \varphi'_{dk} \varphi_{dl} \varphi_{dm} \varphi'_{dn}) \\
&\quad D_{66} \varphi_{dk} \varphi'_{dl} \varphi_{dm} \varphi'_{dn}] \, dA
\end{aligned}
$$

$$
\begin{aligned}
U_{45}(i,j) &= \int_A [D_{12} \varphi_{ek} \varphi'_{el} \varphi'_{dm} \varphi_{dn} \\
&\quad + D_{16} \varphi'_{ek} \varphi_{el} \varphi'_{dm} \varphi_{dn} \\
&\quad + D_{26} \varphi_{ek} \varphi'_{el} \varphi_{dm} \varphi'_{dn} \\
&\quad + D_{66} \varphi'_{ek} \varphi_{el} \varphi_{dm} \varphi'_{dn}] \, dA
\end{aligned}
$$

$$
\begin{aligned}
U_{55}(i,j) &= \int_A [h_c \overline{A}_{44} \varphi_{ek} \varphi_{el} \varphi_{em} \varphi_{en} \\
&\quad + D_{22} \varphi_{ek} \varphi'_{el} \varphi_{em} \varphi'_{en} \\
&\quad + D_{26} (\varphi_{ek} \varphi'_{el} \varphi'_{em} \varphi_{en} \\
&\quad + \varphi'_{ek} \varphi_{el} \varphi_{em} \varphi'_{en}) \\
&\quad + D_{66} \varphi'_{ek} \varphi_{el} \varphi'_{em} \varphi_{en}] \, dA
\end{aligned}
$$

for $i = (m-1) * NT + n$ and $j = (k-1) * NT + l$.

Now, using the trial solutions (Equation 3.8) in Equation 3.7, the work becomes

$$
\begin{aligned}
W &= \sum_{k=1}^{N} \int_V \rho_k a_{c_z} \left(\sum_{m=1}^{NT} \sum_{n=1}^{NT} c_{mn} \varphi_{cm} \varphi_{cn} \right) dV \\
&= \mathbf{F}^T \left\{ \begin{array}{c} \mathbf{c} \\ \mathbf{d} \\ \mathbf{e} \end{array} \right\}
\end{aligned}
\tag{3.11}
$$

where $\mathbf{F}$ is the force vector and can be written as

$$
\mathbf{F} = \left\{ \begin{array}{c} V_3 \\ V_4 \\ V_5 \end{array} \right\}
$$

and

$$\begin{aligned} V_3 &= \sum_{k=1}^{N} \int_V \rho_k a_z \varphi_{cm} \varphi_{cn} dV \\ V_4 &= 0 \\ V_5 &= 0 \end{aligned}$$

The total potential energy for the problem is

$$\Pi = \mathbf{U} - \mathbf{W}. \tag{3.12}$$

Seeking a stationary value of Π with respect to c_{mn}, d_{mn} and e_{mn} yields the following set of equilibrium equations

$$\mathbf{K} \left\{ \begin{array}{c} \mathbf{c} \\ \mathbf{d} \\ \mathbf{e} \end{array} \right\} = \mathbf{F} \tag{3.13}$$

which gives the solution for the unknown coefficient vectors **c**, **d** and **e** of the bending problem.

3.2 Vibration Equations

The equations of motion are obtained using Lagrange's equations:

$$\frac{d}{dt}\left(\frac{\partial L}{\partial \dot{q}_i}\right) - \frac{\partial L}{\partial q_i} = 0 \qquad\qquad i = 1, 2, \cdots, n \tag{3.14}$$

where the Lagrangian L is given by $L \equiv T - U$, T is the kinetic energy, U is the strain energy and q_i are the generalised coordinates. The over dot on q_i implies differentiation with regard to time.

3.2.1 The Kinetic Energy

The kinetic energy expression is

$$T = \frac{1}{2} \int_V \rho \, \dot{\mathbf{u}}^T \dot{\mathbf{u}} \, dV \tag{3.15}$$

For a composite sandwich plate, the kinetic energy is obtained by differentiating Equations 3.3 with respect to time and then substituting into Equation 3.15 and integrating with respect to z:

$$T = \sum_{k=1}^{N} \left\{ \frac{1}{2} \int_A \rho_k \left[\dot{w}_o^2 (z_k - z_{k-1}) + \left(\dot{\zeta}^2 + \dot{\xi}^2 \right) \frac{\left(z_k^3 - z_{k-1}^3 \right)}{3} \right] dA \right\}. \tag{3.16}$$

3.2.2 Solution Procedure

Since the free vibration problem is periodic, the coefficients of the trial functions can be written in the form

$$\begin{aligned} c_{mn}(t) &= c_{mn} e^{i\Omega t} \\ d_{mn}(t) &= d_{mn} e^{i\Omega t} \\ e_{mn}(t) &= e_{mn} e^{i\Omega t} \end{aligned} \tag{3.17}$$

where c_{mn}, d_{mn} and e_{mn} are constants to be determined and Ω is the frequency of vibration.

When Equations 3.8 are differentiated with respect to time and substituted into Equation 3.16, the kinetic energy becomes

$$\begin{aligned} T &= \sum_{k=1}^{N} \left\{ \frac{1}{2} \int_A \rho_k \left\{ (h_{i+1} - h_i) \left(\sum_{m=1}^{NT} \sum_{n=1}^{NT} \dot{c}_{mn} \varphi_{cm} \varphi_{cn} \right)^2 \right. \right. \\ &\quad + \frac{(h_{i+1}^3 - h_i^3)}{3} \left[\left(\sum_{m=1}^{NT} \sum_{n=1}^{NT} \dot{d}_{mn} \varphi_{dm} \varphi_{dn} \right)^2 \right. \\ &\quad \left. \left. \left. + \left(\sum_{m=1}^{NT} \sum_{n=1}^{NT} \dot{e}_{mn} \varphi_{em} \varphi_{en} \right)^2 \right] \right\} dA \right\} \\ &= \frac{1}{2} \left[\dot{\mathbf{c}}^T \; \dot{\mathbf{d}}^T \; \dot{\mathbf{e}}^T \right] \mathbf{M} \begin{Bmatrix} \dot{\mathbf{c}} \\ \dot{\mathbf{d}} \\ \dot{\mathbf{e}} \end{Bmatrix} \end{aligned} \tag{3.18}$$

where $\mathbf{M}$ is the mass matrix written as

$$\mathbf{M} = \begin{bmatrix} \mathbf{T}_{33} & \mathbf{0} & \mathbf{0} \\ \mathbf{0} & \mathbf{T}_{44} & \mathbf{0} \\ \mathbf{0} & \mathbf{0} & \mathbf{T}_{55} \end{bmatrix} \tag{3.19}$$

and the matrix $\mathbf{T_{33}}$, $\mathbf{T_{44}}$ and $\mathbf{T_{55}}$ are given by

$$
\begin{aligned}
T_{33}(i,j) &= \sum_{k=1}^{N} \rho_k (h_{i+1} - h_k) \int_A \varphi_{ck}\varphi_{cl}\varphi_{cm}\varphi_{cn}\, dA \\
T_{44}(i,j) &= \sum_{k=1}^{N} \rho_k \frac{(h_{k+1}^3 - h_k^3)}{3} \int_A \varphi_{dk}\varphi_{dl}\varphi_{dm}\varphi_{dn}\, dA \\
T_{55}(i,j) &= \sum_{k=1}^{N} \rho_k \frac{(h_{k+1}^3 - h_k^3)}{3} \int_A \varphi_{dk}\varphi_{dl}\varphi_{dm}\varphi_{dn}(y)\, dA
\end{aligned}
$$

The substitution of the strain (Equation 3.9) and kinetic energy (Equation 3.18) expressions into the Lagrange's Equation 3.14 and then using Equation 3.17 yields the following system of equations:

$$
\left(\mathbf{K} - \Omega^2 \mathbf{M}\right) \left\{ \begin{array}{c} c_{mn} \\ d_{mn} \\ e_{mn} \end{array} \right\} = \mathbf{0}, \tag{3.20}
$$

from which the natural frequencies Ω and mode shapes Ψ are determined.

3.3 Numerical Results

A FORTRAN code was written for two types of plate: a rectangular sandwich plate simply-supported on all four boundaries and a rectangular sandwich plate with all boundaries free. To verify the code, a series of problems were solved and the results compared with values available in literature.

3.3.1 Simply-Supported Sandwich Plate

For a simply-supported sandwich plate, the basis functions used to represent the displacement and rotations are

$$
\begin{aligned}
\varphi_{cm}(x) &= sin\left(\frac{m\pi x}{a}\right) & \varphi_{cn}(y) &= sin\left(\frac{n\pi y}{b}\right) \\
\varphi_{dm}(x) &= cos\left(\frac{m\pi x}{a}\right) & \varphi_{dn}(y) &= sin\left(\frac{n\pi y}{b}\right) \\
\varphi_{em}(x) &= sin\left(\frac{m\pi x}{a}\right) & \varphi_{en}(y) &= cos\left(\frac{n\pi y}{b}\right).
\end{aligned}
$$

Description	Dimension
a [m (in)]	1.83 (72.)
b [m (in)]	1.22 (48.)
h_f [mm (in)]	6.350 (0.25)
h_c [mm (in)]	0.406 (0.016)

Table 3.1: Dimensions of the Isotropic Sandwich Plate.

These functions are orthogonal, linearly independent, and satisfy the forced boundary conditions of a simply-supported rectangular plate:

$$w = 0 \quad \text{at} \quad x = 0 \text{ and } a$$

$$w = 0 \quad \text{at} \quad y = 0 \text{ and } b$$

These functions also satisfy the natural boundary condition if the plate is orthotropic.

A sandwich plate with isotropic facesheets will be considered initially. Tables 3.1 and 3.2 present the dimensions and the material properties of this plate, respectively. The mass and stiffness matrices are calculated numerically using Gauss-Legendre quadrature; this requires the determination of the appropriate number of integration points. Also, in order that these matrices be evaluated accurately the number of terms retained in the series must be selected. Both of the above were based on a meticulous evaluation of the first four natural frequencies of this plate. It is noted that for an isotropic plate only one term is necessary to determine the first natural frequency, since the modes are orthogonal. Table 3.3 illustrates the solution convergence.

From an analysis of Table 3.3, it is possible to conclude that with 3x3 terms in the series expansion and 9x9 integration points, the solution converges for the first four natural frequencies.

Considering the results in Table 3.3, it may be noted that for a fixed number of terms in the series the calculated natural frequency for a small number of integration points is less than the final converged solution which corresponds to a greater number of integration points. Furthermore, as the number of integration points is increased, the predicted results exhibit a sharp increase and then decrease asymptotically to the final converged result. It is known that the results converge to the exact solution from above, when using the Ritz

Property	Aluminium Sheet	Aluminium Honeycomb
E_{11} [GPa (10^6 psi)]	68.95 (10)	
ν_{12}	0.3	
G_{1z} [MPa (10^3 psi)]		134.4 (19.50)
G_{2z} [MPa (10^3 psi)]		51.71 (7.50)
ρ [kg/m^3 (10^{-5} lb sec^2/in)]	2767. (0.1)	121.79 (0.0044)

Table 3.2: Material Properties of the Isotropic Facesheet Sandwich Plate.

Number of Terms	Number of Points	1^{st} Nat. Frequency	2^{nd} Nat. Frequency	3^{rd} Nat. Frequency	4^{th} Nat. Frequency
2x2	4x 4	23.35	43.14	68.84	85.26
2x2	5x 5	23.33	44.94	70.50	92.02
2x2	6x 6	23.33	44.69	70.28	91.00
2x2	7x 7	23.33	44.71	70.30	91.08
2x2	8x 8	23.33	44.71	70.30	91.07
2x2	9x 9	23.33	44.71	70.30	91.07
3x3	4x 4	23.17	43.08	68.84	85.26
3x3	5x 5	23.33	44.94	70.50	75.42
3x3	6x 6	23.33	44.69	70.28	81.32
3x3	7x 7	23.33	44.71	70.30	79.80
3x3	8x 8	23.33	44.71	70.30	80.01
3x3	9x 9	23.33	44.71	70.30	79.99
3x3	10x10	23.33	44.71	70.30	79.99
4x4	4x 4	23.17	33.13	33.28	39.14
4x4	5x 5	23.33	43.92	63.52	75.42
4x4	6x 6	23.33	44.68	70.19	81.32
4x4	7x 7	23.33	44.71	70.30	79.80
4x4	8x 8	23.33	44.71	70.30	80.01
4x4	9x 9	23.33	44.71	70.30	79.99
4x4	10x10	23.33	44.71	70.30	79.99

Table 3.3: Convergence for Simply-Supported Isotropic Facesheet Sandwich Plate.

Vibration Mode	Raville & Ueng [86]		Present Study (Hz)
	Experimental Results (Hz)	Theoretical Results (Hz)	
1	—	23.	23.33
2	45.	45.	44.71
3	69.	71.	70.30
4	78.	80.	79.99

Table 3.4: Sandwich Plate with Isotropic Facesheets

Description	Dimension
a [m (in)]	1.27 (50.)
b [m (in)]	0.64 (25.)
h_f [mm (in)]	3.18 (0.125)
h_c [mm (in)]	2.54 (1.)

Table 3.5: Plate Dimensions: Isotropic Facesheets.

technique for the calculation of natural frequencies . The behaviour of these results is due to the fact that the number of integration points are initially insufficient to integrate the terms in the stiffness matrix accurately; this error is the source of the anomalous behaviour.

The converged solutions were then compared to experimental results presented by Raville and Ueng [86]. In their paper, the authors showed theoretical and experimental results for the natural frequencies of vibration of a simply supported sandwich plate with thin isotropic facings of equal or unequal thicknesses separated by an orthotropic core. For the theoretical results, they used the Ritz method by interpolating τ_{xz}, τ_{yz} and w. Table 3.4 shows close agreement between the results of the present study and those of Raville and Ueng.

The next step to verification of the code was the analysis of a sandwich plate with facesheets of laminated material. The dimensions and material properties of this plate are given in Table 3.5 and 3.6, respectively. The facesheets are a two layer laminate [-15^o, 15^o]. Table 3.7 presents how the solution converges when the number of series terms and integration points increase for this sandwich plate. For this problem, the solution converges for 3x3 terms in the series expansion and 10x10 integration points, respectively.

Property	Graphite Epoxy Fibre	Glass Fabric Honeycomb
E_{11} [GPa (10^6 psi)]	207. (30.)	
E_{22} [GPa (10^6 psi)]	5.17 (0.75)	
G_{12} [GPa (10^6 psi)]	5.17 (0.75)	
ν_{12}	0.25	
G_{z1} [MPa (10^3 psi)]		117. (17.)
G_{2z} [MPa (10^3 psi)]		241. (35.)
ρ [kg/m^3 (10^{-5} lb sec^2/in)]	1604. (0.15)	2354. (0.22)

Table 3.6: Material Properties of the Composite Sandwich Plate.

Next, the first four natural frequencies for cross-ply and angle-ply sandwich plates were calculated and compared with results presented by Ibrahim *et al.* [42] as shown in Tables 3.8 to 3.13. In this paper, they used the Modified Stiffness Method for the dynamic analysis of unbalanced anisotropic sandwich plates.

The analyses of these tables show that both formulations yield similar results. The values obtained in the present study are always less than the ones shown by Ibrahim *et al.*.

To verify the code for bending problems, the displacements and moments at the centre of an isotropic and a composite sandwich plate are determined and compared with results presented by Khatua & Cheung [47]. In this paper, elements were developed based on the finite element displacement method to analyse multi-layer sandwich beam and plate structures. The dimensions and material properties of the analysed plates are given in Tables 3.14 and 3.15, respectively. These plates are subjected to an uniform distributed load of 2435. N/m^2 (1. lb/in^2). Tables 3.16 and 3.17 show displacement and moment results respectively, given by the code using 3x3 terms in the series expansion and 10x10 integration points. The results are in close agreement with those presented by Khatua & Cheung.

3.3.2 Free-Free Sandwich Plate

For a free-free sandwich plate the trial functions used to represent the displacement and

Number of Terms	Number of Points	1^{st} Nat. Frequency	2^{nd} Nat. Frequency	3^{rd} Nat. Frequency	4^{th} Nat. Frequency
2x 2	3x 3	85.61	208.24	251.75	486.77
2x 2	4x 4	87.41	151.82	187.97	233.11
2x 2	5x 5	87.32	169.36	193.41	262.41
2x 2	6x 6	87.32	167.06	192.75	258.25
2x 2	7x 7	87.32	167.25	192.80	258.60
2x 2	8x 8	87.32	167.24	192.80	258.57
2x 2	9x 9	87.32	167.24	192.80	258.58
2x 2	10x10	87.32	167.24	192.80	258.58
3x 3	4x 4	85.95	151.30	187.37	233.11
3x 3	5x 5	87.30	169.36	192.61	193.38
3x 3	6x 6	87.32	167.06	192.75	258.25
3x 3	7x 7	87.32	167.25	192.80	249.97
3x 3	8x 8	87.32	167.24	192.80	252.53
3x 3	9x 9	87.32	167.24	192.80	252.25
3x 3	10x10	87.32	167.24	192.80	252.27
3x 3	11x11	87.32	167.24	192.80	252.27
4x 4	4x 4	46.20	61.69	75.68	85.95
4x 4	5x 5	87.30	157.86	168.05	192.61
4x 4	6x 6	87.32	163.33	192.26	206.69
4x 4	7x 7	87.32	167.23	192.79	249.97
4x 4	8x 8	87.32	167.24	192.80	252.53
4x 4	9x 9	87.32	167.24	192.80	252.25
4x 4	10x10	87.32	167.24	192.80	252.27
4x 4	11x11	87.32	167.24	192.80	252.27

Table 3.7: Convergence for Cross-Ply Sandwich Plate

Vibration Mode	Ibrahim *et al.* [42] Theoretical Results (Hz)	Present Study (Hz)	Difference (%)
1	152.6	146.7374	-3.84
2	197.6	187.6823	-5.02
3	273.7	254.6068	-6.98
4	422.7	390.3775	-7.65

Table 3.8: Sandwich Plate [0^o, 90^o, 0^o, 0^o, 90^o]

Vibration Mode	Ibrahim *et al.* [42] Theoretical Results (Hz)	Present Study (Hz)	Difference (%)
1	146.0	142.4696	-2.42
2	196.4	185.7885	-5.40
3	279.5	254.2777	-9.02
4	401.1	383.7216	-4.33

Table 3.9: Sandwich Plate [0^o, 90^o, 0^o, 90^o, 0^o]

Vibration Mode	Ibrahim *et al.* [42] Theoretical Results (Hz)	Present Study (Hz)	Difference (%)
1	159.3	150.5499	-5.49
2	199.2	189.1329	-5.05
3	268.7	254.4242	-5.31
4	444.3	396.0267	-10.87

Table 3.10: Sandwich Plate [90^o, 0^o, 0^o, 0^o, 90^o]

Vibration Mode	Ibrahim *et al.* [42] Theoretical Results (Hz)	Present Study (Hz)	Difference (%)
1	90.60	87.3237	-3.62
2	179.4	167.2388	-6.78
3	199.9	192.7994	-3.55
4	275.0	252.2724	-8.26

Table 3.11: Sandwich Plate [-15^o, 15^o, 0^o, -15^o, 15^o]

Vibration Mode	Ibrahim *et al.* [42] Theoretical Results (Hz)	Present Study (Hz)	Difference (%)
1	122.6	116.8771	-4.67
2	209.2	194.7108	-6.93
3	283.3	269.1800	-4.98
4	300.4	275.2259	-8.38

Table 3.12: Sandwich Plate $[-30^{o}, 30^{o}, 0^{o}, -30^{o}, 30^{o}]$

Vibration Mode	Ibrahim *et al.* [42] Theoretical Results (Hz)	Present Study (Hz)	Difference (%)
1	152.9	145.5077	-4.83
2	227.3	211.6824	-6.87
3	308.6	283.5613	-8.11
4	382.1	356.6542	-6.66

Table 3.13: Sandwich Plate $[-45^{o}, 45^{o}, 0^{o}, -45^{o}, 45^{o}]$

Description	Dimension
a [m (in)]	0.25 (10.)
b [m (in)]	0.25 (10.)
h_f [mm (in)]	0.71 (0.028)
h_c [mm (in)]	19.05 (0.75)

Table 3.14: Dimensions of the Isotropic and Composite Facesheet Plate.

Property	Isotropic Plate	Composite Plate
E_{11} [GPa (10^6 psi)]	689. (100.)	689. (100.)
E_{22} [GPa (10^6 psi)]	689. (100.)	276. (40.)
G_{12} [GPa (10^6 psi)]	265. (38.46)	12.9 (1.875)
ν_{12}	0.3	0.3
G_{z1} [kPa (10^3 psi)]	206. (30.)	206. (30.)
G_{2z} [kPa (10^3 psi)]	206. (30.)	82. (12.)
q_o [N/m^2 (lb/in^2)]	2435. (1.)	2435. (1.)

Table 3.15: Material Properties of the Composite Sandwich Plate.

Facesheet	Khatua & Cheung [47]	Present Study	Difference (%)
Isotropic	7.361×10^{-4}	7.572×10^{-4}	2.87
Composite	1.213×10^{-3}	1.244×10^{-3}	2.56

Table 3.16: Displacement at the Centre of the Plate.

Facesheet	Khatua & Cheung [47]	Present Study	Difference (%)
Isotropic	4.7789	4.699	-1.67
Composite	7.4433	7.414	-0.39

Table 3.17: Moment at the Centre of the Plate.

rotations are [60]:

$$\varphi_{c0}(x) = 1 \qquad \varphi_{c0}(y) = 1$$

$$\varphi_{c1}(x) = (x - \tfrac{a}{2}) \qquad \varphi_{c1}(y) = \left(y - \tfrac{b}{2}\right)$$

$$\varphi_{cm}(x) = [cos(\beta_r a) - cosh(\beta_r a)][sin(\beta_r x) + sinh(\beta_r x)] - [sin(\beta_r a) - sinh(\beta_r a)][cos(\beta_r x) + cosh(\beta_r x)]$$

$$\varphi_{cn}(x) = [cos(\beta_r b) - cosh(\beta_r b)][sin(\beta_r y) + sinh(\beta_r y)] - [sin(\beta_r b) - sinh(\beta_r b)][cos(\beta_r y) + cosh(\beta_r y)]$$

$$\varphi_{d0}(x) = 1 \qquad \varphi_{d0}(y) = 1$$

$$\varphi_{d1}(x) = (x - \tfrac{a}{2}) \qquad \varphi_{d1}(y) = \left(y - \tfrac{b}{2}\right)$$

$$\varphi_{dm}(x) = [cos(\beta_r a) - cosh(\beta_r a)][cos(\beta_r x) + cosh(\beta_r x)] - [sin(\beta_r a) - sinh(\beta_r a)][-sin(\beta_r x) + sinh(\beta_r x)]$$

$$\varphi_{dn}(x) = [cos(\beta_r b) - cosh(\beta_r b)][sin(\beta_r y) + sinh(\beta_r y)] - [sin(\beta_r b) - sinh(\beta_r b)][cos(\beta_r y) + cosh(\beta_r y)]$$

$$\varphi_{e0}(x) = 1 \qquad \varphi_{e0}(y) = 1$$

$$\varphi_{e1}(x) = (x - \tfrac{a}{2}) \qquad \varphi_{e1}(y) = \left(y - \tfrac{b}{2}\right)$$

$$\varphi_{em}(x) = [cos(\beta_r a) - cosh(\beta_r a)][cos(\beta_r x) + cosh(\beta_r x)] - [sin(\beta_r a) - sinh(\beta_r a)][-sin(\beta_r x) + sinh(\beta_r x)]$$

$$\varphi_{en}(x) = [cos(\beta_r b) - cosh(\beta_r b)][cos(\beta_r y) + cosh(\beta_r y)] - [sin(\beta_r b) - sinh(\beta_r b)][-sin(\beta_r y) + sinh(\beta_r y)]$$

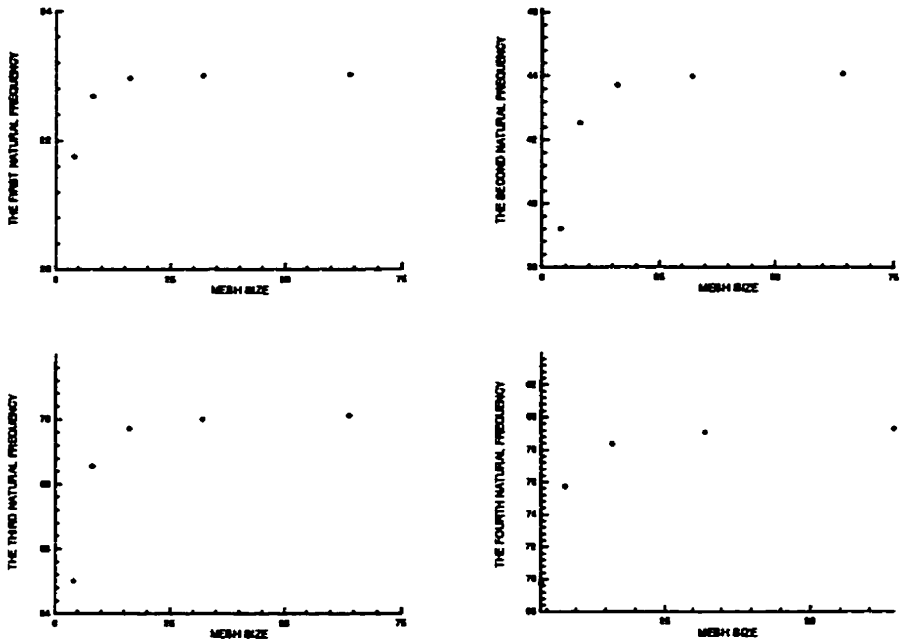

Figure 3.2: Convergence of the Finite Element Mesh.

where β_r is the solution of the transcendental equation $cos(\beta_r l)cosh(\beta_r l) = 1$.

These functions are orthogonal and linearly independent. To check the code, solutions were compared with results given by MSC/NASTRAN [89], using the QUAD4 element, since no solution for free-free vibration problem of a sandwich plate was found in the literature. The first step was to determine the size of the finite element mesh suitable for this problem. Figure 3.2 shows how the solution converges for the first four natural frequencies of a free-free sandwich plate with isotropic facesheets, when the size of the finite element mesh increases. From this figure it can be seen that the solution converges for a 32x32 mesh (5253 degrees of freedom, DOF).

Table 3.18 shows the comparison between the results presented by Raville and Ueng [86] and MSC/NASTRAN [89], with this size of mesh, for the first four natural frequencies of a simply-supported sandwich plate with isotropic facesheets. This table shows that a 32x32 mesh size gives good results.

It was then necessary to determine the number of integration points and terms of the series that would be sufficient to solve a free-free vibration problem with the developed code. Table 3.19 summaries the convergence study. From this table it can be seen that

Vibration Mode	Raville & Ueng [86]		MSC/NASTRAN (32x32 mesh) (Hz)
	Experimental Results (Hz)	Theoretical Results (Hz)	
1	—	23.	23.01
2	45.	45.	43.99
3	69.	71.	70.01
4	78.	80	79.08

Table 3.18: Simply-Supported: Isotropic Facesheet Plate.

with 6x6 terms in the series expansion and 8x8 integration points in each direction the solution converges for the first four natural frequencies (108 DOF). This converged solution was compared with results given by MSC/NASTRAN. The results are given in Table 3.20. From these figures it can be concluded that the codes used here are qualified to calculate the natural frequencies of simply-supported and free-free sandwich plates. Now, they can be used together with the optimization package, which was described in Chapter 2, to solve the optimal design problem of lightweight composite sandwich panels.

Number of Terms	Number of Points	1^{st} Nat. Frequency	2^{nd} Nat. Frequency	3^{rd} Nat. Frequency	4^{th} Nat. Frequency
3x3	3x3	14.22	15.42	31.26	34.06
3x3	4x4	15.25	15.75	35.27	36.80
3x3	5x5	15.25	15.78	34.86	36.79
3x3	6x6	15.25	15.78	34.89	36.80
3x3	7x7	15.25	15.78	34.88	36.80
3x3	8x8	15.25	15.78	34.88	36.80
4x4	4x4	14.42	15.75	34.35	36.80
4x4	5x5	14.44	15.78	33.97	36.79
4x4	6x6	14.45	15.78	34.02	36.80
4x4	7x7	14.45	15.78	34.01	36.80
4x4	8x8	14.45	15.78	34.01	36.80
5x5	5x5	14.44	15.42	32.07	35.40
5x5	6x6	14.45	15.64	33.42	36.46
5x5	7x7	14.45	15.64	33.43	36.53
5x5	8x8	14.45	15.64	33.43	36.53
6x6	6x6	14.38	15.64	33.33	36.46
6x6	7x7	14.36	15.64	33.31	36.53
6x6	8x8	14.37	15.64	33.34	36.53
6x6	9x9	14.37	15.64	33.34	36.53

Table 3.19: Convergence for Free-Free Isotropic Sandwich Plate.

Vibration Mode	MSC/NASTRAN (Hz)	Present Study (Hz)	Difference (%)
1	14.17	14.37	1.41
2	15.47	15.64	1.10
3	32.58	33.34	2.33
4	36.12	36.53	0.58

Table 3.20: Free-free Isotropic Sandwich Plate.

Chapter 4

Modelling

The optimization problem being considered is the minimum mass design of a composite sandwich plate whose facesheets have a spatially varying stiffness and density. The spatially varying stiffness is modelled as a nonuniform net of fibre strips oriented in the x and y directions. Figure 4.1 illustrates a portion of a facesheet, outlining one of the basic cells which composes this layer. In this figure Ws_x, We_x, Ws_y and We_y are the parameters used to define the density of the material: Ws_x is the width of the strips in x-direction in this portion of the plate, and We_x is their spacing; Ws_y and We_y are the same, respectively, in y-direction. So, the density (percentage of material) in x-direction is given by $FDX = Ws_x/(Ws_x + We_x)$ while the density in y-direction is given by $FDY = Ws_y/(Ws_y + We_y)$. Thus, the first step of the modelling is to develop an approximation of the nonuniform net as a smoothed heterogeneous orthotropic continuum. This chapter describes this process and its verification against experimental results.

4.1 Homogenised Continuum Model

The theoretical approach to this problem is referred to as homogenisation theory [6] and the results of this analysis are homogenised engineering constants. The facesheet of the sandwich plate is composed of a net of fibre strips and is modelled by a series of cells as shown in Figure 4.1. Since the cell dimensions are much smaller than the plate dimensions, the net is assumed to behave as a continuous sheet. In order to represent a net of fibre strips as a continuous orthotropic layer, the homogenised engineering constants (E^h_{11}, E^h_{22}, ν^h_{12}, ν^h_{21} and G^h_{12}) of the orthotropic layer must be evaluated based on the geometric and

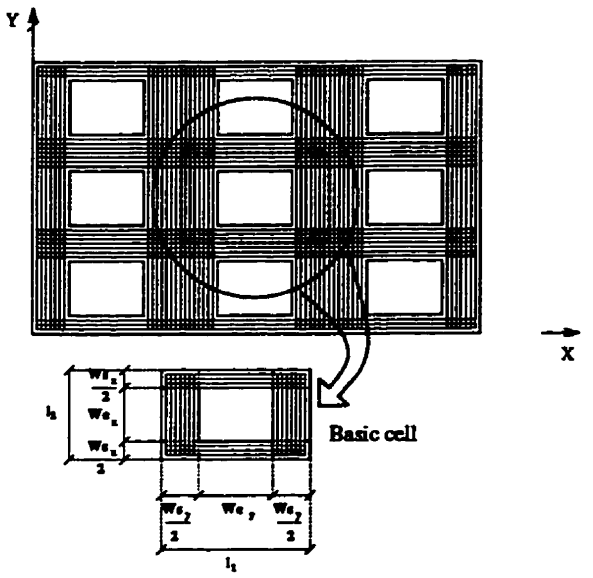

Figure 4.1: Net of Fibre Strips Used as Facesheets of the Composite Sandwich Plate.

material properties of the net.

The homogenised engineering constants can be calculated using the Finite Element Method. Two approaches are presented here: the first uses a basic cell model and the other models part of the fibre-strip net.

4.1.1 The Basic Cell Model Approach

Considering the finite element model of a basic cell presented in Figure 4.2, the procedure adopted here is to apply a boundary condition to this model, and then determine the displacements and the strain energy. Making this strain energy equal to the strain energy of a homogenised cell under the same boundary condition, it is possible to evaluate the homogenised engineering constants. An important issue in this procedure is to set the boundary conditions on the basic cell model properly, so that the model fully represents the periodicity of the structure under a specified load case [99].

Determination of E_{11}^h and ν_{12}^h

In order to calculate E_{11}^h and ν_{12}^h it is assumed that the structure is very large (x and y dimensions are infinite) and the structure is subjected to a uniform stress in the x-direction at its boundary. It is also assumed that the structure remains planar under the application of in-plane loads. Since the cell structure is periodic in both the x and y directions, it follows that under the conditions of a uniform x stress at infinity that the stress and displacement

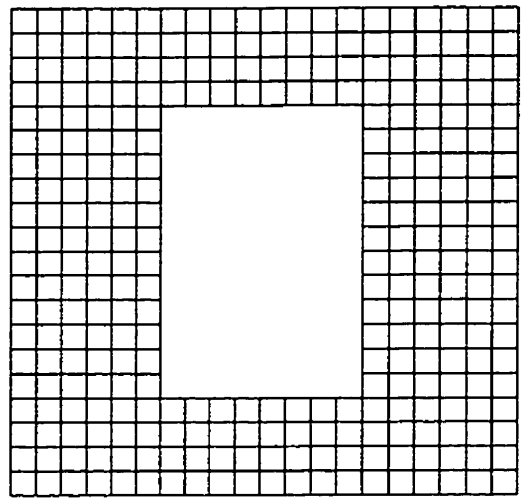

Figure 4.2: The Finite Element Model of a Basic Cell.

solutions must be periodic and they are periodic over each cell. Furthermore, if lines are drawn parallel to the x and y axes forming a rectangular grid and each rectangle of the grid contains only one cell the following may be concluded: 1) The u displacement on lines parallel to the y–axis is constant; 2) The v displacement on lines parallel to the x–axis is constant. This is so because the displacement solution must be periodic.

Having noted the above, it is clear what boundary conditions must be applied to model a single cell of this system. These are the following, according the nomenclature presented in Figure 4.3:

- the structure remains planar;
- no u nor v-displacements for Node 1;
- no v-displacement for the nodes on Side 1;
- no u-displacement for the nodes on Side 2;
- unitary u-displacement for all nodes on Side 3;
- all nodes on Side 4 have equal v-displacement.

Applying these boundary conditions and solving, the strain energy of the model will be U_m^x. The strain energy U_h^x generated in the homogenised cell due to the same boundary

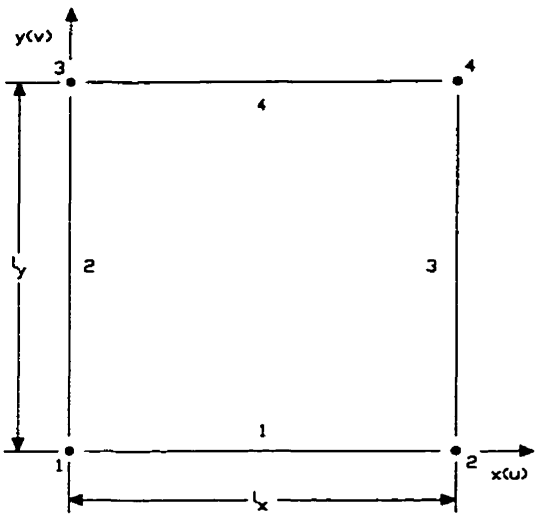

Figure 4.3: Nomenclature Used to Define the Boundary Conditions on the Basic Cell.

conditions is:

$$U_h^x = \frac{1}{2}\int_V \sigma_x^h \epsilon_x^h dV \tag{4.1}$$

Note that the strain energy adopts this simple form because $\sigma_y^h \equiv 0$ and $\tau_{xy}^h \equiv 0$ from the cell boundary conditions. σ_x^h and ϵ_x^h are the homogenised stress and strain in the x-direction, respectively, and V is the volume of the cell. Now, using the stress-strain equation, $\sigma_x^h = E_{11}^h \epsilon_x^h$ (since $\sigma_y^h \equiv 0$), and knowing that $\epsilon_x^h = 1/l_x$ and $V = l_x l_y h_f$, for a cell of thickness h_f, then the strain energy is given by

$$U_h^x = \frac{1}{2}E_{11}^h \left(\frac{1}{l_x}\right)^2 l_x l_y h_f = \frac{1}{2}E_{11}^h \frac{l_y}{l_x} h_f \tag{4.2}$$

The hypothesis behind the homogenisation is that the equivalent structure and the original one should contain the same strain energy when subjected to the same load. Thus setting U_m^x equal to U_h^x, E_{11}^h is evaluated as

$$E_{11}^h = 2U_m^x \frac{l_x}{l_y h_f} \tag{4.3}$$

Also, the homogenised Poisson's ratio ν_{12}^h is given by

$$\nu_{12}^h = -\frac{\Delta_y^x / l_y}{\Delta_x^x / l_x} \tag{4.4}$$

where Δ_x^x is the cell extension in the x-direction and Δ_y^x is the cell compression in the y-direction, with the applied boundary conditions. Since $\Delta_x^x = 1.$, then

$$\nu_{12}^h = -\frac{\Delta_y^x l_x}{l_y} \tag{4.5}$$

Determination of E_{22}^h and ν_{21}^h

The determination of E_{22}^h and ν_{21}^h, follows in exactly the same manner except that the roles of x and y are interchanged. So, the boundary conditions applied to the basic cell finite element model are:

- the structure remains planar;
- no u nor v-displacements for Node 1;
- no v-displacement for the nodes on Side 1;
- no u-displacement for the nodes on Side 2;
- all nodes on Side 3 have equal u-displacement;
- unitary v-displacement for all nodes on Side 4.

Following the same procedure as used to determined E_{11}^h and ν_{12}^h, E_{22}^h is evaluated as:

$$E_{22}^h = 2U_m^y \frac{l_y}{l_x h_f} \tag{4.6}$$

and ν_{21}^h is equal to

$$\nu_{21}^h = -\frac{\Delta_x^y l_y}{l_x} \tag{4.7}$$

Determination of G_{12}^h

In order to calculate G_{12}^h it is assumed that the system is subjected to a uniform shear at infinity. Again the displacement field and stresses are periodic. Based on this periodicity it may be seen that the rectangular grid of undeformed cells is deformed in a periodic manner. This implies that the corners of the original grid lie on a grid of parallelograms. The deformation of the edges of a cell are not straight lines however as the deformation must be periodic in both the x and y directions; thus, the deformation on one side of a cell is equal to the deformation at the corresponding location on the opposite side of that cell plus the

addition of a factor resulting from the shift of the corners of the cell from a rectangular to a parallelogram grid. Thus in the analysis of a single cell using the finite element technique the appropriate boundary conditions which must be imposed are (Figure 4.3):

- the structure remains planar;
- no u nor v-displacements for Node 1;
- all nodes on Side 2 have u and v-displacements equal to the u and v-displacements of the correspondent nodes on Side 3;
- unitary u-displacement for Node 3;
- all nodes on Side 4 have v-displacement equal to the v-displacement of the correspondent nodes on Side 1 and u-displacement equal to the u-displacement of the correspondent nodes on Side 1 plus one.

Under this boundary conditions, the strain energy in the model will be U_m^{xy}. For the same boundary conditions, the strain energy in the homogenised cell is:

$$U_h^{xy} = \frac{1}{2}\int_V \tau_{xy}^h \gamma_{xy}^h dV \tag{4.8}$$

where τ_{xy}^h and γ_{xy}^h are the homogenised shear stress and shear strain, respectively. Substituting the stress-strain equation $\tau_{12}^h = G_{12}^h \gamma_{12}^h$ in Equation 4.8, and knowing that $\gamma_{12}^h = 1/l_y$, the strain energy can be written as

$$U_h^{xy} = \frac{1}{2}G_{12}^h \left(\frac{1}{l_y}\right)^2 l_x l_y h_f = \frac{1}{2}G_{12}^h \frac{l_x}{l_y} h_f \tag{4.9}$$

Again, G_{12}^h is determined by setting U_m^{xy} equal to U_h^{xy}.

$$G_{12}^h = 2U_m^{xy}\frac{l_y}{l_x h_f} \tag{4.10}$$

To verify this approach, the mesh illustrated in Figure 4.2 was used with the finite element code MSC/NASTRAN (QUAD4) [89] to determine the homogenised properties of a structure whose geometric and material properties ($E_{1111} = E_{2222} = 30$ and $E_{1122} = E_{1212} = 10$) of its basic cell are presented by Bendsøe and Kikuchi [9]. In this paper Bendsøe and Kikuchi solve shape optimization problems as material distribution problems by assuming

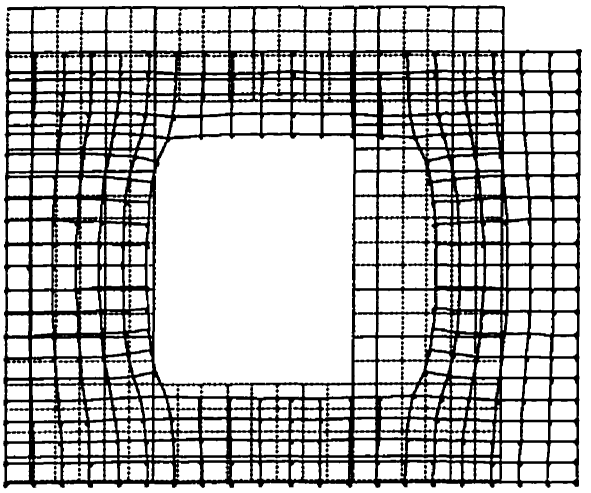

Figure 4.4: Deformation of the Basic Cell under Tension Boundary Conditions.

Reduced Stiffnesses	Bendsøe & Kikuchi [9]	MSC/NASTRAN 1 Cell
$E^h_{11}/(1-\nu^h_{12}\nu^h_{21})$	13.051	12.981
$E^h_{22}/(1-\nu^h_{12}\nu^h_{21})$	17.552	17.526
G_{12}	2.785	2.758
$\nu^h_{21}E_{11}/(1-\nu^h_{12}\nu^h_{21})$	3.241	3.223

Table 4.1: The Reduced Stiffnesses for a Homogenised Material: basic cell approach.

that the material has two constituents: substance and void. Then the microscopic optimal void distribution is considered instead of shape optimization. The homogenisation method is applied in this methodology to determine macroscopic constitutive equations for the material with microscopic material constituents.

Figures 4.4 and 4.5 illustrate how this basic cell is deformed under the tension and shear boundary conditions, respectively. Table 4.1 shows the reduced stiffnesses for the homogenised material obtained by Bendsøe and Kikuchi and by the approach described here. The results are in close agreement.

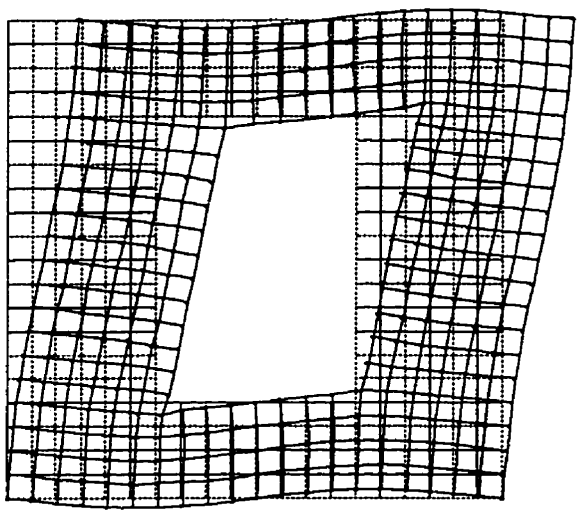

Figure 4.5: Deformation of the Basic Cell under Shear Boundary Conditions.

4.1.2 The Fibre-Strip Net Model Approach

Another way to calculate the homogenised properties is to model a *large* segment of the facesheet (the assumption is that the dimensions of this segment are large compared to the cell dimensions). In this case the boundary conditions and the load applied to the model should represent the boundary conditions and load of an equivalent laboratory experiment. It is important to note that the internal nodal forces and displacements are determined on the boundary of the basic cell closest to the centre of the model.

Assume that the cell problem has been solved using the finite element technique and that the equilibrium solution has been obtained. Furthermore let (u_i,v_i) represent the solution of the problem at the nodes on the perimeter of the cell closest to the centre of the model, where i varies over the perimeter nodes. Also, the internal nodal forces may be determined and the nodal forces at the perimeter nodes are represented as (X_i,Y_i).

Now in an equilibrium configuration two times the strain energy equals the work done; therefore for the cell

$$2U_m^x = \sum_{i=1}^{N_{bc}} (X_i u_i + Y_i v_i) \tag{4.11}$$

where N_{bc} is the number of nodes on the boundary of the basic cell.

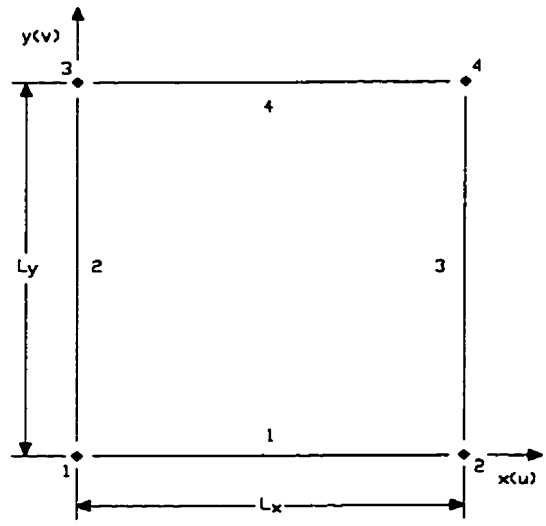

Figure 4.6: Nomenclature Used to Define the Boundary Conditions on the Fibre-Strip Net Model.

From the point of view of the homogenisation principal it will be imposed that

$$U_m^x = U_h^x \tag{4.12}$$

Determination of E_{11}^h and ν_{12}^h

To calculate E_{11}^h and ν_{12}^h, the boundary conditions specified later are applied on the boundary of the model. The description of the boundary conditions is done according to the nomenclature presented in Figure 4.6 for the whole model and Figure 4.3 for the basic cell closest to the centre of the model.

- the structure remains planar;
- no u nor v-displacements for Node 1;
- no u-displacement for the nodes on Side 2;
- unitary u-displacement for all nodes on Side 3.

The strain energy of the homogenised basic cell under these boundary conditions is:

$$U_h^x = \frac{1}{2}\int_V \sigma_x^h \epsilon_x^h dV = \frac{1}{2}\int_V E_{11}^h (\epsilon_x^h)^2 dV \tag{4.13}$$

In the homogeneous state, the strains are:

$$\epsilon_x^h = \frac{1}{L_x} \qquad \epsilon_y^h = -\frac{\nu_{12}^h}{L_x} \tag{4.14}$$

and therefore

$$U_h^x = \frac{1}{2} E_{11}^h \left(\frac{1}{L_x}\right)^2 l_x l_y h_f \tag{4.15}$$

Thus setting the energy expressions (Equation 4.11 and Equation 4.15) equal yields

$$E_{11}^h = \left(\frac{L_x^2}{l_x l_y h_f}\right) \sum_{i=1}^{N_{bc}} (X_i u_i + Y_i v_i) \tag{4.16}$$

The Poisson's ratio is calculated using Equation 4.4. Here, Δ_x^x and Δ_y^x are assumed to be the displacement average of the nodes on Side 3 and 4, respectively. So, ν_{12}^h can be determined by

$$\nu_{12}^h = -\frac{\Delta_y^x / l_y}{\Delta_x^x / l_x} = -\frac{\left(\sum_{i=1}^{n_4} v_i\right) / (n_4 l_y)}{\left(\sum_{i=1}^{n_3} u_i\right) / (n_3 l_x)} \tag{4.17}$$

where u_i are the displacements in the x-direction for the nodes on Side 3 and v_i are the displacements in the y-direction for the nodes on Side 4, n_3 and n_4 are the number of nodes on Side 3 and 4, respectively, of the basic cell.

Determination of E_{22}^h and ν_{21}^h

The boundary conditions which should be applied to calculate E_{22}^h and ν_{21}^h are the following:

- the structure remains planar;
- no u nor v-displacements for Node 1;
- no v-displacement for the nodes on Side 1;
- unitary v-displacement for all nodes on Side 4.

Following the same procedure used to determined E_{11}^h and ν_{12}^h, E_{22}^h is evaluated as:

$$E_{22}^h = \left(\frac{L_y^2}{l_x l_y h_f}\right) \sum_{i=1}^{N_{bc}} (X_i u_i + Y_i v_i) \tag{4.18}$$

The Poisson's ratio ν_{21}^h is equal to

$$\nu_{21}^h = -\frac{\left(\sum_{i=1}^{n_3} u_i\right) / (n_3 l_x)}{\left(\sum_{i=1}^{n_4} v_i\right) / (n_4 l_y)} \tag{4.19}$$

where u_i are the displacements in the x-direction of the nodes on Side 3 and v_i are the displacements in the y-direction of the nodes on Side 4.

Determination of G_{12}^h

The G_{12}^h is determined applying the following boundary conditions:

- the structure remains planar;
- no u nor v-displacements for Node 1;
- no v-displacement for all nodes on Side 1;
- the nodes on Side 2 have u-displacements that vary linearly from zero at Node 1 to one at Node 3;
- the nodes on Side 3 have u-displacements that vary linearly from zero at Node 2 to one at Node 4;
- no v-displacement and unitary u-displacement for all nodes on Side 4.

The strain energy of the homogenised basic cell under these boundary conditions is:

$$U_h^{xy} = \frac{1}{2}\int_V \tau_{xy}^h \gamma_{xy}^h dV = \frac{1}{2}\int_V G_{12}^h (\gamma_{xy}^h)^2 dV \tag{4.20}$$

In the homogeneous state, the shear strain is:

$$\gamma_{xy}^h = \frac{1}{L_y} \tag{4.21}$$

and therefore

$$U_h^{xy} = \frac{1}{2} G_{12}^h \left(\frac{1}{L_y}\right)^2 l_x l_y h_f \tag{4.22}$$

Thus setting the energy expression equal: $U_m^{xy} = U_h^{xy}$, yields

$$G_{12}^h = \left(\frac{L_y^2}{l_x l_y h_f}\right) \sum_{i=1}^{N_{bc}} (X_i u_i + Y_i v_i) \tag{4.23}$$

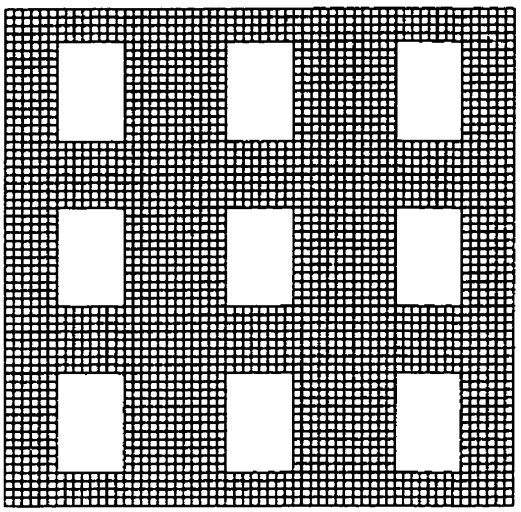

Figure 4.7: The Finite Element Model of 9 Basic Cells.

Three finite element meshes were created with 1, 9 and 81 basic cells (Figures 4.2, 4.7 and 4.8, respectively). These meshes were used with the MSC/NASTRAN code to solve the homogenised problem presented before. Figures 4.9 to 4.11 show the deformation of these meshes under a uniform stretch condition and Figures 4.12 to 4.14 illustrate the deformation of these meshes under uniform shear strain.

From the results showed in Table 4.2, it is possible to compare the reduced stiffnesses for the homogenised material obtained using the three meshes with the values presented by Bendsøe and Kikuchi. Doing this comparison, it is clear that it is necessary to use at least the mesh with 9 basic cells to calculate the E^h_{11}, E^h_{22}, ν^h_{12} and ν^h_{21} and the mesh with 81 basic cells to determine G^h_{12}.

Once the procedure used to determine the homogenised properties of a fibre-strip net was verified, it was then used to create tables with values of these homogenised properties for different material densities in the x and y directions. During the optimization process, the homogenised properties of a specific design are determined by interpolating the values from these tables.

Using the finite element model, five tables were generated for E^h_{11}, E^h_{22}, ν^h_{12}, G^h_{12} and homogenised density (Tables 4.3 to 4.7, respectively), varying the material density from 10% to 90% in the x and y-directions and with steps of 10%. Figures 4.15 to 4.19 illustrate graphically the results in these tables. These results show that for a fixed value of material

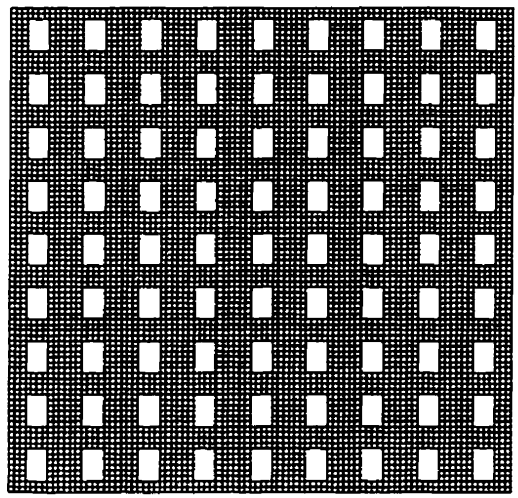

Figure 4.8: The Finite Element Model of 81 Basic Cells.

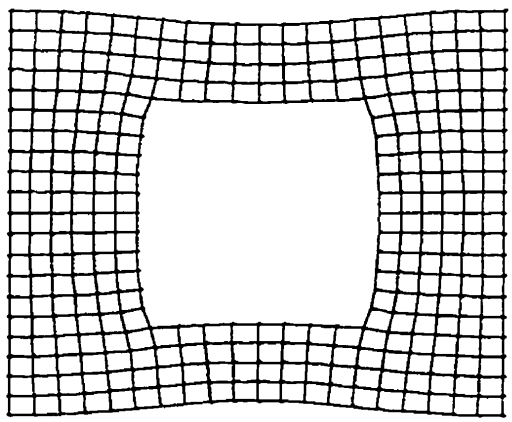

Figure 4.9: Mesh Deformation of a Basic Cell under Uniform Stretch Condition.

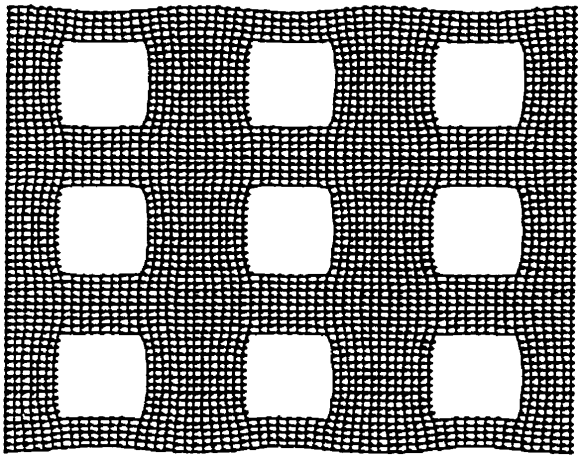

Figure 4.10: Mesh Deformation of 9 Basic Cells under Uniform Stretch Condition.

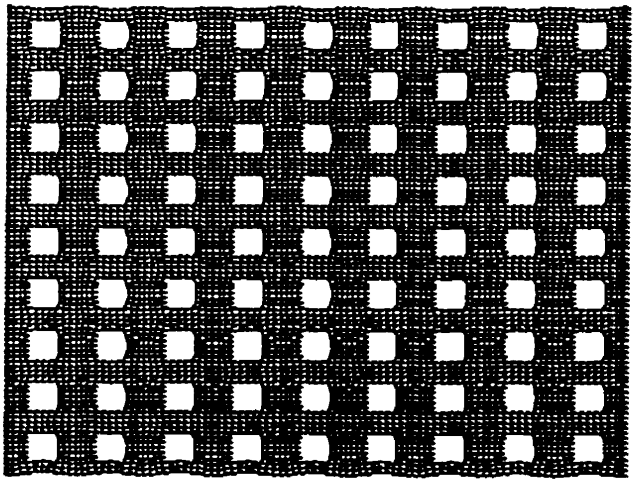

Figure 4.11: Mesh Deformation of 81 Basic Cells under Uniform Stretch Condition.

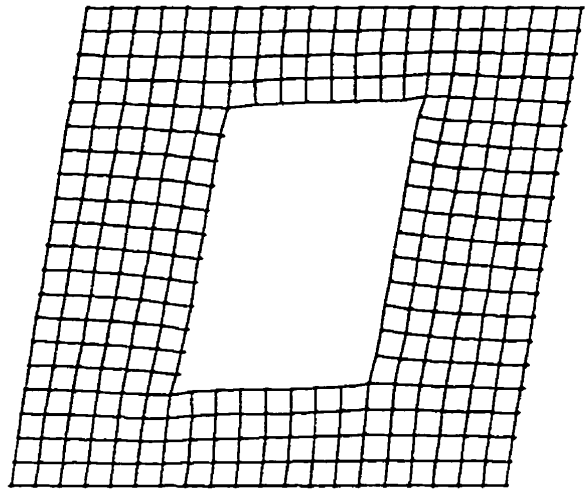

Figure 4.12: Mesh Deformation of a Basic Cell under Uniform Shear Strain.

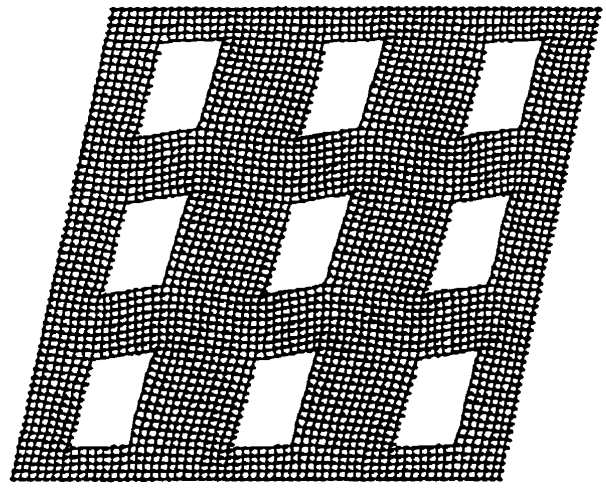

Figure 4.13: Mesh Deformation of 9 Basic Cells under Uniform Shear Strain.

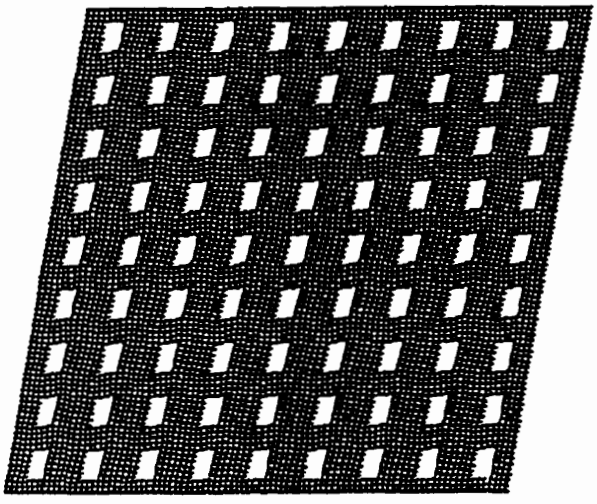

Figure 4.14: Mesh Deformation of 81 Basic Cells under Uniform Shear Strain.

Reduced Stiffnesses	Bendsøe & Kikuchi [9]	MSC/NASTRAN		
		1 Cell	9 Cells	81 Cells
$E^h_{11}/(1-\nu^h_{12}\nu^h_{21})$	13.051	11.977	12.540	12.852
$E^h_{22}/(1-\nu^h_{12}\nu^h_{21})$	17.552	16.739	17.116	17.477
G_{12}	2.785	4.863	3.299	2.800
$\nu^h_{21}E_{11}/(1-\nu^h_{12}\nu^h_{21})$	3.241	1.089	3.306	3.371

Table 4.2: The Reduced Stiffnesses for a Homogenised Material: Fibre-Strip Net Model Approach

Material Density	Material Density in X-Direction								
Y-Direction	10%	20%	30%	40%	50%	60%	70%	80%	90%
10%	21.606	43.186	64.769	86.355	107.94	129.54	151.13	172.73	194.33
20%	21.754	43.410	65.069	86.731	108.40	130.07	151.74	173.41	195.06
30%	21.949	43.683	65.419	87.158	108.90	130.65	152.39	174.12	195.80
40%	22.195	44.007	65.821	87.638	109.46	131.27	153.08	174.84	196.54
50%	22.496	44.386	66.278	88.171	110.06	131.94	153.79	175.58	197.28
60%	22.856	44.823	66.790	88.753	110.70	132.63	154.51	176.31	198.02
70%	23.275	45.317	67.353	89.378	111.38	133.34	155.24	177.05	198.77
80%	23.755	45.866	67.963	90.038	112.08	134.06	155.97	177.89	199.51
90%	24.297	46.469	68.615	90.729	112.80	134.80	156.71	178.53	200.25

Table 4.3: Homogenised Young's Modulus E_{11}^h (GPa).

density in one direction, the homogenised properties have a smooth behaviour when the material density changes in the other direction. Therefore, it may be concluded that these tables with 10% steps yield a satisfactory interpolation of the homogenised properties in the range from 10% to 90%.

4.2 Comparison with Experimental Results

To validate the process of approximating the net of fibre strips by an equivalent homogenised continuum-layer, a free-free modal test was completed; the sandwich plate had facesheets manufactured from an aluminium net and the core was an aluminium honeycomb. Aluminium was chosen for the facesheets instead of a composite material because it was easier to manufacture the net with this material.

The sandwich plate is a five layer symmetric laminate with length of 406 mm and width of 201 mm (Figure 4.20). The outside layers are the aluminium nets with a 0.4 mm thicknesses. Figure 4.21 illustrates the layout of the net. The second layers are adhesive films, with a 0.12 mm thickness. The core is 4.46 mm thick 3/8-5052-.007 aluminium honeycomb. Table 4.8 presents the mechanical properties of the three materials.

To simulate the free-free boundary conditions, the plate was suspended by four springs located at the middle of the plate edges, which corresponded to the nodes of the first elastic

Material Density	Material Density in X-Direction								
Y-Direction	10%	20%	30%	40%	50%	60%	70%	80%	90%
10%	21.606	21.754	21.949	22.195	22.496	22.856	23.275	23.755	24.297
20%	43.186	43.410	43.683	44.007	44.386	44.823	45.317	45.866	46.469
30%	64.769	65.069	65.419	65.821	66.278	66.790	67.353	67.963	68.615
40%	86.355	86.731	87.158	87.638	88.171	88.753	89.378	90.038	90.729
50%	107.94	108.40	108.90	109.46	110.06	110.70	111.38	112.08	112.80
60%	129.54	130.07	130.65	131.27	131.94	132.63	133.34	134.06	134.80
70%	151.13	151.74	152.39	153.08	153.79	154.51	155.24	155.97	156.71
80%	172.73	173.41	174.12	174.84	175.58	176.31	177.05	177.89	178.53
90%	194.33	195.06	195.80	196.54	197.28	198.02	198.77	199.51	200.25

Table 4.4: Homogenised Young's Modulus E^h_{22} (GPa).

Material Density	Material Density in X-Direction								
Y-Direction	10%	20%	30%	40%	50%	60%	70%	80%	90%
10%	.27E-2	.57E-2	.92E-2	.13E-1	.18E-1	.23E-1	.29E-1	.35E-1	.42E-1
20%	.28E-2	.53E-2	.81E-2	.11E-1	.14E-1	.18E-1	.22E-1	.26E-1	.30E-1
30%	.31E-2	.54E-2	.76E-2	.10E-1	.13E-1	.16E-1	.19E-1	.23E-1	.26E-1
40%	.34E-2	.57E-2	.78E-2	.10E-1	.12E-1	.15E-1	.18E-1	.20E-1	.23E-1
50%	.38E-2	.60E-2	.81E-2	.10E-1	.12E-1	.14E-1	.17E-1	.19E-1	.21E-1
60%	.41E-2	.63E-2	.84E-2	.10E-1	.12E-1	.14E-1	.16E-1	.18E-1	.20E-1
70%	.45E-2	.66E-2	.87E-2	.10E-1	.12E-1	.14E-1	.15E-1	.17E-1	.19E-1
80%	.48E-2	.70E-2	.89E-2	.10E-1	.12E-1	.14E-1	.15E-1	.17E-1	.18E-1
90%	.53E-2	.72E-2	.91E-2	.10E-1	.12E-1	.14E-1	.15E-1	.17E-1	.18E-1

Table 4.5: Homogenised Poisson's Ratio ν^h_{12}.

Material Density	Material Density in X-Direction								
Y-Direction	10%	20%	30%	40%	50%	60%	70%	80%	90%
10%	2.3790	3.3156	4.2522	5.3963	6.6333	7.9354	9.2760	10.663	12.145
20%	3.3156	6.0623	7.1388	8.2965	9.5156	10.780	12.083	13.436	14.894
30%	4.2522	7.1388	9.4849	10.651	11.863	13.113	14.397	15.728	17.160
40%	5.3963	8.2965	10.651	12.619	13.827	15.071	16.348	17.671	19.089
50%	6.6333	9.5156	11.863	13.827	15.409	16.656	17.937	19.262	20.678
60%	7.9354	10.780	13.113	15.071	16.656	17.905	19.199	20.535	21.957
70%	9.2760	12.083	14.397	16.348	17.937	19.199	20.191	21.545	22.978
80%	10.663	13.436	15.728	17.671	19.262	20.535	21.545	22.358	23.806
90%	12.145	14.894	17.160	19.089	20.678	21.957	22.978	23.806	24.523

Table 4.6: Homogenised Shear Modulus G_{12}^h (GPa).

Material Density	Material Density in the X-Direction								
Y-Direction	10%	20%	30%	40%	50%	60%	70%	80%	90%
10%	330.	495.	660.	825.	990.	1155.	1320.	1485.	1650.
20%	495.	660.	825.	990.	1155.	1320.	1485.	1650.	1815.
30%	660.	825.	990.	1155.	1320.	1485.	1650.	1815.	1980.
40%	825.	990.	1155.	1320.	1485.	1650.	1815.	1980.	2145.
50%	990.	1155.	1320.	1485.	1650.	1815.	1980.	2145.	2310.
60%	1155.	1320.	1485.	1650.	1815.	1980.	2145.	2310.	2475.
70%	1320.	1485.	1650.	1815.	1980.	2145.	2310.	2475.	2640.
80%	1485.	1650.	1815.	1980.	2145.	2310.	2475.	2640.	2805.
90%	1650.	1815.	1980.	2145.	2310.	2475.	2640.	2805.	2970.

Table 4.7: Homogenised Mass Density (kg/m^3).

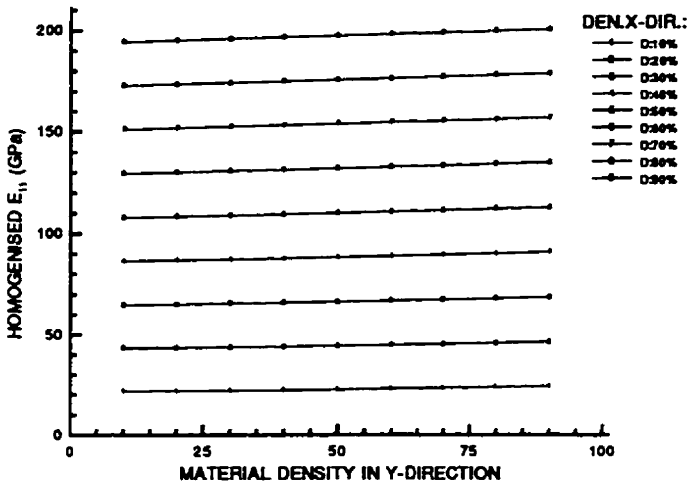

Figure 4.15: Homogenised Young's Modulus E_{11}^h as a Function of the Material Density in the x and y Directions.

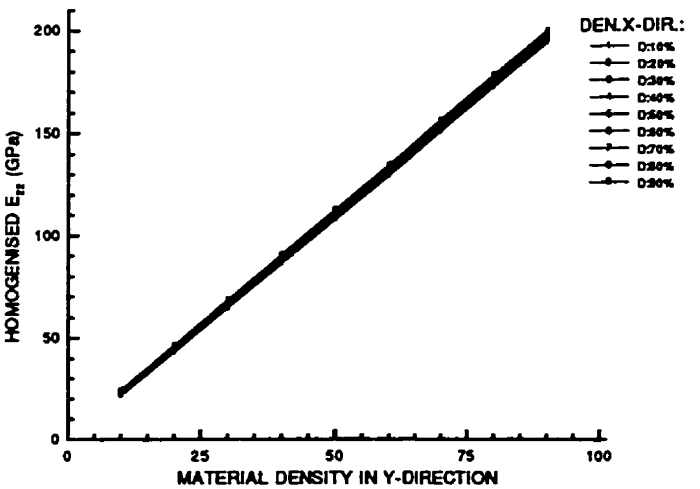

Figure 4.16: Homogenised Young's Modulus E_{22}^h as a Function of the Material Density in the x and y Directions.

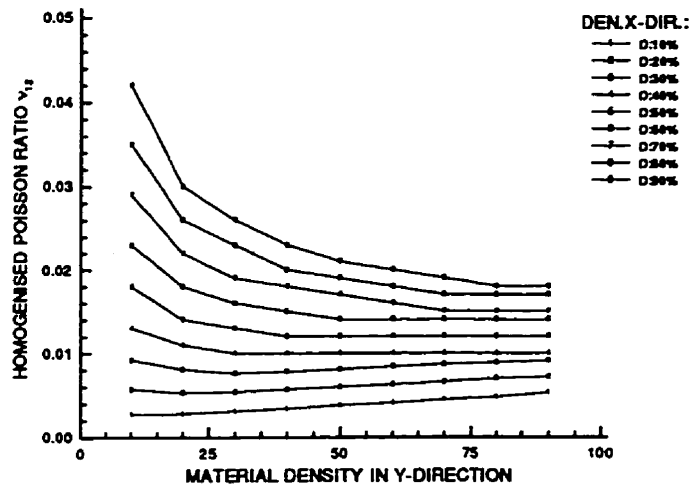

Figure 4.17: Homogenised Poisson Ratio ν_{12}^h as a Function of the Material Density in the x and y Directions.

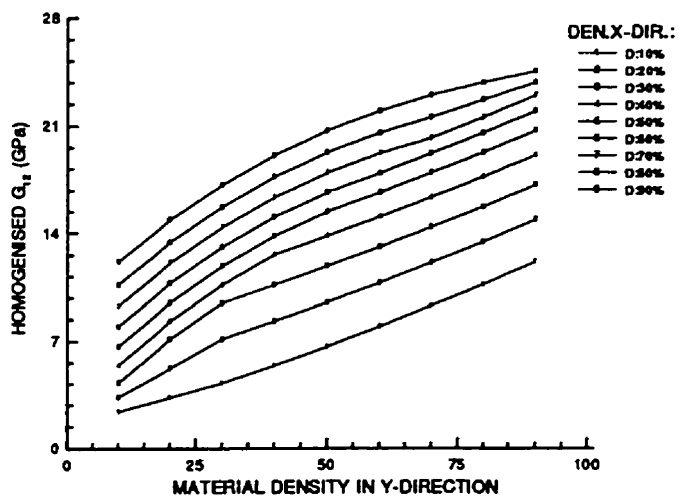

Figure 4.18: Homogenised Shear Modulus G_{12}^h as a Function of the Material Density in the x and y Directions.

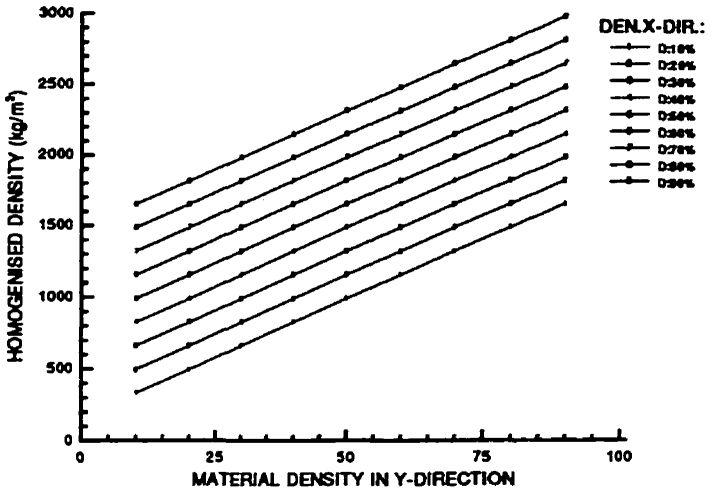

Figure 4.19: Homogenised Mass Density as a Function of the Material Density in the x and y Directions.

Property	Aluminium	Adhesive Film	Honeycomb
E_{11} [GPa (10^6psi)]	72.4 (12.26)	11.00 (1.86)	
E_{22} [GPa (10^6psi)]	72.4 (12.26)	11.00 (1.86)	
G_{12} [GPa (10^6psi)]	27.2 (4.60)	3.92 (0.66)	
ν_{12}	0.33	0.40	
G_{1z} [MPa (10^3psi)]			82.74 (14.01)
G_{2z} [MPa (10^3psi)]			48.28 (8.17)
ρ [kg/m^3(10^{-3}lbm/in^3)]	2800. (101.16)	1110. (40.10)	16.018 (0.58)

Table 4.8: Material properties.

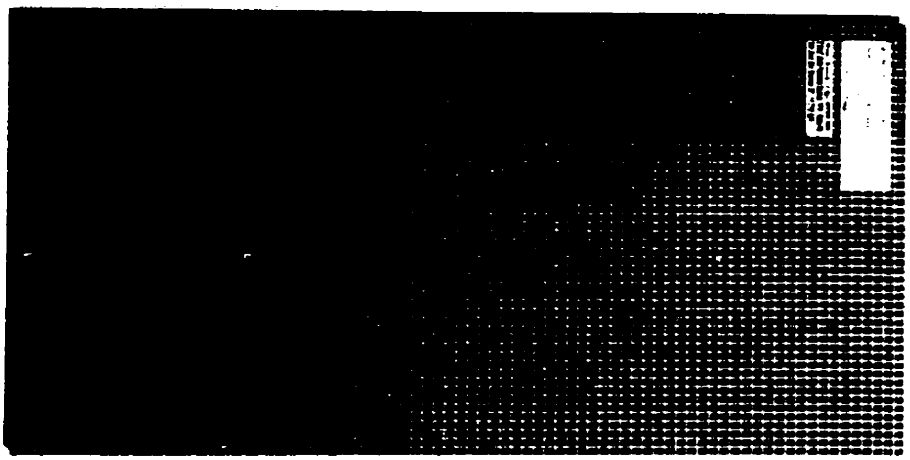

Figure 4.20: Sandwich Plate with Uniform Net in the Facesheets.

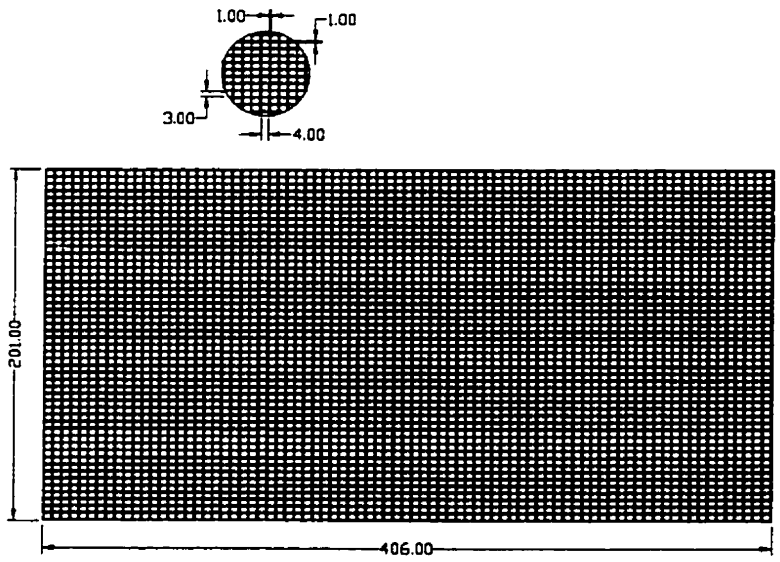

Figure 4.21: Layout of the Facesheets.

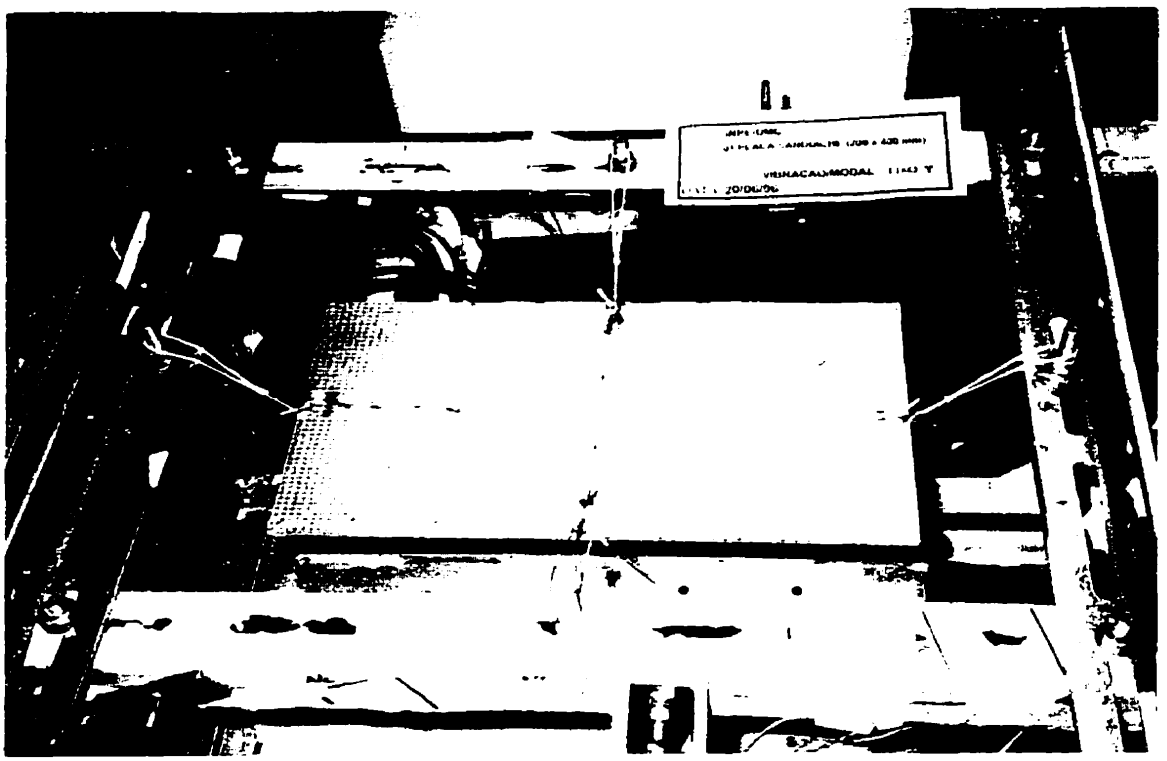

Figure 4.22: Plate Ready to be Tested.

mode. Figure 4.22 illustrates the plate ready to be tested. In this figure the elastic supports, accelerometers and cables can be seen. For this test, fifteen accelerometers were bonded to the plate (eight Endevco Model 22 and seven Endevco Model 2222C). Their positions are sketched in Figure 4.23. Fifteen load amplifiers were connected to the accelerometers. In addition, an impact hammer instrumented with a B & K Model 8200 was connected to the load amplifiers.

The modal test was done using a digital data acquisition and analysis system, GEN-RAD 2515 in conjunction with the analysis software SDRC MODAL-PLUS Version 9.2. This work was done at the Integration and Test Laboratory (LIT) of the National Institute for Space Research (INPE), in Brazil. The first three elastic modes and their natural frequencies are illustrated in Figures 4.24 to 4.26.

Since the analysis program developed in this research (see Chapter 3) cannot simulate

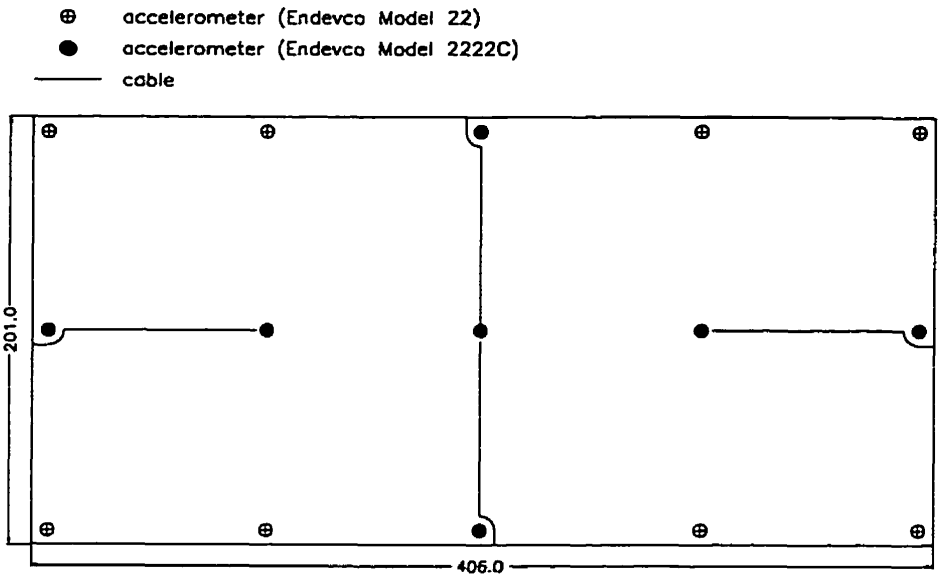

Figure 4.23: Position of the Accelerometers.

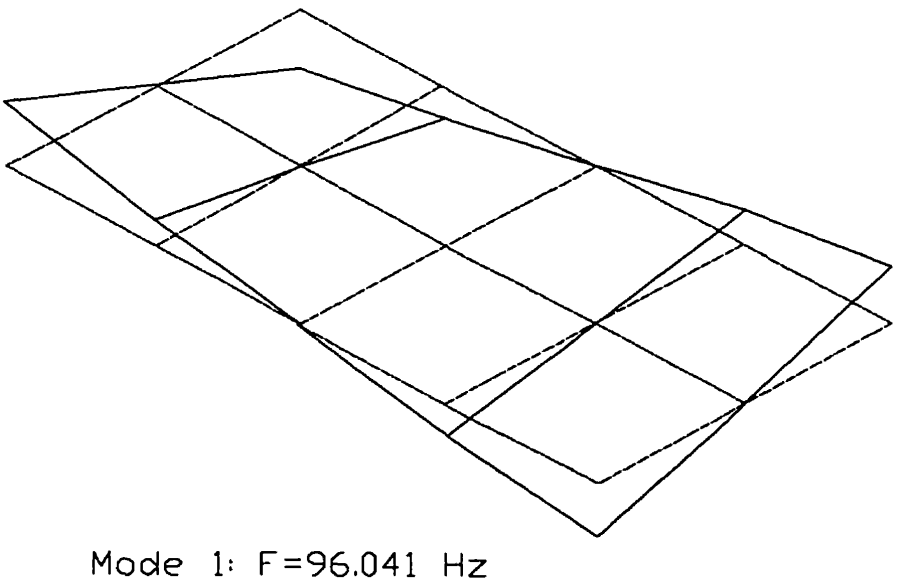

Figure 4.24: The First Elastic Mode - Experimental Result.

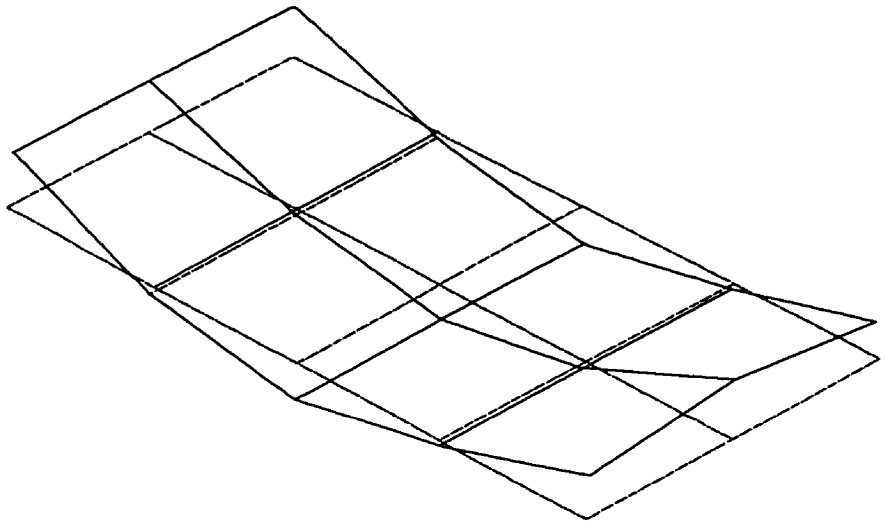

Figure 4.25: The Second Elastic Mode - Experimental Result.

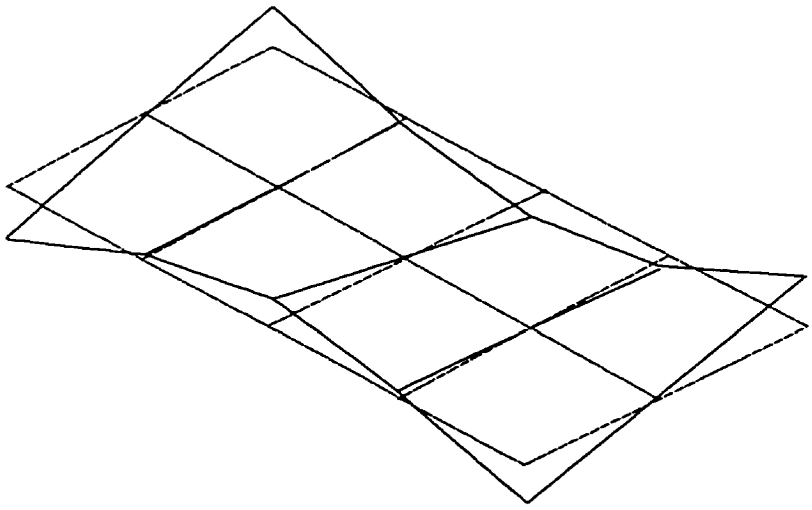

Figure 4.26: The Third Elastic Mode - Experimental Result.

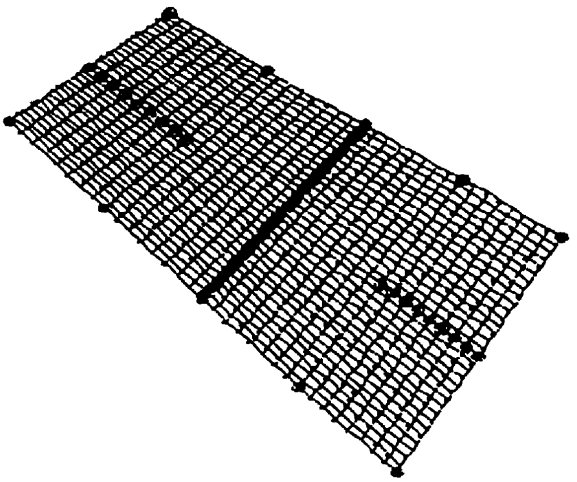

Figure 4.27: The First Elastic Mode - MSC/NASTRAN Result with Concentrated Masses.

concentrated masses due to the accelerometers used in the test, the test results were compared with numerical results obtained from the finite element program MSC/NASTRAN. A finite element model of the tested plate was developed, including the concentrated masses of the accelerometers and cables used in the experiment. In this model, the mechanical properties of the aluminium net were calculated using the homogenisation process described in the first part of this chapter. Figures 4.27 to 4.29 present the first three elastic modes and their frequencies given by this model. These modes are the same as the ones determined in the experiment and these frequencies are close to the ones measured in the experiment.

In a second step, all the concentrated masses are removed from the finite element model using MSC/NASTRAN and the results (Figures 4.30 to 4.32) are compared with the results of the analysis program described in Chapter 3, that uses the process of approximation described in the first part of this present chapter (Figures 4.33 to 4.35). From Figures 4.30 to 4.35 and Table 4.9, it is possible to see that the program results agree closely with the results of MSC/NASTRAN model without concentrated mass. These results validate the process of approximating the net of fibre strips by an equivalent homogenised orthotropic continuum-layer.

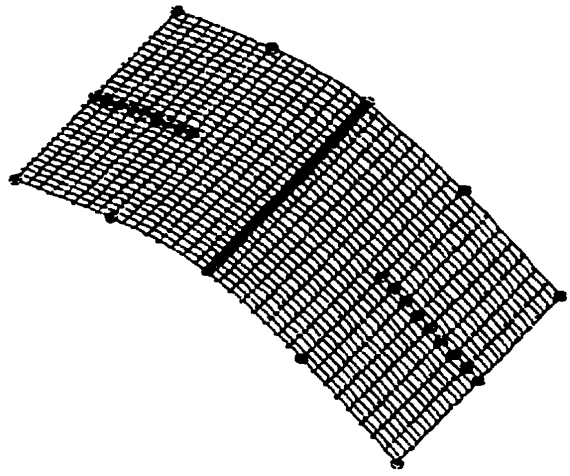

Figure 4.28: The Second Elastic Mode - MSC/NASTRAN Result with Concentrated Masses.

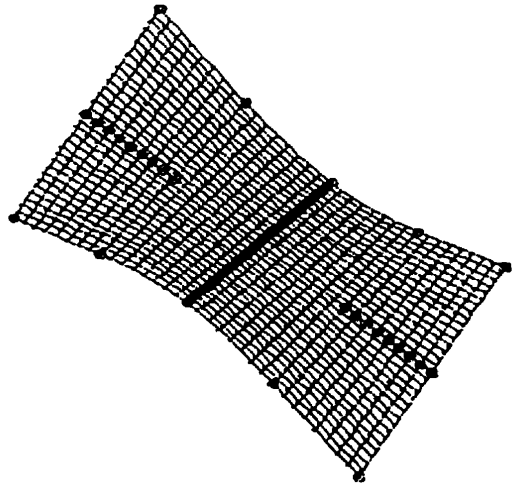

Figure 4.29: The Third Elastic Mode - MSC/NASTRAN Result with Concentrated Masses.

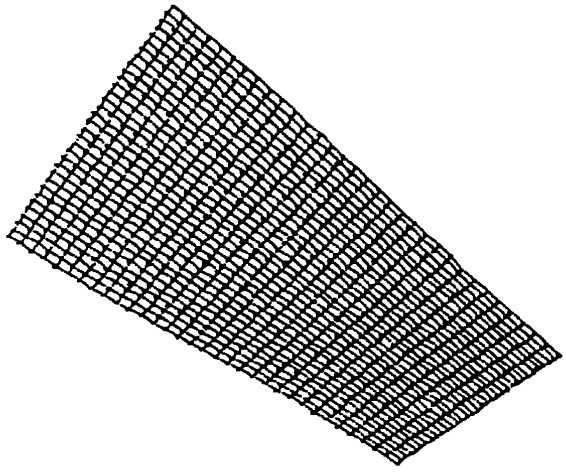

Figure 4.30: The First Elastic Mode - MSC/NASTRAN Result without Concentrated Masses.

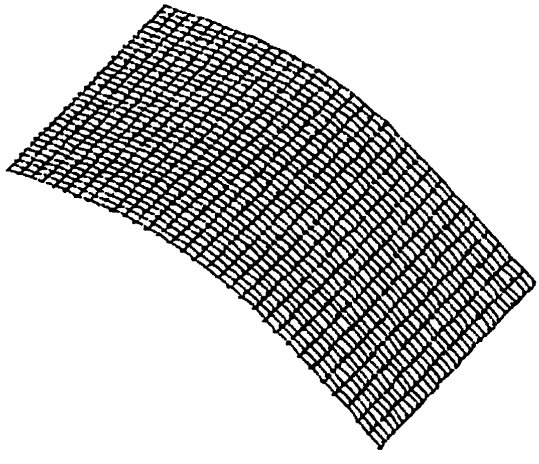

Figure 4.31: The Second Elastic Mode - MSC/NASTRAN Result without Concentrated Masses.

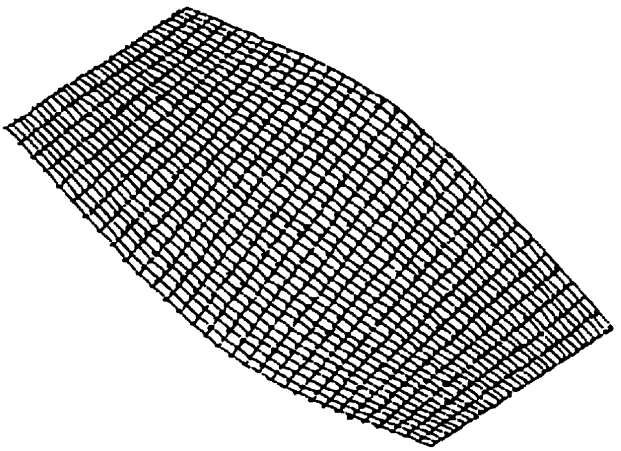

Figure 4.32: The Third Elastic Mode - MSC/NASTRAN Result without Concentrated Masses.

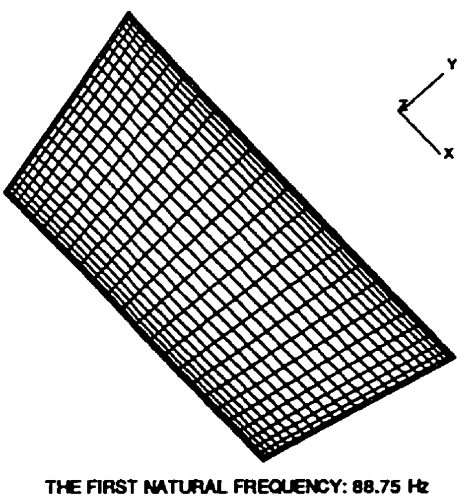

Figure 4.33: The First Elastic Mode - Present Result.

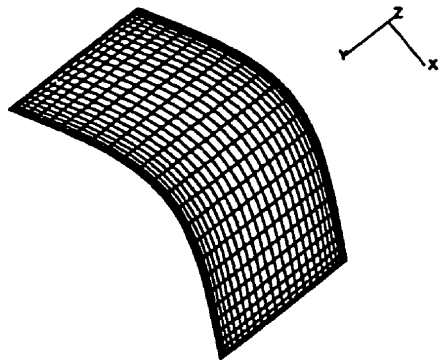

Figure 4.34: The Second Elastic Mode - Present Result.

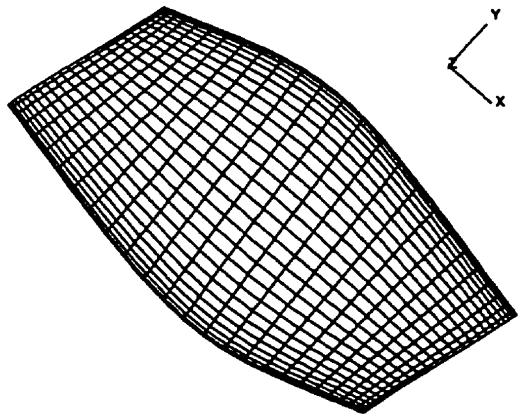

Figure 4.35: The Third Elastic Mode - Present Result.

Vibration Mode	MSC/NASTRAN Results (Hz)	Present Study (Hz)
1	92.58	88.75
2	177.15	178.08
3	255.62	253.38

Table 4.9: Natural Frequencies from the Numerical Models without Concentrated Masses.

Chapter 5

Method of Optimization

The problem studied here is the minimization of the mass of a composite sandwich plate while maintaining the first natural frequency and some failure loads greater than prescribed values. The choice of natural frequency and failure load constraints is based on design requirements for satellite structures. In this problem, the facesheets are assumed to be composed of an orthotropic net of unidirectional composite fibre strips. Thus, the facesheet stiffness is altered by changing the width and spacing between these strips.

This chapter is divided in four sections. The first describes the approaches used to define the design variables. Then, the following section presents the failure loads considered in this work. The third section explains the sensitivity analysis, while the final section outlines the optimization algorithms used.

5.1 Approaches to Define the Design Variables

The definition of the design variables is accomplished using two techniques. In the first, an independent design approach, the facesheets are discretized into regions with uniform design parameters. In the second, a reduced basis formulation, the design parameter is specified by a linear combination of orthogonal basis functions.

5.1.1 Approach 1: Independent Design

In this technique the facesheets are discretized into bands in both the x and y-directions. The material densities (FDX and FDY) are the design variables x_i and are assumed to be constant in each band (Figure 5.1). The optimization procedure for this approach can be

formulated as follows

$$\begin{aligned} \text{Minimize} \quad &: \quad M_{fs} = 2\int_A \rho(x_i) h_f dA \\ \text{Subject to} \quad &: \quad \Omega_1 \geq \overline{\Omega}_1 \\ &\qquad \sigma(x,y) \leq \overline{FS}_j \qquad j = 1, \cdots, \text{NFM} \\ &\qquad x_l \leq x_i \leq x_u \qquad i = 1, \cdots, \text{NDV} \end{aligned} \tag{5.1}$$

where

M_{fs} : mass of the facesheets

$\rho(x_i)$: density of the facesheets

x_i : the i^{th} design variable

h_f : thickness of the facesheets

Ω_1 : the first natural frequency

$\overline{\Omega}_1$: specified value for the first natural frequency.

$\sigma(x,y)$: stress at (x,y) position

$\overline{FS}_j$: the specified value for the j^{th} failure stress

NFM : number of failure modes

NDV : number of design variables

x_l : lower limit for design variables

x_u : upper limit for design variables

This approach is easy to implement. However, it has the disadvantage of allowing sharp changes in the design variables from one band to the other. In addition, from a practical structural point of view these jumps in properties may induce stress concentrations in the structure.

5.1.2 Approach 2: Reduced Basis Formulation

In this approach, the material density of the facesheets is approximated by a linear combination of orthogonal functions superimposed on an initial design. Here, the design variables

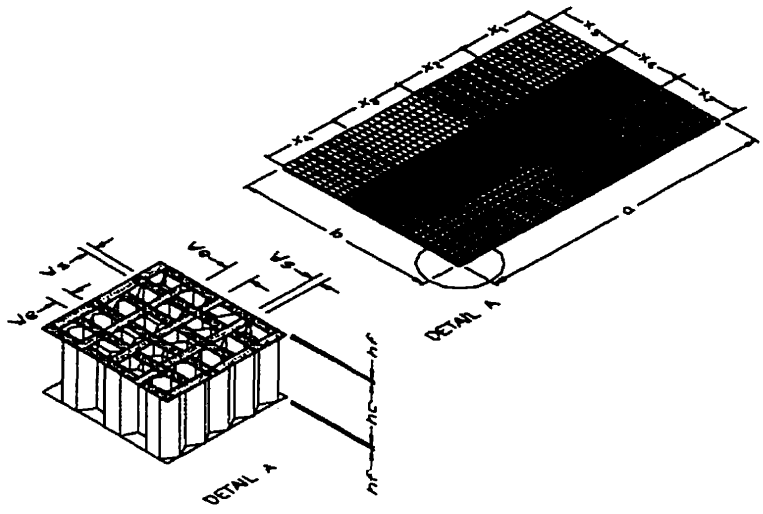

Figure 5.1: Independent Design Approach.

x_i are the coefficients which multiply each orthogonal function. This global description enforces a smooth material distribution, but it restricts the optimal design to the class of curves that can be obtained by a finite number of such functions. Pedersen [75–77] used this strategy to obtain the optimal shape design for minimum stress or energy concentration. Mathematically, the material distributions in the x and y-directions are given by

$$FDX = x_1 + \sum_{i=2}^{NDV/2} x_i f_i(y) \tag{5.2}$$

$$FDY = x_{NDV/2+1} + \sum_{i=NDV/2+2}^{NDV} x_i f_i(x) \tag{5.3}$$

where

f_i : the i^{th} preselected orthogonal basis function.

Two sets of orthogonal functions were tested for this approach. These were the odd eigenfunctions of a vibrating beam for the two cases of simple supported and fully clamped

boundary conditions. These functions are easy to work with and form a complete set. These eigenfunctions are

- For a simply-supported vibrating beam (Approach 2A)

$$f_i(x) = \sin\left(\frac{i\pi x}{a}\right) \tag{5.4}$$

- For a clamped vibrating beam (Approach 2B)

$$\begin{aligned} f_i(x) \;=\; & \cosh(k_i x) - \cos(k_i x) - \\ & \frac{\cos(k_i a) - \cosh(k_i a)}{\sin(k_i a) - \sinh(k_i a)}[\sinh(k_i x) - \sin(k_i x)] \end{aligned} \tag{5.5}$$

where a is the length of the beam. The values of $k_i a$ are obtained from the solution of the transcendental equation

$$\cos(k_i a)\cosh(k_i a) = 1. \tag{5.6}$$

The optimization procedure for this approach can be formulated as follows

$$\begin{aligned} \text{Minimize} \;:\; & M_{fs} = 2\int_A \rho(x_i) h_f dA \\ \text{Subject to} \;:\; & \Omega_1 \geq \overline{\Omega}_1 \\ & \sigma(x,y) \leq \overline{FS}_j \qquad\qquad j = 1, \cdots, \text{NFM} \\ & FDX_l \leq FDX \leq FDX_u \\ & FDY_l \leq FDY \leq FDY_u \end{aligned} \tag{5.7}$$

where

FDX_l : lower limit of the material density in x-direction (Equation 5.2)

FDX_u : upper limit of the material density in x-direction (Equation 5.2)

FDY_l : lower limit of the material density in y-direction (Equation 5.3)

FDY_u : upper limit of the material density in y-direction (Equation 5.3)

In this approach, besides the constraint which imposes that the first natural frequency must be greater than a specified value, other constraints have to be considered: the material density must be between the lower and upper limits ($FDX_l \leq FDX \leq FDX_u$ and $FDY_l \leq FDY \leq FDY_u$). One way to define these constraints is to look for the points that have the lowest and the highest material density. The lowest material density is constrained to be higher than the lower limit and the highest material density is constrained to be smaller than the upper limit.

However, this procedure can bring some instability to the numerical solution, since the solution can possibly to oscillate between two designs. In this work, some points of the plate are selected and lower and upper limits are imposed for the material density at these points. The positions of these points are related to the peaks of the orthogonal functions used to define the material distribution.

The advantage of this approach is the fact that the design variables change slowly from one region to another in the structure.

5.2 Failure Load Constraints

A composite sandwich construction is composed of two thin facesheets that support the membrane and bending loads, bonded to a thick core which resists the shear loads. A sandwich structure should be designed to meet strength and buckling requirements [11, 22, 50, 79, 111], such as: the strength of the facesheets should be enough to withstand the tensile, compressive, and in-plane shear stresses generated by the design load conditions; the thickness and shear modulus of the core should be sufficient to support the transverse shear stresses due to the design loads, and to avoid overall buckling and excessive deflection as well as shear failure of the facesheets; the size and density of the core should be such to prevent the monocell buckling (face dimpling); and the normal compressive strength of the core and the in-plane tensile strength of the facesheets should be sufficient to prevent wrinkling and crimping instability of the facesheets.

In this research, besides the fundamental frequency, three failure modes were considered as constraints: fibre failure, intercell buckling and wrinkling. These are related to the requirements that are affected by changing the stiffness distribution of the facesheets, considering that in the optimization process neither the dimensions nor the material properties

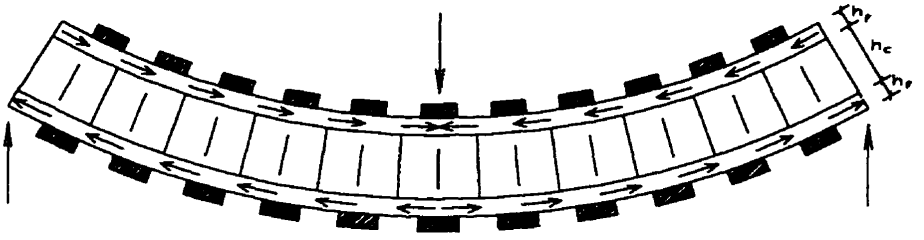

Figure 5.2: Stress Distribution in the Facesheets.

of the core are changed.

5.2.1 Fibre Failure Constraint

This constraint must guarantee that the tensile and compressive stresses in the strips of the facesheet net are less than the tensile and compressive allowable stresses of the strip material, respectively (Figure 5.2). The stresses in the x and y-directions are given by

$$\sigma_x = E_{11}\left(h_f + \frac{h_c}{2}\right)\kappa(1) \tag{5.8}$$

$$\sigma_y = E_{22}\left(h_f + \frac{h_c}{2}\right)\kappa(2) \tag{5.9}$$

where $\kappa(1)$ and $\kappa(2)$ are the x and y-curvatures, respectively, and h_c is the thickness of the core. The strip stresses are determined in the region where there is no overlap of strips, since in the overlap region the stress level is less. Doing so, ensures that the worst region has been considered.

The constraint equations for this failure mode are

$$X_c \leq \sigma_x \leq X_t \qquad\qquad X_c \leq \sigma_y \leq X_t \tag{5.10}$$

where X_c is the compression allowable stress and X_t is the tensile allowable stress.

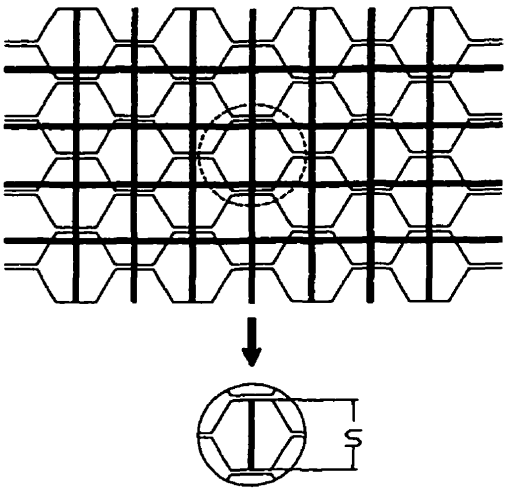

Figure 5.3: Intercell Buckling Constraint.

5.2.2 Intercell Buckling Constraint

This constraint imposes that, at a point of the plate, the compression stress on the fibre strip is less than the stress necessary to cause local buckling of the fibre strip in and out of the honeycomb cell. To determine this critical buckling stress, it is assumed that the fibre strip on the top of a cell is a simply supported beam and its buckling equation is [12, page 22]:

$$F_{ib_x} = \frac{\pi^2 E_{11}^h}{12}\left(\frac{h_f}{s}\right)^2 \tag{5.11}$$

$$F_{ib_y} = \frac{\pi^2 E_{22}^h}{12}\left(\frac{h_f}{s}\right)^2 \tag{5.12}$$

where s is the honeycomb-core cell size, Figure 5.3.

The constraint equations for this failure mode is

$$\sigma_x \geq -F_{ib_x} \qquad \sigma_y \geq -F_{ib_y} \tag{5.13}$$

where σ_x and σ_y are the compression stress in x and y-directions as defined in Equations 5.8 and 5.9, respectively.

Assuming that the strip buckling length is equal to the honeycomb cell size is in fact a

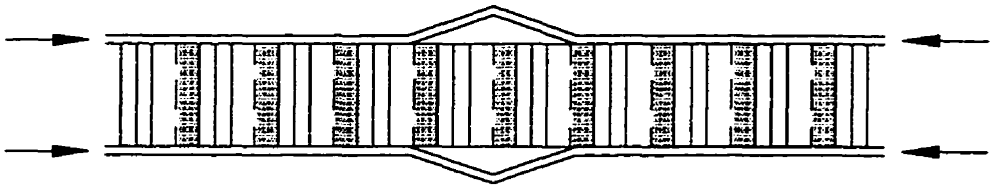

Figure 5.4: Face Wrinkling Instability.

conservative approach, as in most cases the strip is supported by a perpendicular strip in the domain of the open honeycomb cell (see Figure 5.3).

5.2.3 Wrinkling Constraint

Wrinkling is a phenomenon in which a facesheet buckles inwardly or outwardly depending on whether there is core compression failure or adhesive bond failure (Figure 5.4). Empirical equations for compressive strength used for the facesheet wrinkling strength evaluation are given in [40] as

$$F_{wc_x} = 0.82E_{11}^h \left(\frac{E_c h_f}{E_{11}^h h_c}\right)^{1/2} \tag{5.14}$$

$$F_{wc_y} = 0.82E_{22}^h \left(\frac{E_c h_f}{E_{22}^h h_c}\right)^{1/2} \tag{5.15}$$

where E_c is the compressive Young's modulus of the core.

The constraint equations for this failure mode is

$$\sigma_x \geq -F_{wc_x} \qquad \sigma_y \geq -F_{wc_y} \tag{5.16}$$

where σ_x and σ_y are the compressive stresses in x and y-directions, respectively.

5.3 Sensitivity Analysis

Information needed for the optimal design process is the way in which the objective function and the constraints change with the design variables (the sensitivity of structural response). To obtain this information requires a major computational effort during the optimization process. Therefore, efficient computational techniques are essential.

In all the procedures discussed before (Approaches 1 and 2), the derivatives of the objective function with respect to the design variables are straightforward. However, the sensitivity derivatives of stress and eigenvalue constraints cannot be determined analytically because they are both implicit function of the design variables, so a semi-analytical approach is used in which the derivatives are approximated by finite difference expressions.

5.3.1 The Sensitivity Derivatives of Stress

Using the Direct Method [49], the derivatives of the stress are calculated using the stress-displacement equations

$$\boldsymbol{\sigma} = \mathbf{S}\mathbf{u} \tag{5.17}$$

Implicit differentiation of Equation 5.17 with respect to the design variable x_i yields

$$\frac{\partial \boldsymbol{\sigma}}{\partial x_i} = \frac{\partial \mathbf{S}}{\partial x_i}\mathbf{u} + \mathbf{S}\frac{\partial \mathbf{u}}{\partial x_i} \tag{5.18}$$

The derivatives of the displacement are calculated using the displacement analysis equations

$$\mathbf{K}\mathbf{u} = \mathbf{F} \tag{5.19}$$

Differentiating of Equation 5.19 with respect to the design variable x_i yields

$$\frac{\partial \mathbf{K}}{\partial x_i}\mathbf{u} + \mathbf{K}\frac{\partial \mathbf{u}}{\partial x_i} = \frac{\partial \mathbf{F}}{\partial x_i} \tag{5.20}$$

Moving the first term of the left side to the right side and premultiplying Equation 5.20 by $\mathbf{K}^{-1}$ yields

$$\frac{\partial \mathbf{u}}{\partial x_i} = \mathbf{K}^{-1}\left(\frac{\partial \mathbf{F}}{\partial x_i} - \frac{\partial \mathbf{K}}{\partial x_i}\mathbf{u}\right) \tag{5.21}$$

Substituting Equation 5.21 into Equation 5.18 the derivatives of the stresses can be given as

$$\frac{\partial \boldsymbol{\sigma}}{\partial x_i} = \frac{\partial \mathbf{S}}{\partial x_i}\mathbf{u} + \mathbf{S}\mathbf{K}^{-1}\left(\frac{\partial \mathbf{F}}{\partial x_i} - \frac{\partial \mathbf{K}}{\partial x_i}\mathbf{u}\right) \tag{5.22}$$

where $\partial \mathbf{S}/\partial x_i$ and $\partial \mathbf{K}/\partial x_i$ are calculated using forward finite differences

$$\frac{\partial \mathbf{S}}{\partial x_i} \approx \frac{\mathbf{S}(x_i + \Delta x_i) - \mathbf{S}(x_i)}{\Delta x_i} \tag{5.23}$$

$$\frac{\partial \mathbf{K}}{\partial x_i} \approx \frac{\mathbf{K}(x_i + \Delta x_i) - \mathbf{K}(x_i)}{\Delta x_i} \tag{5.24}$$

5.3.2 The Sensitivity Derivatives of an Eigenvalue

The constraint equation for the first natural frequency is given by

$$g = \overline{\Omega}_1 - \Omega_1. \tag{5.25}$$

The derivative of this constraint with respect to the design variable x_i is given by

$$\frac{\partial g}{\partial x_i} = -\frac{\partial \Omega_1}{\partial x_i}. \tag{5.26}$$

Using the semi-analytical approach, the derivative of the first eigenvalue with respect to a design variable is given by [38]

$$\frac{\partial \Omega}{\partial x_i} = \frac{1}{2\Omega} \frac{\mathbf{u}^T \left(\partial \mathbf{K}/\partial x_i - \Omega^2 \partial \mathbf{M}/\partial x_i\right) \mathbf{u}}{\mathbf{u}^T \mathbf{M} \mathbf{u}} \tag{5.27}$$

where $\mathbf{u}$ is the mode shape corresponding to the least natural frequency. The expression to determine $\partial \mathbf{K}/\partial x_i$ is given in Equation 5.24 and $\partial \mathbf{M}/\partial x_i$ are calculated as

$$\frac{\partial \mathbf{M}}{\partial x_i} \approx \frac{\mathbf{M}(x_i + \Delta x_i) - \mathbf{M}(x_i)}{\Delta x_i} \tag{5.28}$$

5.4 Optimization Algorithm

Many survey articles have been published in the field of structural optimization [2, 34, 37, 78, 82, 101]. From these papers, it is possible to see that there is no consensus regarding the numerical methods that are most suitable to determine an optimal design. Because of this, it is necessary to evaluate a number of the available methods on the specific problem of interest.

As mentioned in the Chapter 2, if the designer intends to use a method based on gradients of the objective function and constraints, it is necessary to consider three related

procedures. The first deals with the constraints, the second defines the search direction and the third completes the unidirectional search.

From all the methods discussed in Section 2.7, it is possible to form many combinations or sets of algorithms to solve the optimization problem. Before choosing some of these sets, it is worth reviewing a number of points mentioned in Chapter 2.

In Section 2.7, there are five strategies for considering the constraints: four penalty function methods and the method of centres. Since some of the problems presented in this work has only one constraint (the first natural frequency to be greater than a specified value), the method of the centres in not recommended, because in this case the problems are underconstrained and the linear approximations are unbounded. Among the penalty function methods, Powell [81] emphasized the importance of including Lagrange multipliers in penalty function methods, making the Augmented Lagrange Multiplier Method the most recommended penalty function method. Vanderplaats [108, pages 147–150] show this by comparing the performance of all four methods when applied to find the optimal design of a cantilevered beam under concentrated load at its free edge. His results illustrate that for this specific problem, the Augmented Lagrange Multiplier Method performs best.

Five methods are described in Section 2.7 which may be used to define the search direction. Figure 2.11 shows clearly that unless the objective function has no slope eccentricity, the steepest descent method should not be used to define the search direction. However, it has been using as an initial search direction in other algorithms. The gradient projection method also has weak points; it has satisfactory performance only when the active constraints (constraints close to be violated) are convex, otherwise the solution can be trapped at every point where the active constraint is concave.

Once the search direction has been defined, Section 2.7 presents two methods for the one directional search. The polynomial approximation usually requires fewer function evaluations to reach the optimum. However, it can define infeasible designs that results in convergence difficulties for some optimization algorithms.

Considering all the above, four sets were chosen to test the constraint enforcement strategies. The dimensional characteristics of the plate used to test the four sets are given in Table 5.1, while the material properties are presented in Table 5.2. The algorithm sets are defined in Table 5.3. Four different algorithms were chosen to deal with the constraints: Exterior Penalty Function Method, Linear Extended Interior Penalty Function Method,

Description	Dimension
a [m (in)]	1.75 (69.09)
b [m (in)]	2.58 (101.61)
h_f [mm (in)]	0.15 (0.0059)
h_c [mm (in)]	21.70 (0.8543)

Table 5.1: Dimensions of the Isotropic Sandwich Plate.

Property	Facesheet	Core
E_{11} [GPa (10^6 psi)]	200. (31.18)	
E_{22} [GPa (10^6 psi)]	7.03 (1.02)	
G_{12} [GPa (10^6 psi)]	4.48 (0.65)	
ν_{12}	0.3	
G_{z1} [MPa (10^3 psi)]		138. (20.)
G_{2z} [MPa (10^3 psi)]		82.7 (12.)
ρ [kg/m^3 (10^{-3} lbm/in^3)]	1650. (59.61)	25.6 (0.9259)

Table 5.2: Material Properties of the Composite Sandwich Plate.

Augmented Lagrange Multiplier Method and Sequential Linear Programming Method. For the first three sets, the Conjugate Directions Method was used to define the search direction. The Method of Feasible Directions was included in the fourth set. For all four sets, the Golden Section Method was used for the unidirectional search.

Tables 5.4, 5.5 and 5.6 summarise the performance of these sets when applied in conjunction with Approaches 1, 2A and 2B, respectively. These tables present the optimal value of the objective function and the number of function evaluations needed to reach the optimal design for a different number of design variables (NDV), using the four preselected sets.

From these tables it is possible to see that Sets 3 and 4 give the best results. Set 3 performs better than Sets 1 and 2. This is in agreement with Powell [81], who noted that any Sequential Unconstrained Minimization Technique which does not include Lagrange multipliers is obsolete as a practical optimization tool. However, when the number of function evaluations is considered, it can be concluded that Set 4 requires fewer function evaluations to reach the optimum (less computer time). For this reason this set was chosen

Set 1	Exterior Penalty Function Conjugate Direction Method Golden Section Method
Set 2	Linear Extended Interior Penalty Function Method Conjugate Direction Method Golden Section Method
Set 3	Augmented Lagrange Multiplier Method Conjugate Direction Method Golden Section Method
Set 4	Sequential Linear Programming Method of Feasible Direction Golden Section Method

Table 5.3: The Chosen Sets.

SETS	1		2		3		4	
NDV	Opt. Obj. Func.	N. Func. Eval.	Opt. Obj. Func.	N. Func. Eval.	Opt. Obj. Func.	N. Func. Eval.	Opt. Obj. Func.	N. Func. Eval.
1	1.2903	181	1.2905	335	1.2904	146	1.2343	12
2	1.1989	297	1.1995	610	1.1989	241	1.1988	93
4	1.0201	341	1.0413	737	1.0207	480	1.0190	57
8	1.0223	234	1.0848	718	1.0193	381	0.9969	257
16	1.0222	253	1.3761	650	1.0174	357	0.9970	9

Table 5.4: Performance Using Method 1.

SETS	1		2		3		4	
NDV	Opt. Obj. Func.	N. Func. Eval.	Opt. Obj. Func.	N. Func. Eval.	Opt. Obj. Func.	N. Func. Eval.	Opt. Obj. Func.	N. Func. Eval.
1	1.1763	287	1.1765	489	1.1763	106	1.1756	14
2	1.0839	456	1.0840	551	1.0838	701	1.0830	59
3	1.0251	491	1.0971	397	1.0258	650	1.0240	90
4	1.0286	566	1.0958	402	1.0244	1254	1.0241	169
5	1.0423	577	1.1233	418	1.0080	1135	1.0004	71

Table 5.5: Performance Using Method 2.

SETS	1		2		3		4	
NDV	Opt. Obj. Func.	N. Func. Eval.	Opt. Obj. Func.	N. Func. Eval.	Opt. Obj. Func.	N. Func. Eval.	Opt. Obj. Func.	N. Func. Eval.
1	1.2881	661	1.3051	703	1.2497	476	1.2464	14
2	1.0475	501	1.0476	579	1.0473	706	1.0463	77
3	1.0279	479	1.0352	531	1.0269	1424	1.0267	156
4	1.0278	581	1.0215	579	1.0223	440	1.0290	119
5	1.0345	539	1.0265	588	1.0142	519	1.0233	47

Table 5.6: Performance Using Method 3.

to be used in future calculations.

Comparing convergence of the three approaches as the number of design variables increases, it may be seen that in some cases the convergence is not uniform as expected. The reason for this is that the point defining the optimal design is on a surface corresponding to the natural frequency constraint. Numerically, this surface has an acceptance band; therefore, a point constrained by this surface may violate the constraint (within a prescribed tolerance) and be in the infeasible space. Thus, when the number of design variables increases, the solution is pushed back to the feasible space and sometimes this causes the objective function to increase.

In this chapter the optimization approaches used were investigated and evaluated. The objective function, design variables and constraints were also defined and the numerical optimization method was chosen. In the next chapter several problems will be solved using these parameters in order to understand their effects on the optimal design of composite sandwich plates.

Chapter 6

Composite Sandwich Plate Optimization

This chapter presents the results of several optimization studies. The objective is to minimize the mass of a composite sandwich plate with a prescribed first natural frequency and certain failure loads as constraints. The density of the facesheet material is defined as a design variable. In this case, the facesheets are assumed to be composed of an orthotropic net of unidirectional fibre composite strips. The stiffnesses of the facesheets are altered by changing the widths and the spacings between the strips.

6.1 Rectangular Composite Sandwich Plates

The first structure to be considered is a simple supported square plate with facesheets constructed from an orthogonal net of unidirectional carbon–fibre/epoxy composite strips. The core material is an orthotropic aluminium honeycomb. Figure 6.1 gives an illustration of the plate and its geometry as well as providing an exploded view of the orthogonal composite net and aluminium honeycomb. The mechanical properties of the composite and honeycomb are summarised in Table 6.1. In order to provide a reference value for the optimization, a calculation was completed with 40% of the unidirection composite in both the x any y-directions; the first natural frequency for this design is 21.47 Hz. This natural frequency will be used as a lower bound on the first natural frequency of the plates in the optimization work.

The optimal composite facesheet distribution for a plate of the same geometry is inves-

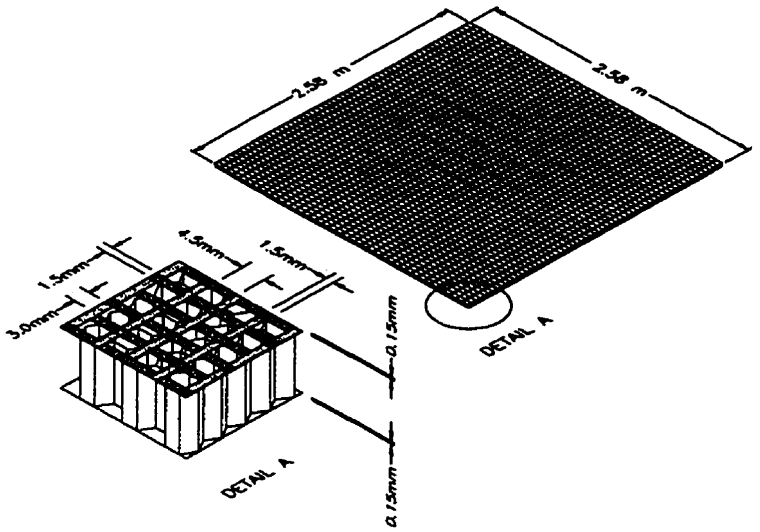

Figure 6.1: Dimensions of the Square Plate.

Property	Carbon Fibre/Epoxy	Aluminium Honeycomb
E_{11} [GPa (10^6 psi)]	215. (36.4)	
E_{22} [GPa (10^6 psi)]	7. (1.02)	
G_{12} [GPa (10^6 psi)]	4.50 (0.65)	
ν_{12}	0.3	
G_{z1} [MPa (10^3 psi)]		138. (20.)
G_{2z} [MPa (10^3 psi)]		138. (20.)
ρ [kg/m^3 (10^{-3} lbm/in^3)]	1650. (59.61)	25.6 (0.9259)

Table 6.1: Material Properties of the Square Plate.

tigated using Approach 1. As described in Chapter 5, in this approach the facesheets are discretized into bands in both x and y-directions and the design variables are the material density in each of this bands. In this problem the mass of the facesheets is minimized and the first natural frequency of 21.47 Hz is alone considered as a lower bound constraint. The optimal layout of the facesheet is investigated when the number of design variables increases (the number of bands are augmented). In this problem, the material density in each band ranges from 10% to 90%. There are two main motivations to impose limits on the material density: first, for practical design applications, it is reasonable to have a minimum amount of material so that the solar cell can be laid on it; and second, when the material density approaches to 0% or 100%, the material properties change rapidly resulting in some numerical instabilities in the optimization process.

Initially, only one design variable is considered in each direction. Then this number is doubled several times until there are sixteen design variables in each direction. Since the plate is square, it is assumed that the optimal material distribution of the facesheet is symmetric. This means that, when there are N design variables in one direction, the plate is divided in 2N bands in that direction and the material distribution is symmetric about the plate centre line.

Figures 6.2 to 6.6 present the optimal designs for 2, 4, 8, 16 and 32 bands (1, 2, 4, 8 and 16 design variables) in each direction, respectively. As may be expected, these results show that the optimal design concentrates the material at the centre region of the plate, in both directions. In this calculation, six terms in the series expansion and thirty integration points were used, in both directions.

Figure 6.7 illustrates the changes in the objective function as the number of design variables increases. The mass of the facesheets for the first optimal design (two design variables) is 2.52 kg. When the number of design variables is increased to 32, the mass of the facesheets decreases to 2.23 kg. This means a 12% saving in the mass of the facesheets.

Another factor investigated in this problem is the influence of the aspect ratio (a/b) on the optimal design. Tables 6.3 to 6.6 present the optimal design for plates with different aspect ratios using 2, 4, 8 and 16 design variables. The results presented in these tables are in accordance with the sketch shown in Figure 6.8. To determine the values of the first natural frequency to be applied as a lower limit constraint for each aspect ratio problem, the first natural frequency of sandwich plates with these aspect ratios and a uniform material

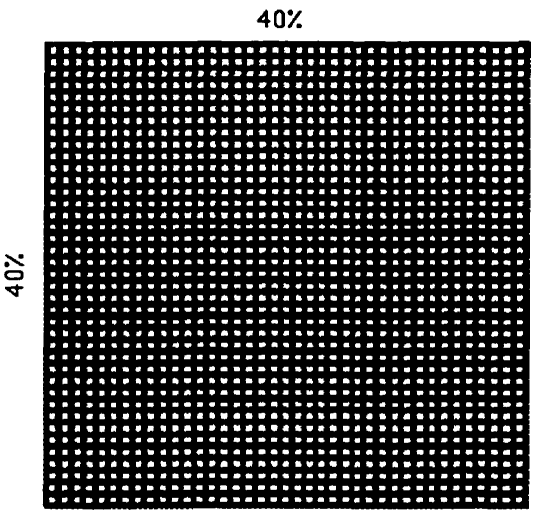

Figure 6.2: Optimal Design with 2 Design Variables.

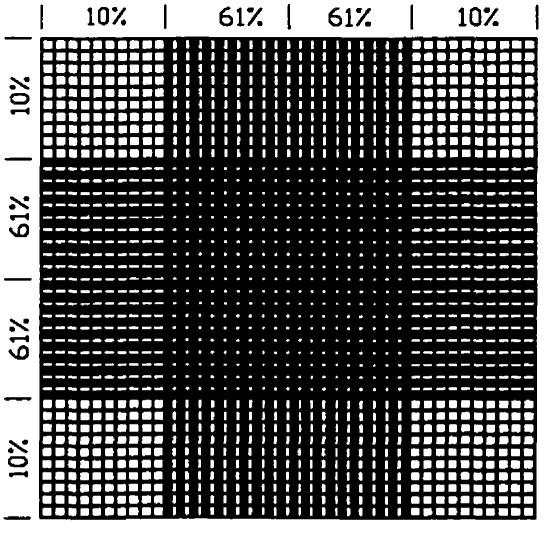

Figure 6.3: Optimal Design with 4 Design Variables.

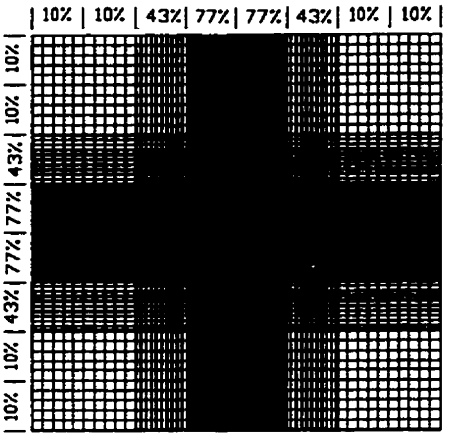

Figure 6.4: Optimal Design with 8 Design Variables.

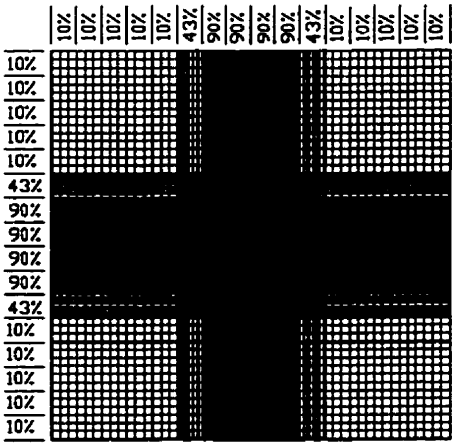

Figure 6.5: Optimal Design with 16 Design Variables.

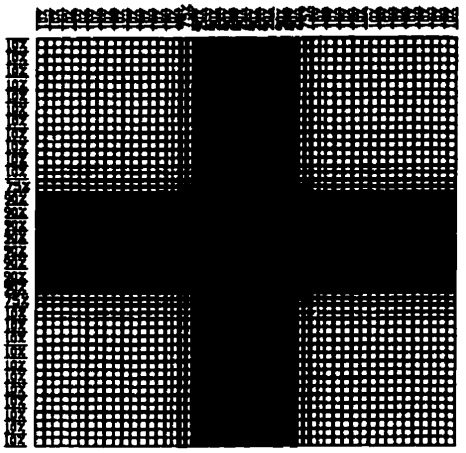

Figure 6.6: Optimal Design with 32 Design Variables.

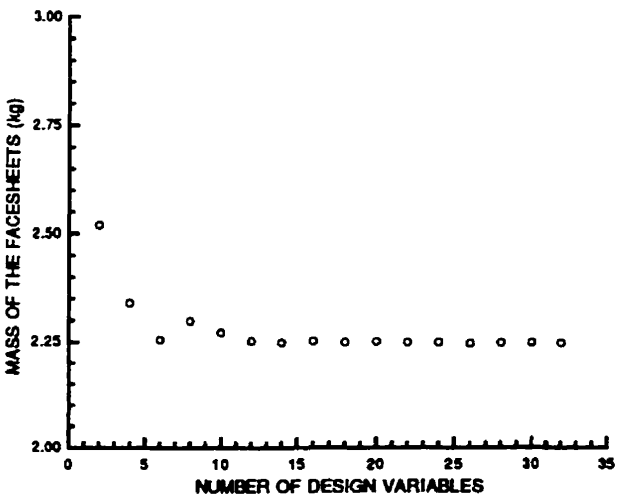

Figure 6.7: Convergence of the Objective Function with the Number of Design Variables Using Approach 1.

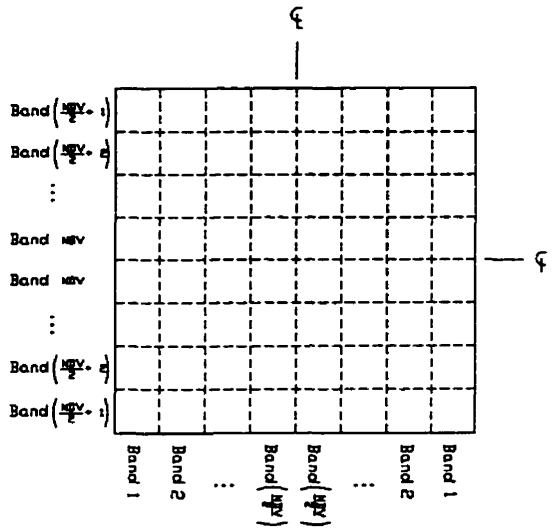

Figure 6.8: Sketch for the Results Presented in Tables 6.2 to 6.6.

distribution were calculated. These reference solutions have, as in the first case, facesheets with a 40% material density in both directions (Table 6.2).

From these results, it is possible to observe that even a small variation in the aspect ratio ($a/b \leq 0.90$) causes large changes on the layout of the optimal plate design. The optimal design has only the minimum amount of material allowed (10%) oriented in the long dimension of the plate. As consequence of this, as the aspect ratio decreases the weight saving increases, as shown in Table 6.7. This provides a simple but useful guideline for designers.

Another interesting observation from these results is that as the aspect ratio decreases, instead of concentrating all the material in the centre region of the plate, the optimizer starts to accumulate material in several regions along the long side of the plate. The spacing of these bands are regular and have the appearance of stiffeners.

All the results given so far were obtained applying Approach 1. Now, the optimal designs using Approaches 2A and 2B are presented and compared with the results obtained using Approach 1.

As described in Chapter 5, Approaches 2A and 2B are reduced basis formulations in which the material density is specified by a linear combination of orthogonal basis functions. Figure 6.9 and 6.10 show the change in material density distribution as the number of design variables increases using Approaches 2A and 2B, respectively. In the calculation of the first

Aspect Ratio (a/b)	First Natural Frequency (Hz)
1.00	21.47
0.95	22.64
0.90	24.05
0.85	25.76
0.80	27.85
0.75	30.43
0.50	58.56
0.25	215.2

Table 6.2: Lower Limit for the First Natural Frequency Constraint.

Aspect Ratio (a/b)	Material Distribution (%)	
	Band in X-Direction	Band in Y-Direction
	1	1
1.00	40.	40.
0.95	46.	29.
0.90	61.	10.
0.85	56.	10.
0.80	51.	10.
0.75	41.	10.
0.50	36.	10.
0.25	32.	10.

Table 6.3: Aspect Ratio Study: 2 Design Variables

Aspect Ratio (a/b)	Material Distribution (%)			
	Bands in X-Direction		Bands in Y-Direction	
	1	2	1	2
1.00	10.	61.	10.	61.
0.95	10.	88.	10.	23.
0.90	10.	87.	10.	10.
0.85	10.	77.	10.	10.
0.80	10.	70.	10.	10.
0.75	10.	63.	10.	10.
0.50	10.	47.	10.	10.
0.25	27.	37.	10.	10.

Table 6.4: Aspect Ratio Study: 4 Design Variables

Aspect Ratio (a/b)	Material Distribution (%)							
	Bands in X-Direction				Bands in Y-Direction			
	1	2	3	4	1	2	3	4
1.00	10.	10.	43.	77.	10.	10.	43.	77.
0.95	10.	10.	90.	90.	10.	10.	10.	31.
0.90	10.	10.	85.	90.	10.	10.	10.	10.
0.85	10.	10.	63.	90.	10.	10.	10.	10.
0.80	10.	10.	46.	90.	10.	10.	10.	10.
0.75	10.	10.	33.	90.	10.	10.	10.	10.
0.50	10.	10.	47.	47.	10.	10.	10.	10.
0.25	10.	39.	28.	35.	10.	10.	10.	10.

Table 6.5: Aspect Ratio Study: 8 Design Variables

Aspect Ratio (a/b)	Band Direction	Material Distribution (%)							
		1	2	3	4	5	6	7	8
1.00	X	10.	10.	10.	10.	10.	43.	90.	90.
	Y	10.	10.	10.	10.	10.	43.	90.	90.
0.95	X	10.	10.	10.	10.	90.	90.	90.	90.
	Y	10.	10.	10.	10.	10.	10.	11.	52.
0.90	X	10.	10.	10.	10.	80.	90.	90.	90.
	Y	10.	10.	10.	10.	10.	10.	10.	10.
0.85	X	10.	10.	10.	10.	42.	82.	90.	90.
	Y	10.	10.	10.	10.	10.	10.	10.	10.
0.80	X	10.	10.	10.	10.	10.	78.	90.	90.
	Y	10.	10.	10.	10.	10.	10.	10.	10.
0.75	X	10.	10.	10.	10.	10.	69.	82.	82.
	Y	10.	10.	10.	10.	10.	10.	10.	10.
0.50	X	10.	10.	10.	10.	22.	81.	54.	29.
	Y	10.	10.	10.	10.	10.	10.	10.	10.
0.25	X	10.	10.	20.	61.	27.	16.	54.	24.
	Y	10.	10.	10.	10.	10.	10.	10.	10.

Table 6.6: Aspect Ratio Study: 16 Design Variables

Aspect Ratio (a/b)	Weight Initial Design	Weight Optimal Design	Weight Saving (%)
1.00	2.52	2.23	-12
0.95	2.39	2.04	-15
0.90	2.27	1.74	-23
0.85	2.14	1.48	-31
0.80	2.02	1.28	-37
0.75	1.89	1.12	-41
0.50	1.26	0.63	-50
0.25	0.63	0.31	-51

Table 6.7: Weight Savings for Different Aspect Ratios.

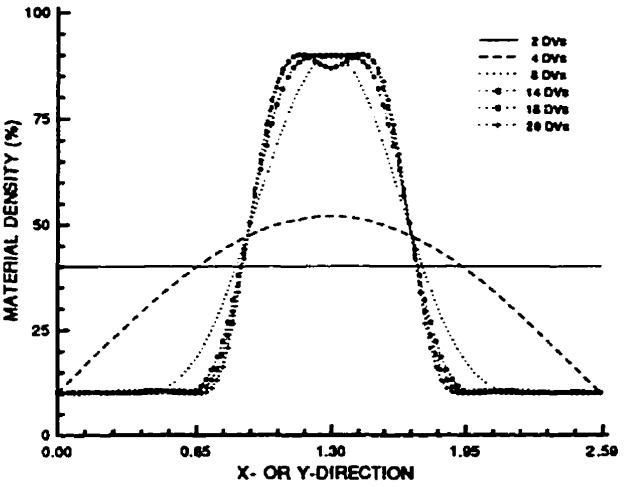

Figure 6.9: Change of Material Distribution Along the One Direction as the Number of Design Variables Increases: Approach 2A.

natural frequency with different facesheet layouts, the analysis subroutine used six terms in the series expansions and twenty-seven integration points in each direction.

The final step is to compare the final optimal designs obtained with the three methods; this comparison is illustrated in Figure 6.11. These results indicate that all three methods converge to similar material distributions. However, the plot of objective function (mass of the facesheets) as a function of number of design variables (Figure 6.12) shows that Approaches 2A and 2B converge to the similar values, but Approach 1 defines a lighter structure. This happens because the solutions given by Approaches 2A and 2B are restricted to the class of curves obtainable by a set of preselected functions. Another conclusion resulting from these calculations is that Approach 2A is preferable to Approach 2B. That is, both methods give almost the same results, but the set of orthogonal functions used in Approach 2B requires more computer time for processing.

In order to overcome the possibility of the optimal solution been trapped in a local minimum, the following procedure was adopted for the three methods. For the simplest problem (two design variables), the initial design was chosen with high material density (a feasible design). Then, for each new optimization problem, with an increased number of design variables, the chosen initial design was the optimal design of the previous problem (with less design variables). This procedure was verified by searching for the optimal solution

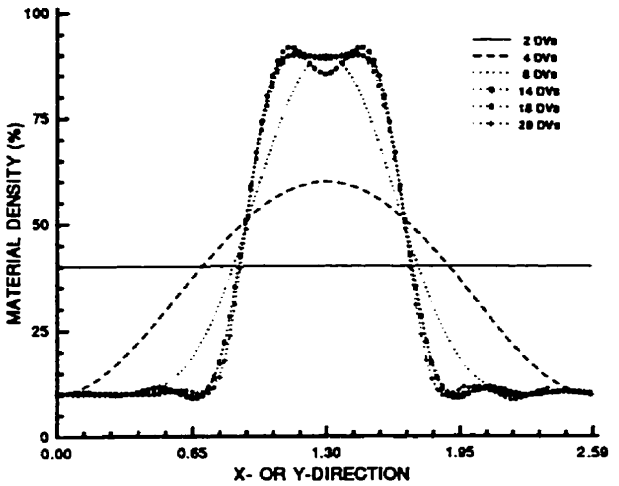

Figure 6.10: Change of Material Distribution Along the One Direction as the Number of Design Variables Increases: Approach 2B.

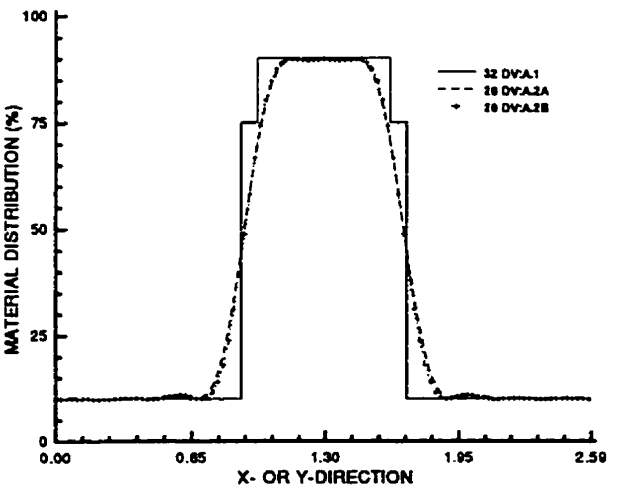

Figure 6.11: Material Distribution Given by the Three Approaches.

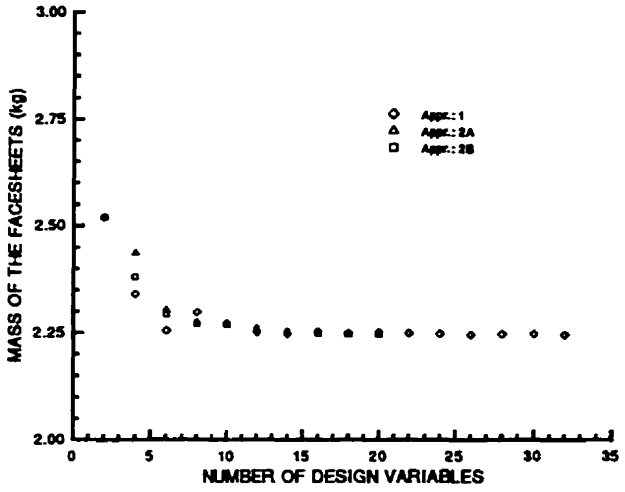

Figure 6.12: Convergence of the Objective Function using the Three Approaches.

based on an initial design in which all strips had the maximum allowed material density. The results of these calculation were that, the optimal objective functions were equal or higher than the objective functions determined using the procedure previously described.

Another strategy was used when the optimal design had any design variable out of the feasible space, (because of the prescribed tolerance for the constraints); in such case the design variables were increased by 1% and the optimization search restarted. This procedure was repeated until all design variables were feasible or until the number of restarted processes reached a predefined limit; in both cases the resulting design was accepted.

One way to determine the efficiency of a method is to determine the number of times that the objective function and the constraints are evaluated, during a run. This count varies as function of the initial design, the number of design variables and other optimization parameters such as the constraint tolerances. A comparison of this numerical effort for the three methods is presented in Figure 6.13. This figure summarises the number of objective function and constraint evaluations as a function of the number of design variables. It can be seen that Approach 1 requires many more function evaluations than Approaches 2A and 2B.

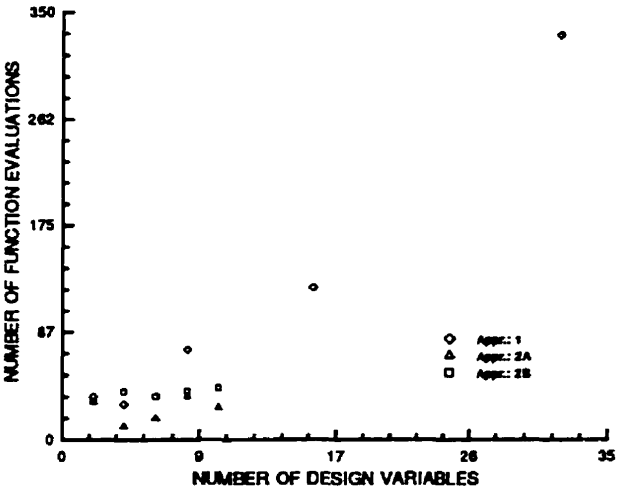

Figure 6.13: The Number of Function Evaluation as Function of the Number of Design Variables.

6.2 Structural Support for Satellite Solar Array

Consider now the composite sandwich plate used as structural support for the solar array of the China-Brazil Earth Resources Satellite - CBERS (Figure 1.1). This remote sensing satellite has been developed in a joint program between the Brazilian and Chinese governments. This sandwich plate has facesheets composed of carbon fibre/epoxy nets and core of aluminium honeycomb (Figure 1.2). The panel schema with its dimensions are given in Figure 1.3. Also, Table 6.8 presents the mechanical properties of the carbon fibre/epoxy strips (M40/epoxy) and the aluminium honeycomb (3/8 5056-.001). These values originate from the CBERS initial design. During the project some of these dimensions were altered.

In the optimization of this panel, the mass of the facesheets is the objective function, because the dimensions and material properties of the core are kept constant. In addition, considering only the mass of the facesheets makes the objective function more sensitive to changes in the design variables. The stiffness constraint is defined by the lower bound of the first natural frequency, which is 36.87 Hz (the first natural frequency of the original panel).

This problem will also be used to compare the performance of the three methods described in Chapter 5 (Approaches 1, 2A and 2B). Figures 6.14 to 6.16 present the optimal

Property	Carbon Fibre/Epoxy	Aluminium Honeycomb
E_{11} [GPa (10^6 psi)]	215. (36.4)	
E_{22} [GPa (10^6 psi)]	7. (1.02)	
G_{12} [GPa (10^6 psi)]	4.50 (0.65)	
ν_{12}	0.3	
G_{z1} [MPa (10^3 psi)]		138. (20.)
G_{2z} [MPa (10^3 psi)]		138. (20.)
ρ [kg/m^3 (10^{-3} lbm/in^3)]	1650. (59.61)	25.6 (0.9259)

Table 6.8: Material Properties of the Solar Array Support.

material distribution in the x-direction using the three approaches. Based on the aspect ratio results of the previous section, it was assumed that the optimal design would have the minimum material volume allowed in the y-direction (10%). Therefore, only the material distribution in the x-direction is considered. These figures illustrate how the material distribution changes when the number of design variables increases for the three methods.

From Figure 6.17 it can be seen that the results of all methods converge to essentially the same design. However, the optimal material distributions obtained from Approaches 2A and 2B are smoother than the distributions obtained from Approach 1, which is felt to be a desirable result.

Figure 6.18 shows how the optimal mass changes when the number of design variables increases. Different from the previous problem, now all the methods converge to the same value. In this problem the objective function decreased from 1.34 kg to 1.06 kg, which represents a 20.9% saving in the mass of the facesheets (7.0 % in the overall mass of the plate). Since the reference design is an actual piece of space hardware this is considered to be a significant improvement.

In order to obtain a more realistic design, the next problem to be presented considers three failure modes: fibre failure, intercell buckling and wrinkling instability.

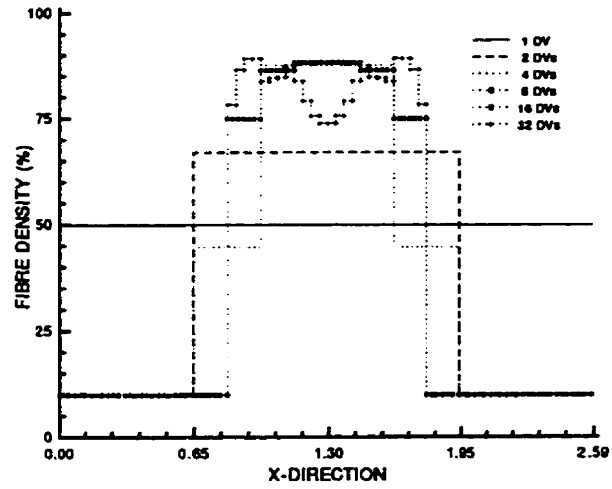

Figure 6.14: Optimal Material Distribution in the Solar Array Support Given by Approach 1.

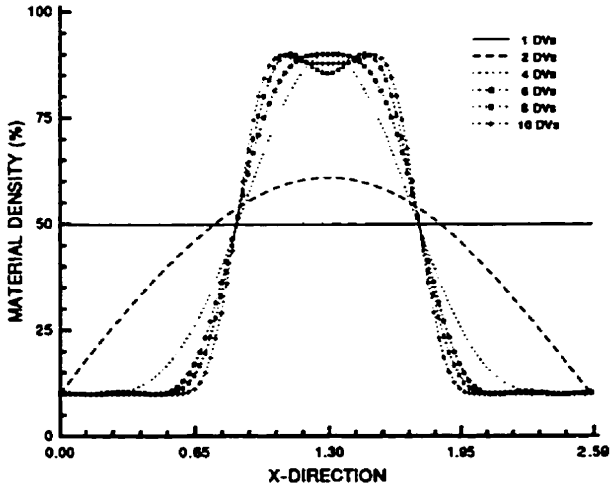

Figure 6.15: Material Distribution in the Solar Array Support Given by Approach 2A.

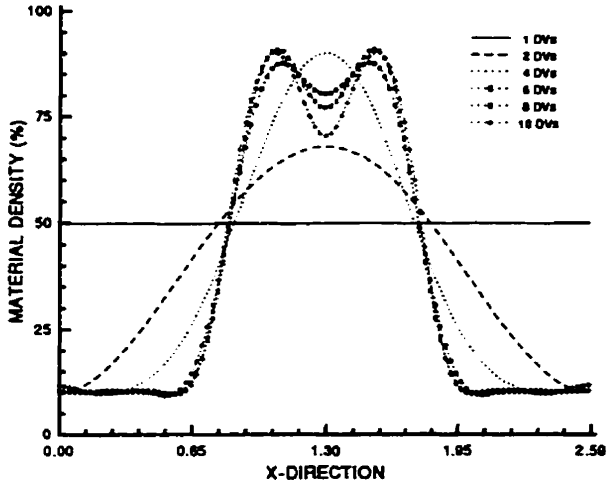

Figure 6.16: Material Distribution in the Solar Array Support Given by Approach 2B.

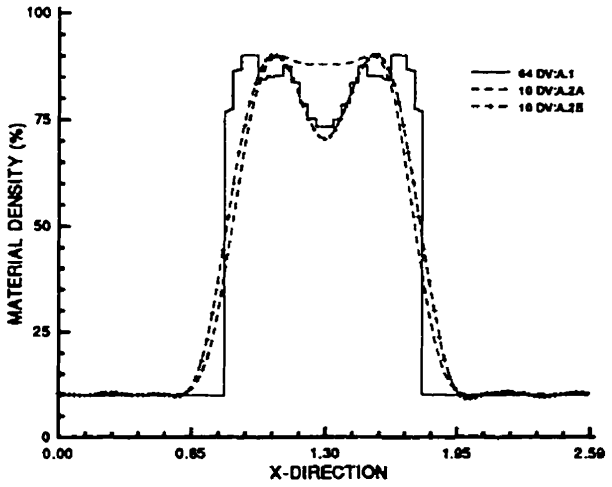

Figure 6.17: Comparison of the Approaches.

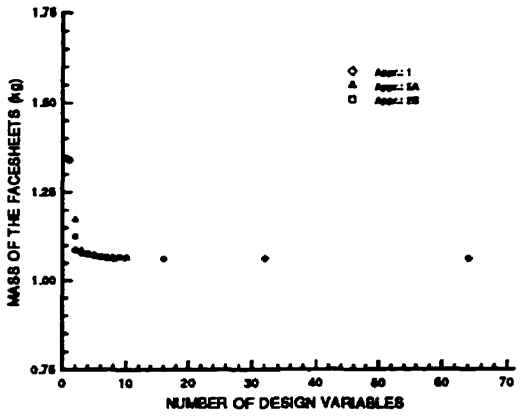

Figure 6.18: Objective function versus NDV for the Solar Array Support.

6.3 Rectangular Plates with Failure Constraints

The optimal design of the square composite sandwich plate is investigated again, but, this time, besides the first natural frequency constraint, three failure load constraints are considered: fibre failure, intercell buckling and wrinkling instability. As described in Section 5.3, these failure constraints are related to the strength and buckling requirements that a composite sandwich plate must fulfill and that are affected by changing the stiffness distribution of the facesheets.

In order to determine a set of reference stresses and strains in the panel, it is assumed that the panel is subjected to a 20 g (196.20 m/s^2) acceleration in a direction perpendicular to the panel. This acceleration value is reasonable for a satellite structure launched by a solid fuel rocket [94] and represents a worse case scenario.

For the same reason that some points have to be selected to verify the material density limit constraints for Approaches 2A and 2B (Section 5.1.2), another set of points is chosen to verify the failure load constraints. In Approach 1, these points are defined at the intersection of the mesh formed by the borders of the bands with uniform material density. In Approaches 2A and 2B, these points are selected in positions related to the nodes and peaks of the orthogonal functions specifying the material distribution.

The dimensions, material properties and the first natural frequency constraint for this problem were presented in Section 6.1. The allowable stresses for carbon fibre/epoxy composite are given in Table 6.9. In this table: X_t is the axial strength in tension; X_C is the

Description	Carbon Fibre
X_t [MPa ($x10^3$ psi)]	310. (49.0)
X_C [MPa ($x10^3$ psi)]	310. (49.0)
S [MPa ($x10^3$ psi)]	155. (24.5)

Table 6.9: Carbon Fibre Composite Strength Allowable.

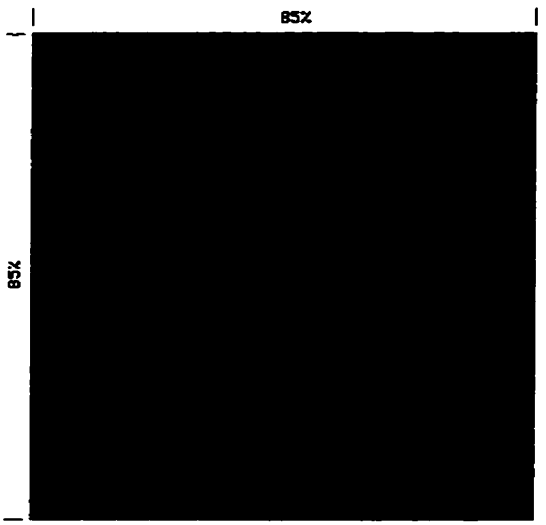

Figure 6.19: Optimal Design with 2 Design Variables.

axial strength in compression; and S is the shear strength allowable.

The optimal design of the plate is analysed following the same procedure described in Section 6.1. Figures 6.19 to 6.23 present the optimal design for 2, 4, 8, 16 and 32 design variables, respectively. The figures illustrate that, as before, the optimal design concentrates material at the centre of the plate, but the change in material density from one band to another is smoother this time. Another interesting result is the fact that as the number of design variables increases, the optimal design has less material at the border and more at the centre of the plate. However, if the number of design variables is further increased and the amount of material at the centre of the plate reaches an upper limit, material is moved from the quarter-point region of the plate and placed at the border. As may be seen by comparing Figures 6.22 and 6.23.

To understand which set of constraints drives the optimal design, Figures 6.24 to 6.38 show the values of the three failure load constraints for different numbers of design variables.

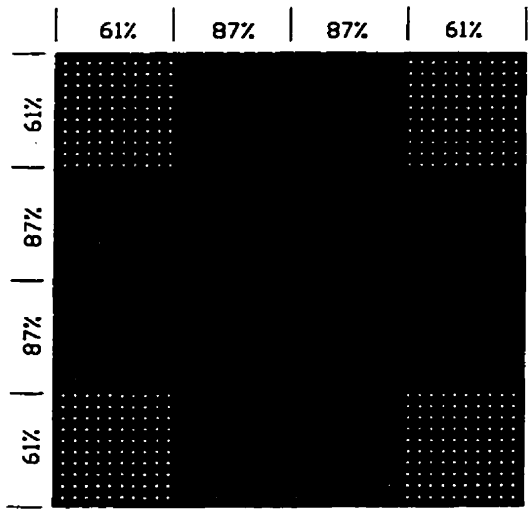

Figure 6.20: Optimal Design with 4 Design Variables.

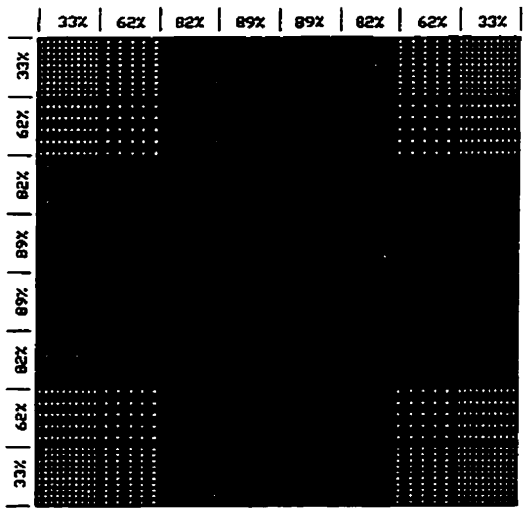

Figure 6.21: Optimal Design with 8 Design Variables.

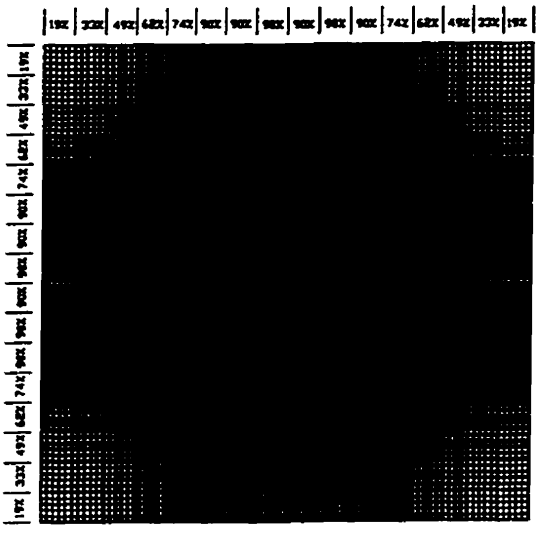

Figure 6.22: Optimal Design with 16 Design Variables.

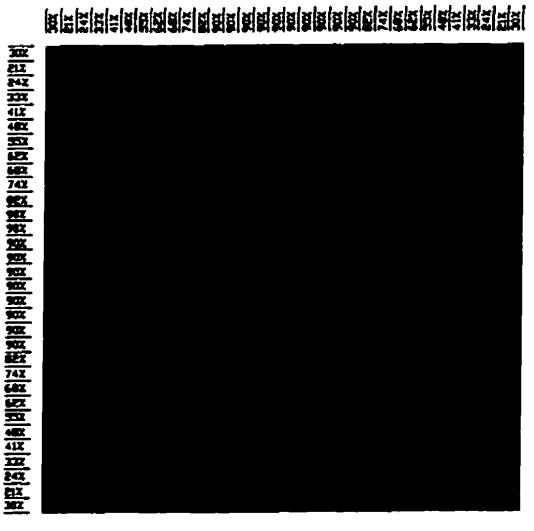

Figure 6.23: Optimal Design with 32 Design Variables.

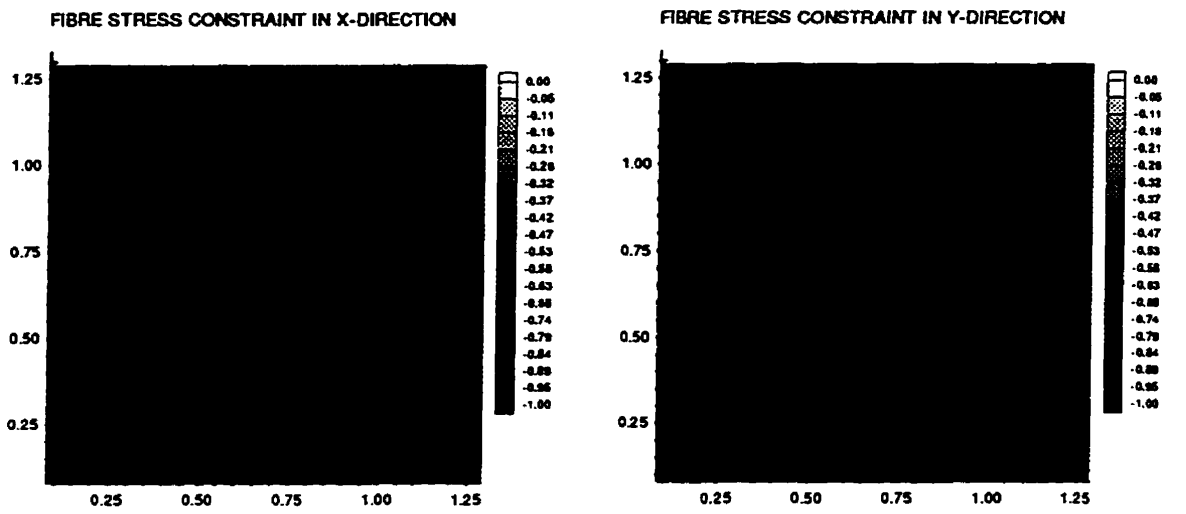

Figure 6.24: Fibre Stress Constraint for Optimal Design with 2 Design Variables.

These figures present only the first quadrant of the plate ($0 \leq x \leq a/2$ and $0 \leq y \leq b/2$), since the plate has four fold symmetry about the centre lines. The table appearing in the figures gives the value of the constraints the way that is considered by the optimization code:

$$g = \frac{\sigma}{\sigma_{adm}} - 1 \tag{6.1}$$

where g is the value of the constraint and it should be less or equal to zero, σ is the actual stress at a point of the plate and σ_{adm} is the allowable stress. So, when $g > 0$ means that the constraint is violated.

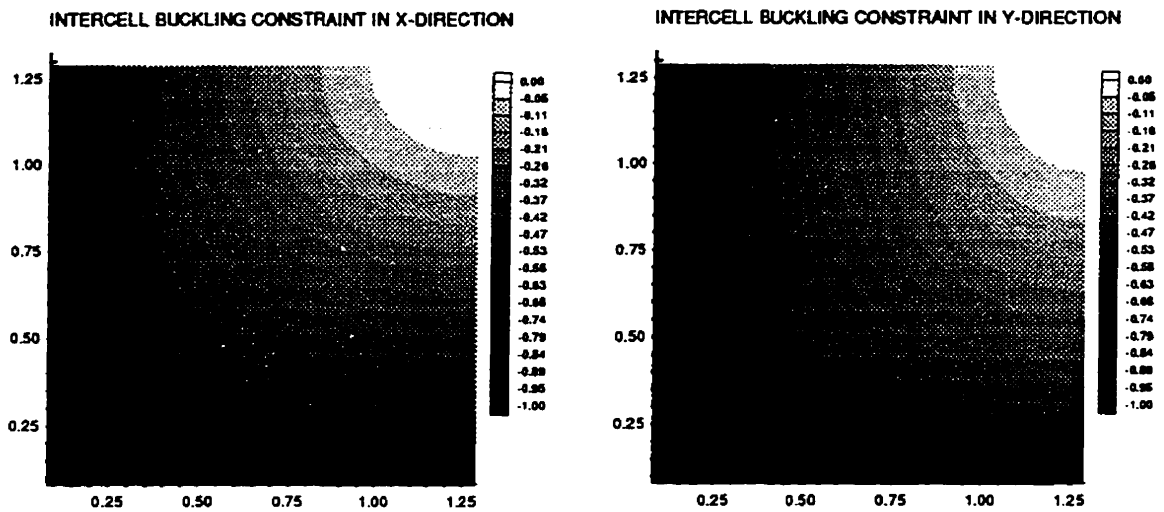

Figure 6.25: Intercell Buckling Constraint for Optimal Design with 2 Design Variables.

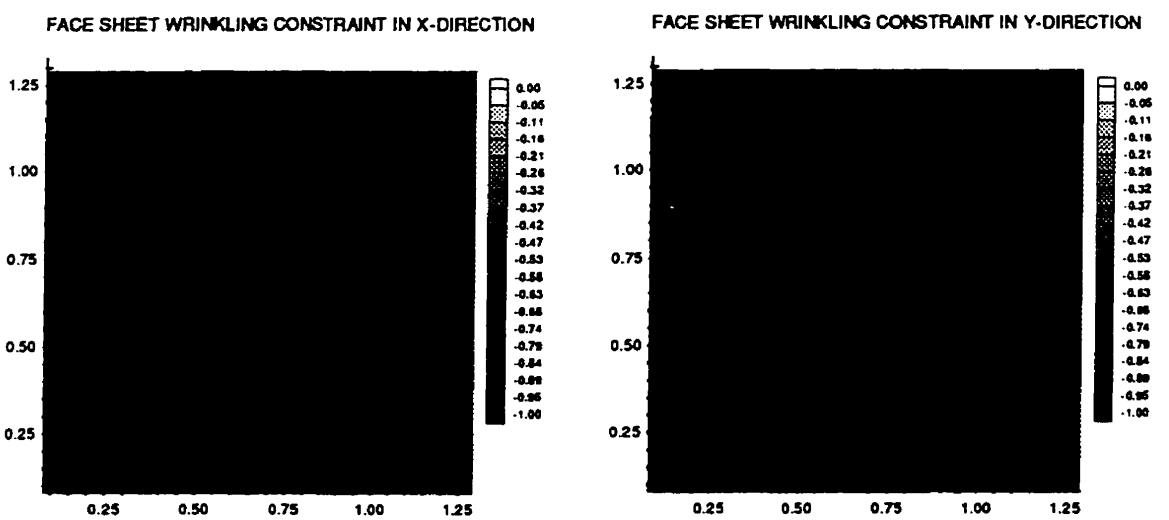

Figure 6.26: Facesheet Wrinkling Constraint for Optimal Design with 2 Design Variables.

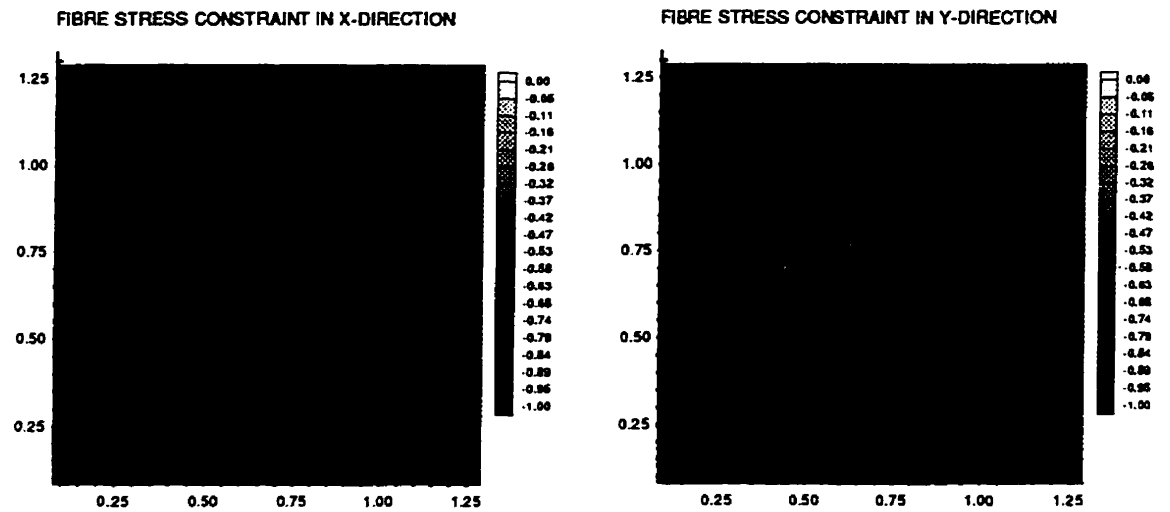

Figure 6.27: Fibre Stress Constraint for Optimal Design with 4 Design Variables.

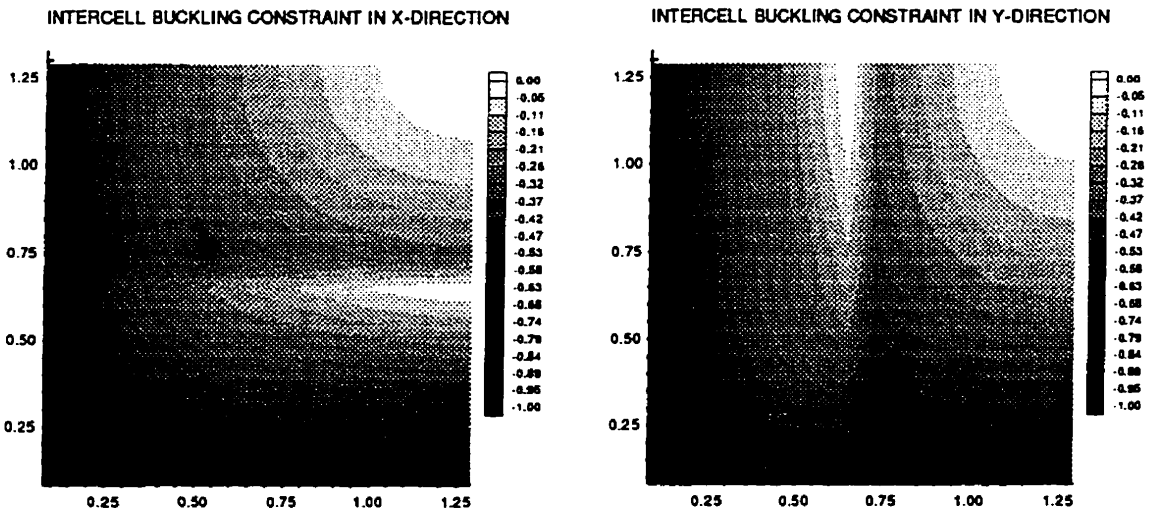

Figure 6.28: Intercell Buckling Constraint for Optimal Design with 4 Design Variables.

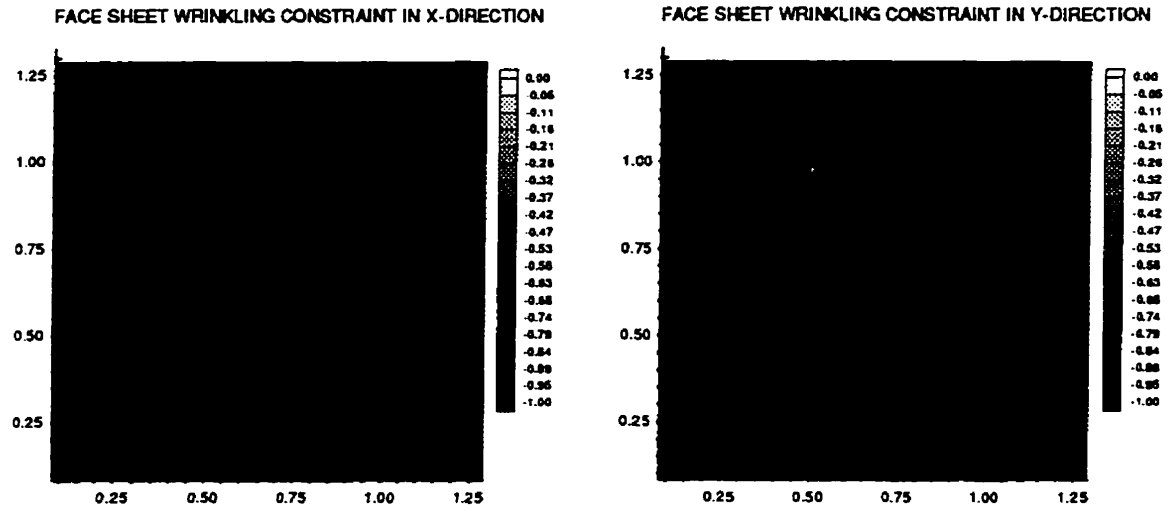

Figure 6.29: Facesheet Wrinkling Constraint for Optimal Design with 4 Design Variables.

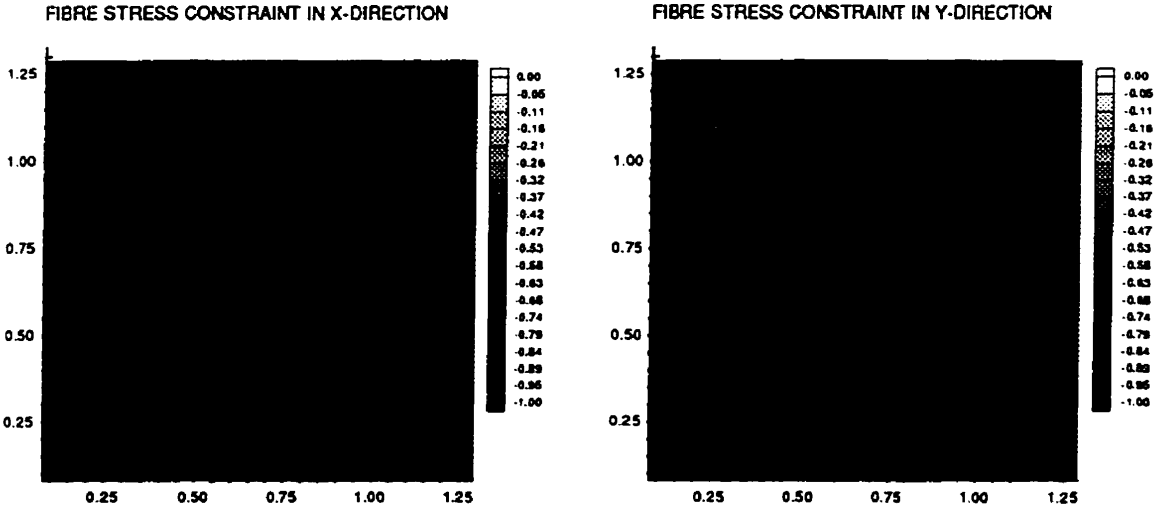

Figure 6.30: Fibre Stress Constraint for Optimal Design with 8 Design Variables.

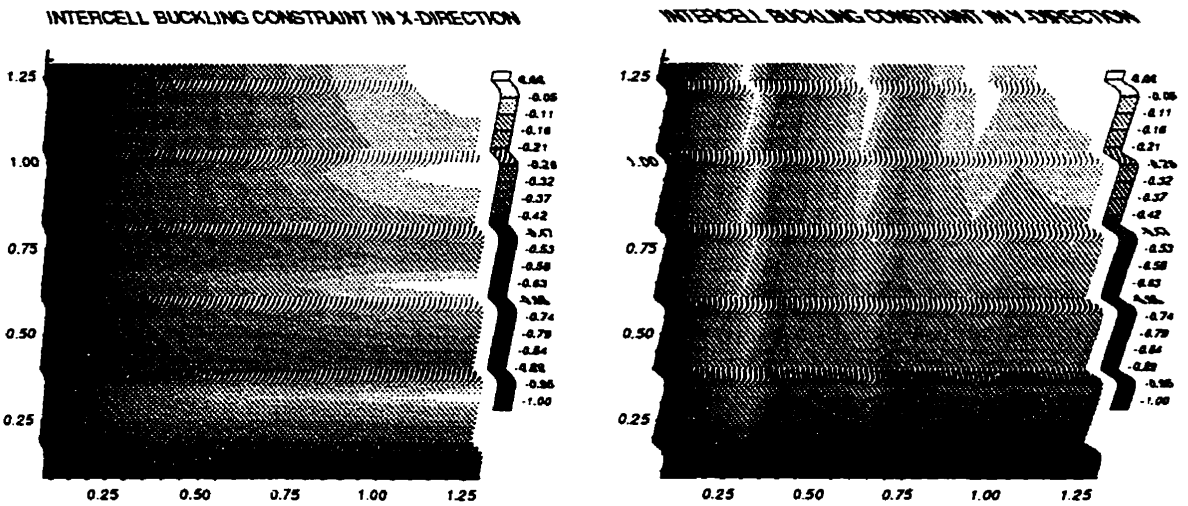

Figure 6.31: Intercell Buckling Constraint for Optimal Design with 8 Design Variables.

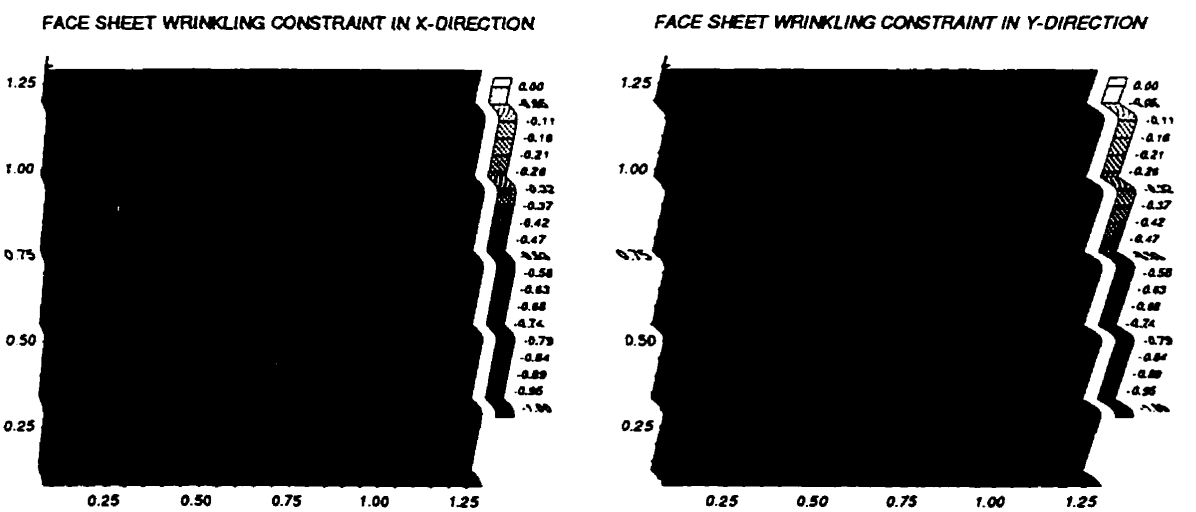

Figure 6.32: Facesheet Wrinkling Constraint for Optimal Design with 8 Design Variables.

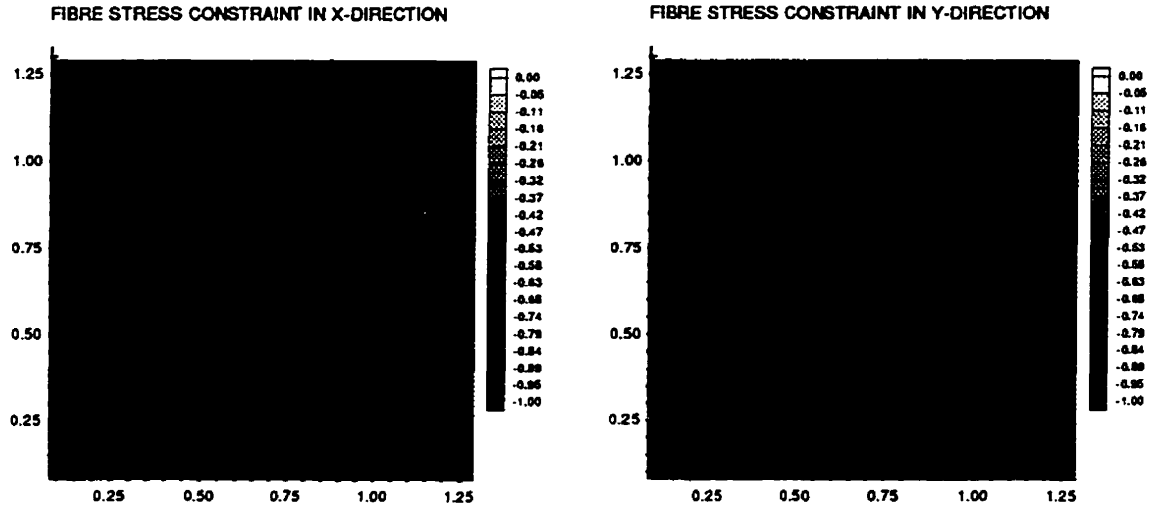

Figure 6.33: Fibre Stress Constraint for Optimal Design with 16 Design Variables.

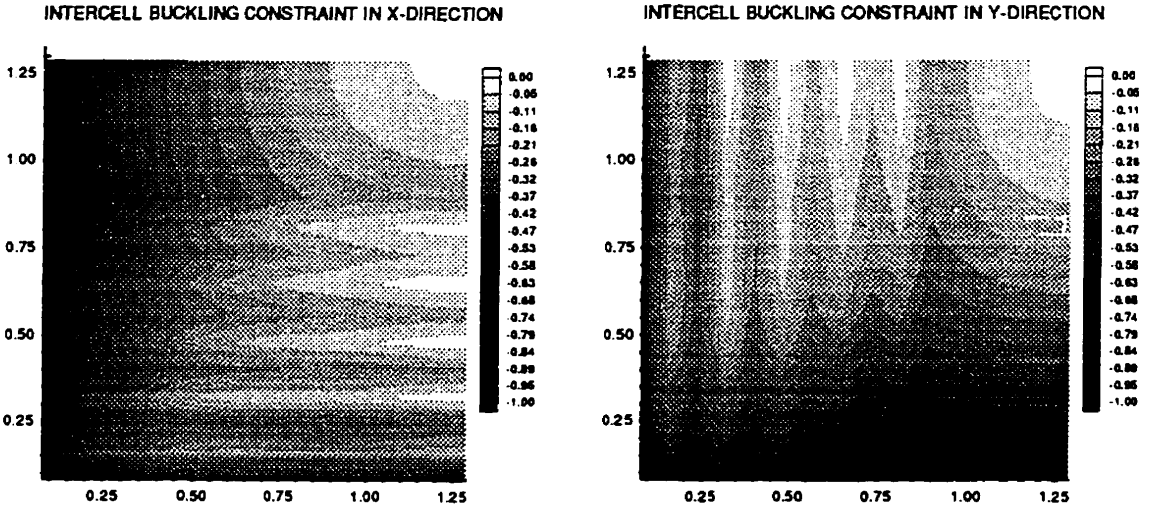

Figure 6.34: Intercell Buckling Constraint for Optimal Design with 16 Design Variables.

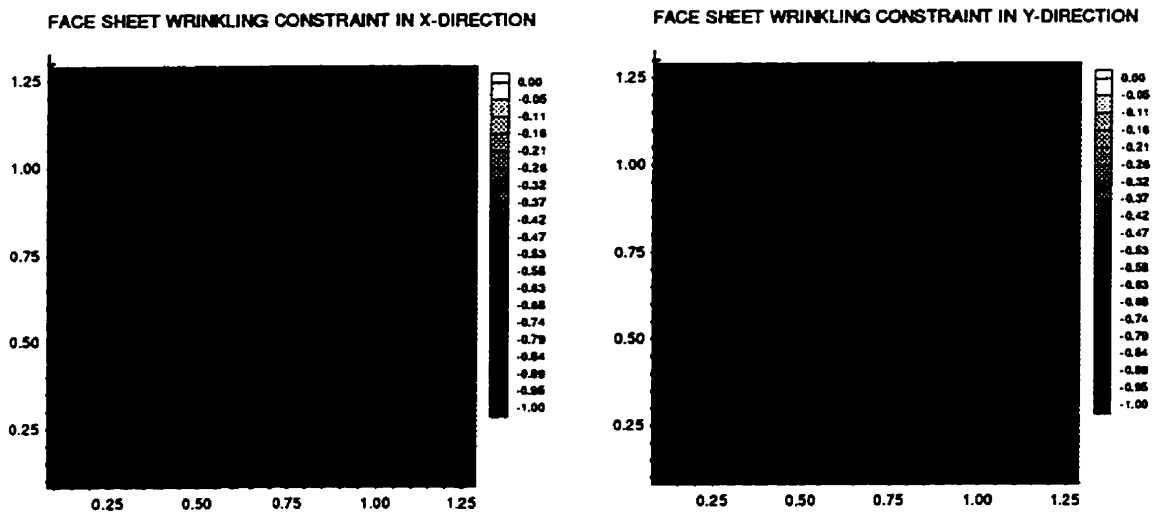

Figure 6.35: Facesheet Wrinkling Constraint for Optimal Design with 16 Design Variables.

Number of Design Variables	First Natural Frequency (Hz)
2	26.07
4	25.81
8	25.55
16	25.46
32	25.36

Table 6.10: The First Natural Frequency for Different Number of Design Variables.

From these figures and from Table 6.10, which gives the first natural frequency of the optimal design for different numbers of design variables, it can be concluded that intercell buckling is the only active constraint for all cases and therefore drives the optimal designs. This is a result of the particular honeycomb core used; the conclusion might change if other core materials were considered.

Figure 6.39 displays how the mass of the facesheets decreases when the number of design variables increases. For 2 design variables, the value of the objective function is 5.60 kg. When the number of design variables increases to 32, the mass of the facesheets falls to 3.84 kg. This is a saving of 32% of the facesheet mass and a saving of 19% of the total plate mass.

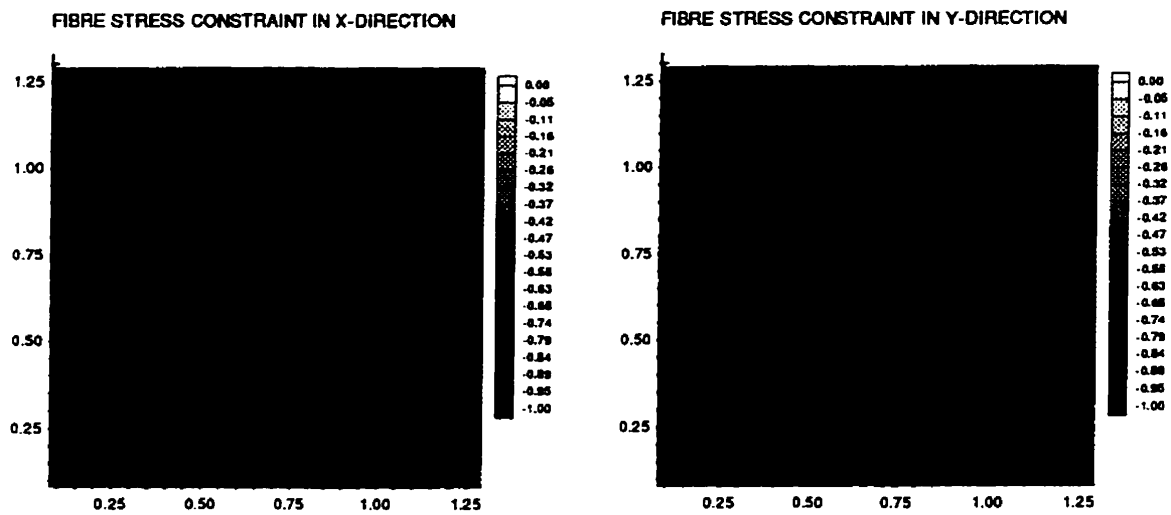

Figure 6.36: Fibre Stress Constraint for Optimal Design with 32 Design Variables.

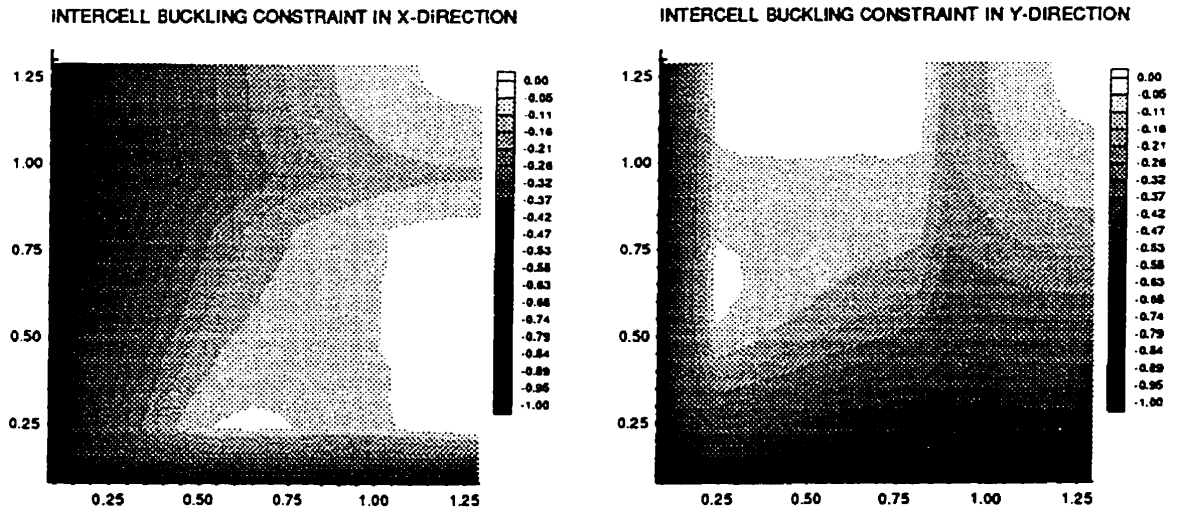

Figure 6.37: Intercell Buckling Constraint for Optimal Design with 32 Design Variables.

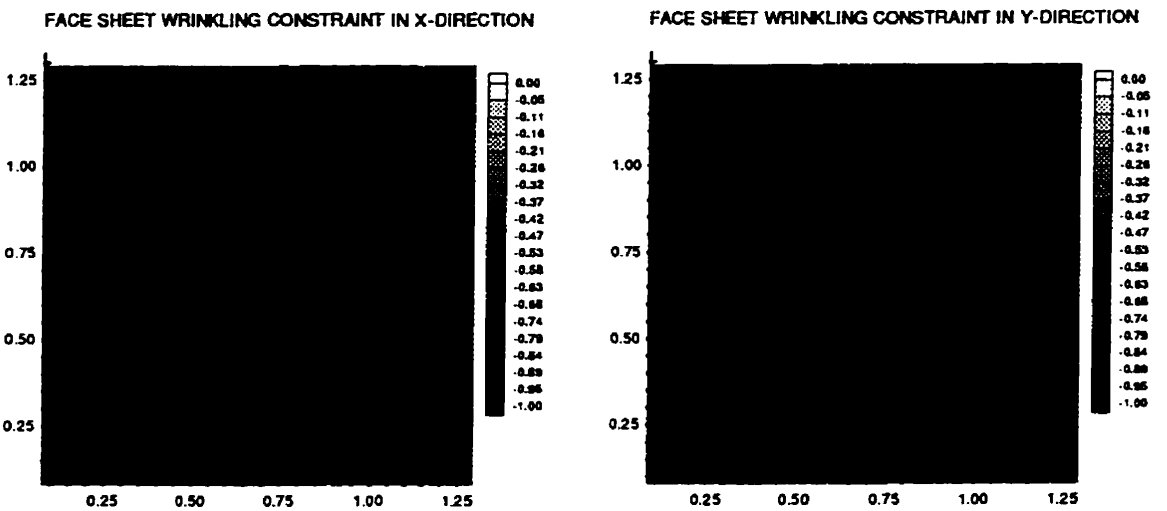

Figure 6.38: Facesheet Wrinkling Constraint for Optimal Design with 32 Design Variables.

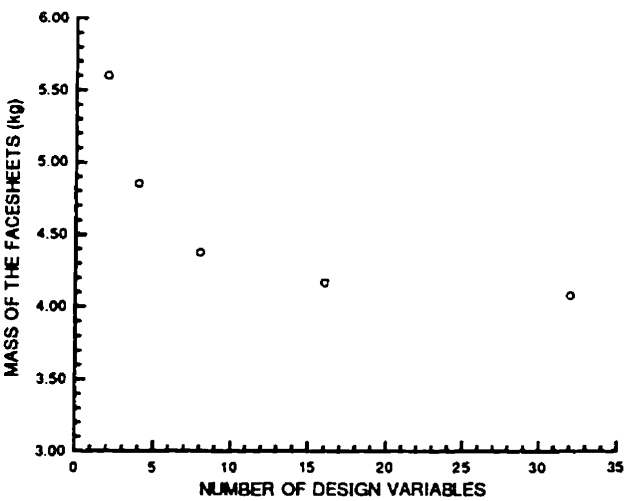

Figure 6.39: Convergence of the Objective Function with the Number of Design Variables.

Aspect Ratio (a/b)	Material Distribution (%)	
	Band in X-Direction	Band in Y-Direction
	1	1
1.00	85.	85.
0.95	87.	76.
0.90	87.	66.
0.85	86.	56.
0.80	83.	47.
0.75	80.	39.
0.50	52.	21.
0.25	32.	10.

Table 6.11: Aspect Ratio Study: 2 Design Variables

The next step is to investigate the effect of the aspect ratio (a/b) on the optimal design for different numbers of design variables. Tables 6.11 to 6.14 present the optimal design for plates with different aspect ratios using 2, 4, 8 and 16 design variables. Again, the results presented in these tables are in accordance with the sketch shown in Figure 6.8. Looking at these results and comparing them with the results presented in Section 6.1 two factors can be noted. The first is that, when the failure load is included there is not an abrupt change in the optimal design for a small variation on the aspect ratio, rather the design is modified gradually as a function of aspect ratio. The other one is that only for a small aspect ratio ($a/b \approx 0.25$) the the minimum allowed amount of material is in the long dimension of the plate.

Following the sequence of Section 6.1, Approaches 2A and 2B were also applied to solve this problem. Prescribed points in the plate were selected to check the material density constraints and other points were chosen to check the failure load constraints. Figure 6.40 and 6.41 present the material density change when the number of design variables increases. These figures show that Approaches 2A and 2B methods converge to essentially the same design.

In order to determine which constraint leads to the optimal design, Figure 6.42 to 6.44 present the value of the failure load constraints when Approach 2A is applied while Figures 6.45 to 6.47 do the same for Approach 2B, for eighteen design variables. Examining

Aspect Ratio (a/b)	Material Distribution (%)			
	Bands in X-Direction		Bands in Y-Direction	
	1	2	1	2
1.00	61.	87.	60.	86.
0.95	62.	89.	54.	77.
0.90	63.	89.	47.	67.
0.85	63.	88.	40.	57.
0.80	62.	85.	35.	48.
0.75	60.	82.	30.	42.
0.50	44.	53.	17.	23.
0.25	27.	35.	10.	10.

Table 6.12: Aspect Ratio Study: 4 Design Variables

Aspect Ratio (a/b)	Material Distribution (%)							
	Bands in X-Direction				Bands in Y-Direction			
	1	2	3	4	1	2	3	4
1.00	33.	62.	82.	89.	33.	62.	82.	89.
0.95	34.	62.	85.	90.	29.	55.	73.	90.
0.90	33.	63.	83.	90.	25.	48.	64.	89.
0.85	35.	64.	90.	90.	22.	40.	52.	58.
0.80	35.	63.	82.	88.	20.	36.	46.	50.
0.75	34.	62.	78.	83.	18.	32.	41.	44.
0.50	28.	45.	52.	53.	10.	18.	23.	25.
0.25	17.	33.	33.	34.	10.	10.	10.	10.

Table 6.13: Aspect Ratio Study: 8 Design Variables

Aspect Ratio (a/b)	Band Direction	Material Distribution (%)							
		1	2	3	4	5	6	7	8
1.00	X	19.	33.	49.	62.	74.	86.	90.	90.
	Y	19.	33.	49.	62.	74.	89.	90.	90.
0.95	X	29.	33.	48.	62.	75.	90.	90.	90.
	Y	21.	29.	43.	55.	65.	90.	90.	90.
0.90	X	30.	33.	48.	62.	90.	90.	90.	90.
	Y	23.	25.	37.	48.	57.	63.	86.	90.
0.85	X	17.	34.	50.	63.	85.	90.	90.	90.
	Y	12.	23.	33.	41.	48.	54.	57.	87.
0.80	X	18.	35.	51.	65.	75.	83.	88.	89.
	Y	11.	22.	30.	37.	43.	48.	50.	50.
0.75	X	17.	35.	50.	63.	72.	79.	84.	85.
	Y	10.	19.	27.	34.	39.	42.	44.	45.
0.50	X	15.	29.	39.	46.	50.	52.	54.	54.
	Y	10.	11.	15.	19.	22.	24.	25.	26.
0.25	X	10.	17.	19.	56.	30.	22.	32.	40.
	Y	10.	10.	10.	10.	10.	10.	10.	10.

Table 6.14: Aspect Ratio Study: 16 Design Variables

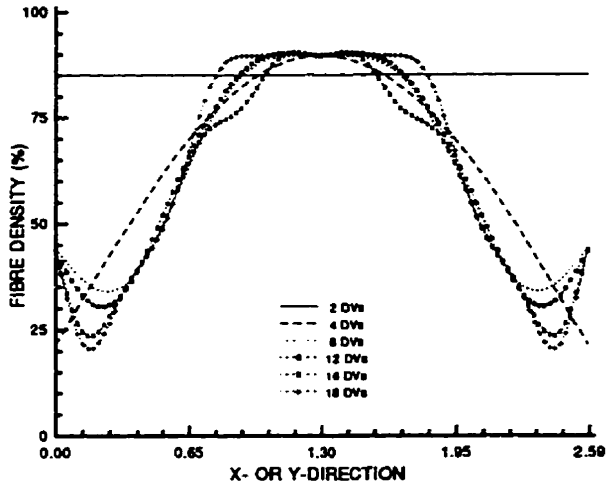

Figure 6.40: Change in Material Distribution with Number of Design Variables: Approach 2A.

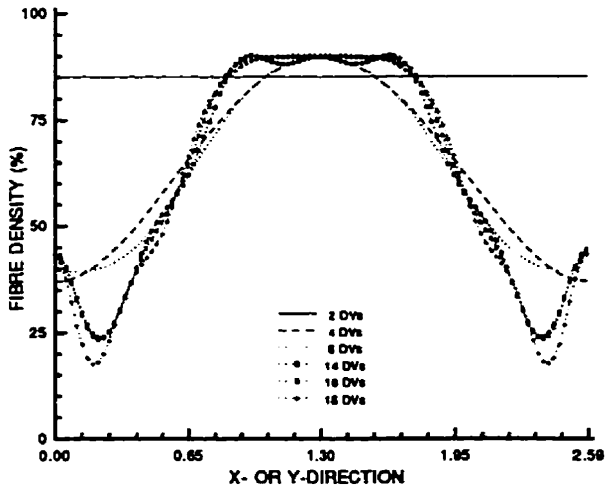

Figure 6.41: Change in Material Distribution with Number of Design Variables: Approach 2B.

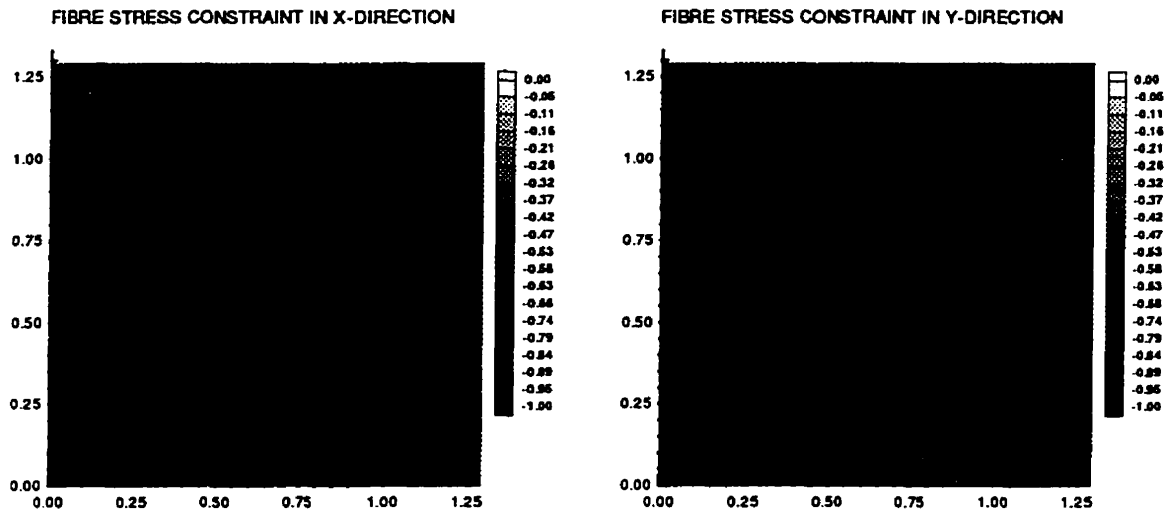

Figure 6.42: Fibre Stress Constraint for Optimal Design with 18 Design Variables: Approach 2A.

these figures it is concluded that intercell buckling is the constraint which drives the optimal design.

Comparing the three methods (Figure 6.48), it is possible to verify that all three methods converge essentially to the same solution. Figure 6.49 shows how the objective function decreases as a function of the number of design variables.

From the results presented certain conclusions can be drawn. First, the two techniques (independent design approach and reduced basic formulation) work well to yield an optimal design. As may be expected, Approaches 2A and 2B produce very similar results. However, the orthogonal functions used in Approach 2B are more complex (they use hyperbolic functions) and demand more computer time to be calculated. Therefore, Approach 2A is preferred over Approach 2B. The design provided by Approaches 2A and 2B has a smoother change in material density, which may be a desirable factor. The inclusion of the failure loads makes the optimal design more realistic, and results in a redistribution of material compared to the analysis, in Section 6.1, without failure constraints. The most important result is that it is possible to considerably reduce mass by defining a nonuniform material distribution in the facesheets.

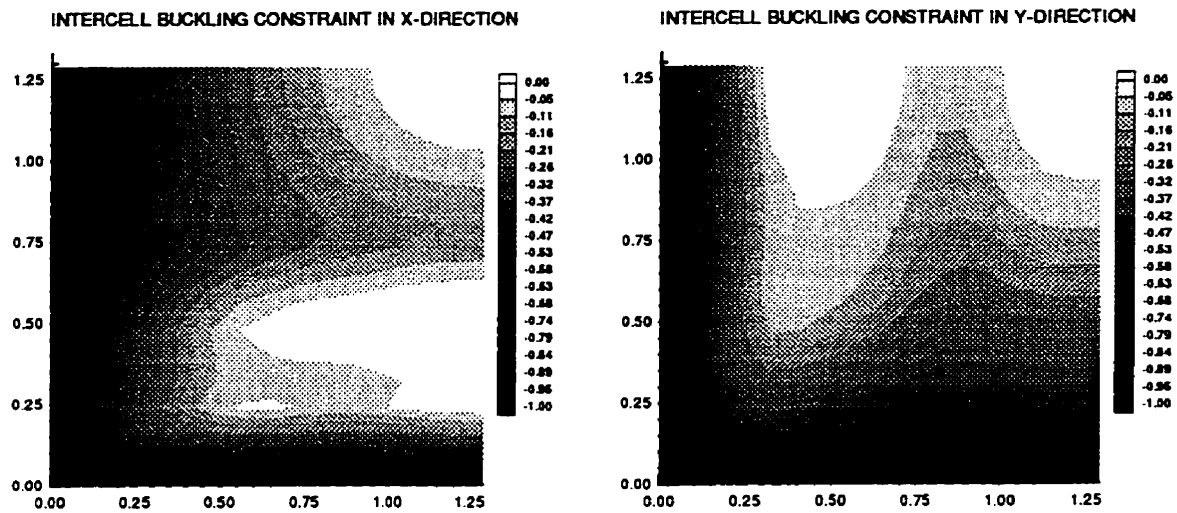

Figure 6.43: Intercell Buckling Constraint for Optimal Design with 18 Design Variables: Approach 2A.

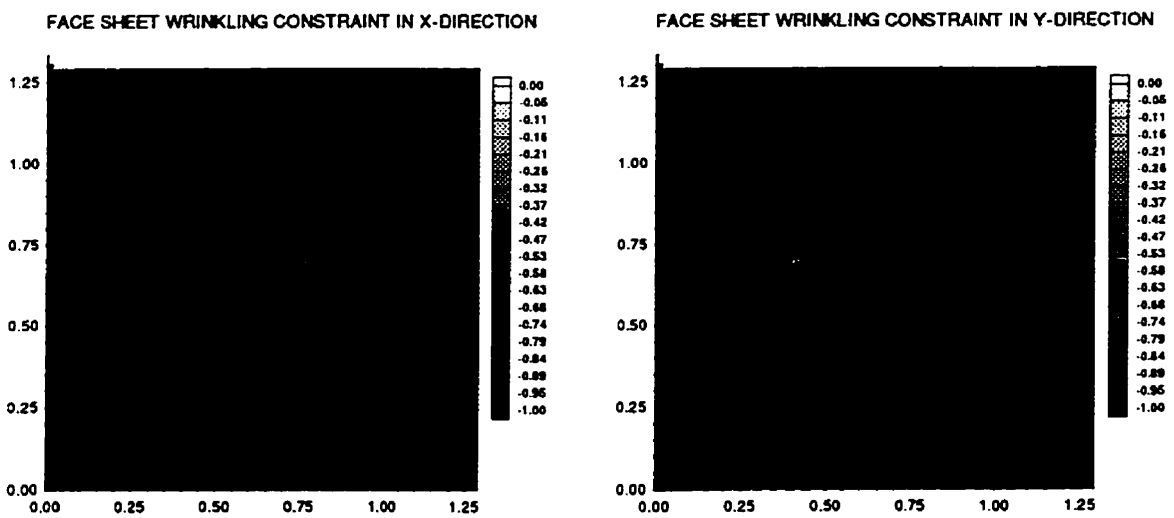

Figure 6.44: Facesheet Wrinkling Constraint for Optimal Design with 18 Design Variables: Approach 2A.

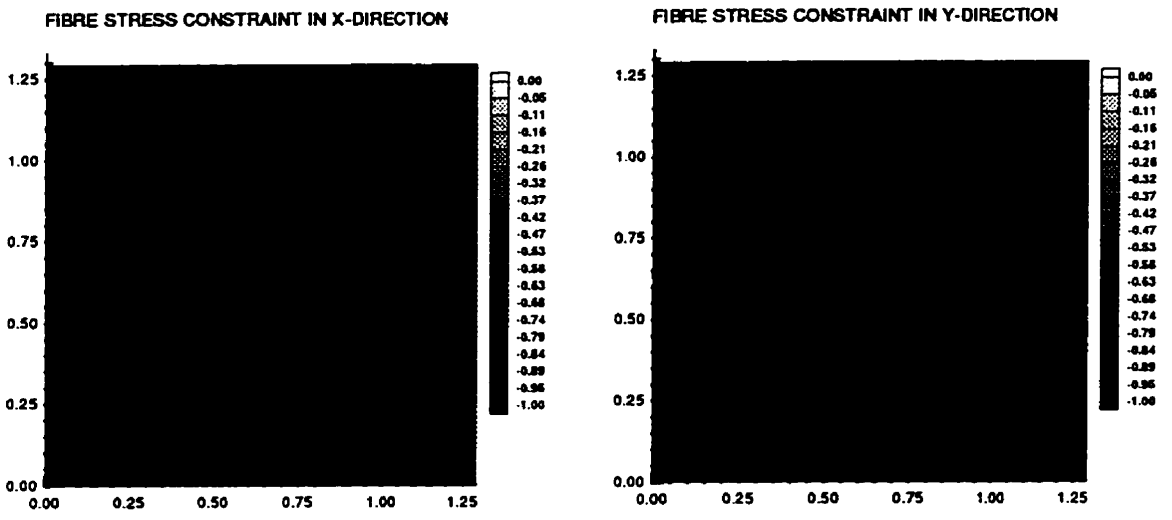

Figure 6.45: Fibre Stress Constraint for Optimal Design with 18 Design Variables: Approach 2B.

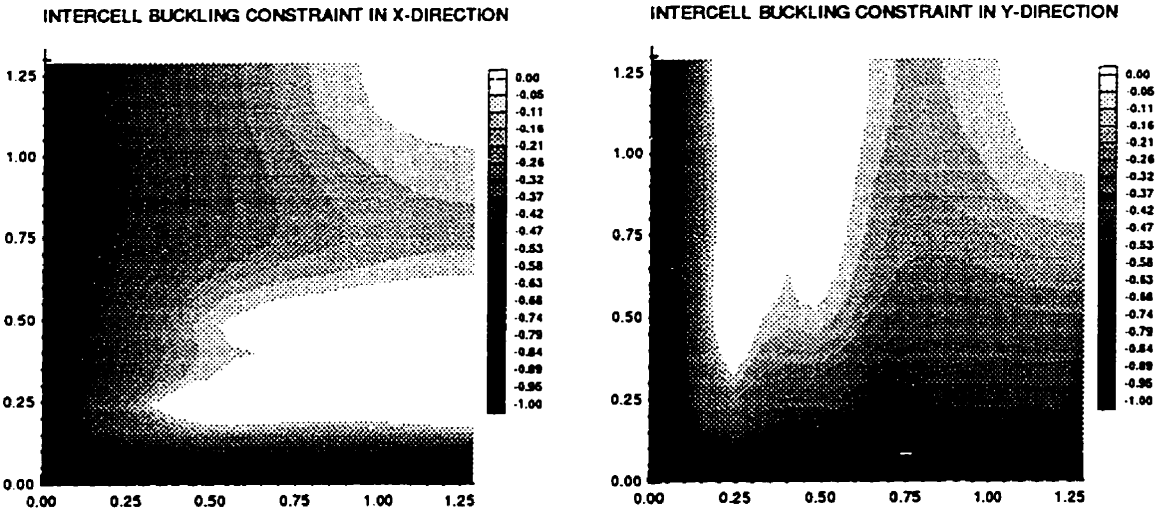

Figure 6.46: Intercell Buckling Constraint for Optimal Design with 18 Design Variables: Approach 2B.

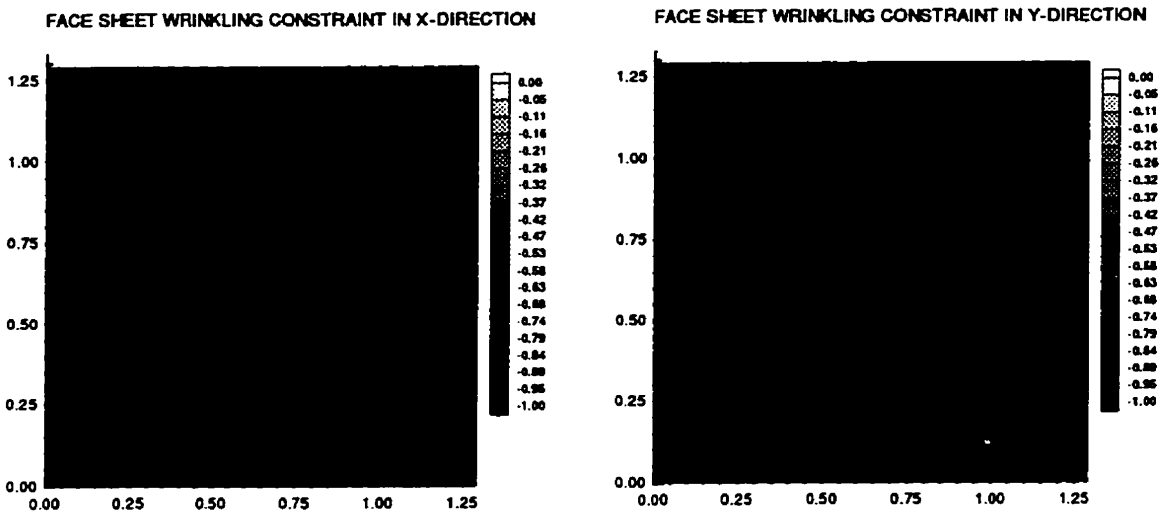

Figure 6.47: Facesheet Wrinkling Constraint for Optimal Design with 18 Design Variables: Approach 2B.

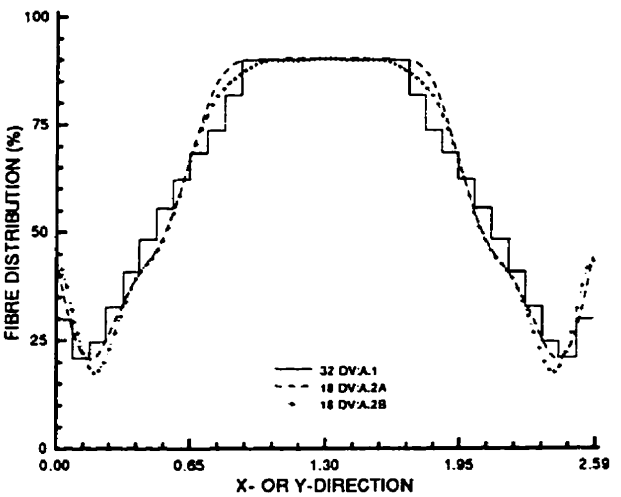

Figure 6.48: Material Distribution.

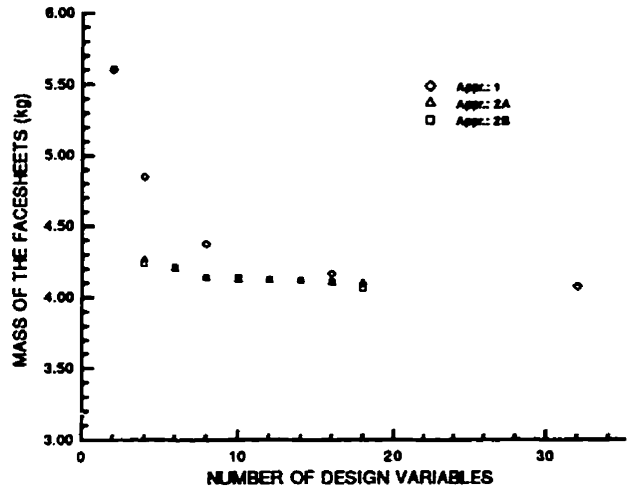

Figure 6.49: Convergence of the Objective Function using the Three Approaches.

6.4 Solar Array Support with Failure Constraints

Here, the optimal design of the structural support for the solar array of the CBERS is studied regarding the first natural frequency and the failure modes (fibre failure, intercell buckling and wrinkling instability) as constraints. The dimensions, material properties and constraints for this problem were given in Section 6.2. The allowable stresses for the carbon fibre/epoxy composite are presented in Table 6.9. It is assumed that the panel is subjected to a 20 g acceleration in a direction perpendicular to the panel.

The first results to be shown are the optimal designs given by the three methods as the number of design variables increases. Figures 6.50 to 6.54 present the optimal solution when Approach 1 was used. Different from the results displayed in Section 6.2, in this problem the optimal layouts have nonuniform material distribution in both directions.

The optimal solutions obtained using Approaches 2A and 2B are illustrated in Figures 6.55 to 6.56 and 6.57 to 6.58, respectively. The comparison of the final optimal designs given by the three methods is shown in Figure 6.59 and 6.60. Once again, the three methods yield similar solutions. Figure 6.61 illustrates how the mass of the facesheets decreases when the number of design variables increases using the three methods.

In order to identify which failure load constraints are active, Figures 6.62 to 6.70 present the failure load constraints in the first quadrant of the plate for the optimal designs obtained

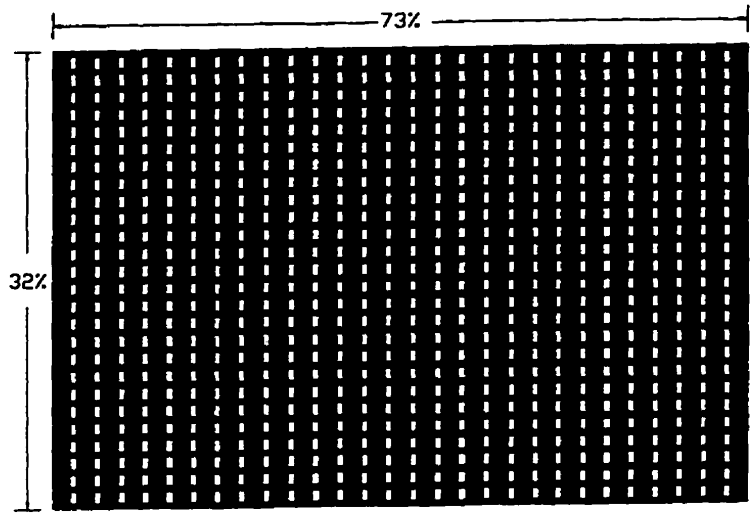

Figure 6.50: Solar Array Support Optimal Design with 2 Design Variables: Approach 1.

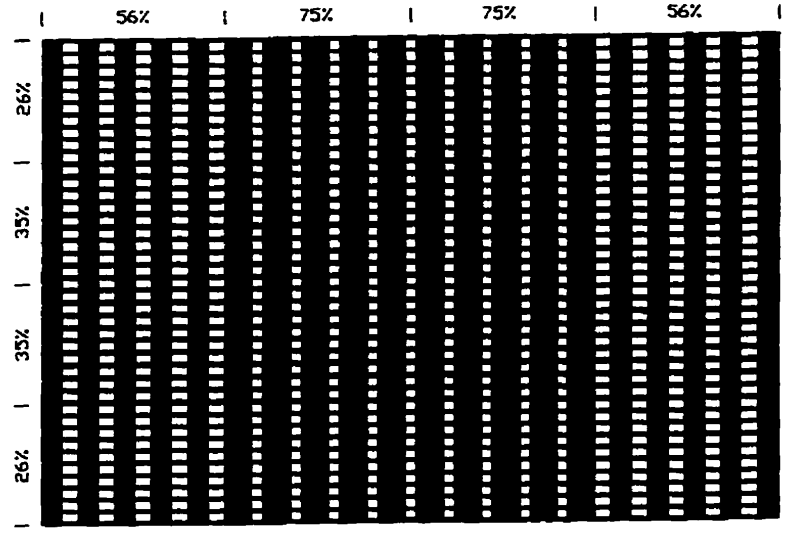

Figure 6.51: Solar Array Support Optimal Design with 4 Design Variables: Approach 1.

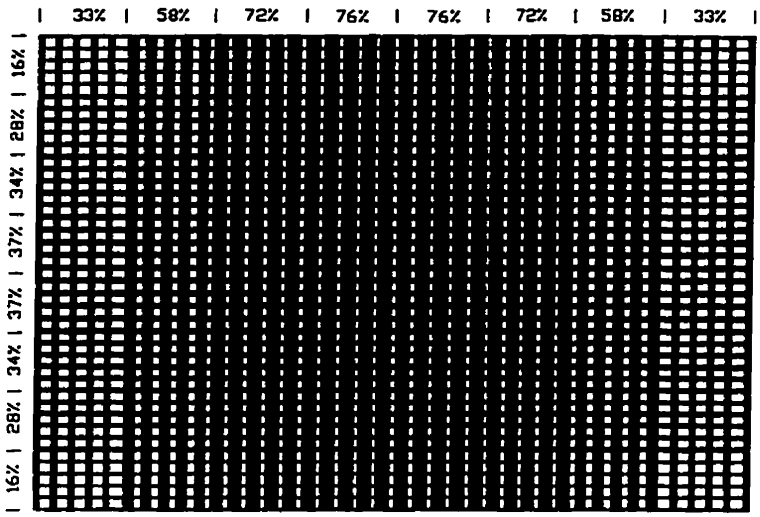

Figure 6.52: Solar Array Support Optimal Design with 8 Design Variables: Approach 1.

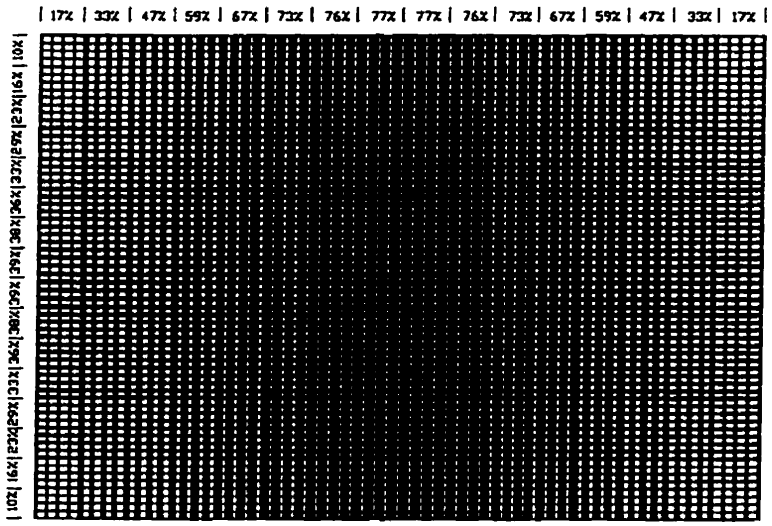

Figure 6.53: Solar Array Support Optimal Design with 16 Design Variables: Approach 1.

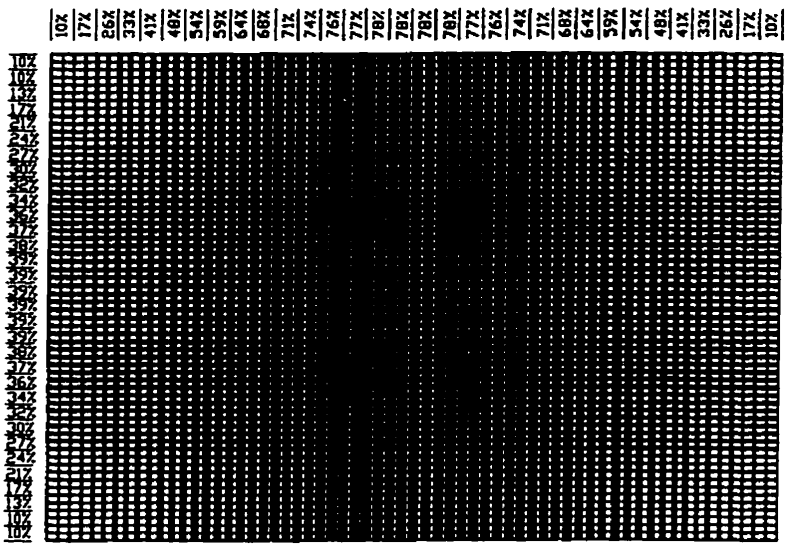

Figure 6.54: Solar Array Support Optimal Design with 32 Design Variables: Approach 1.

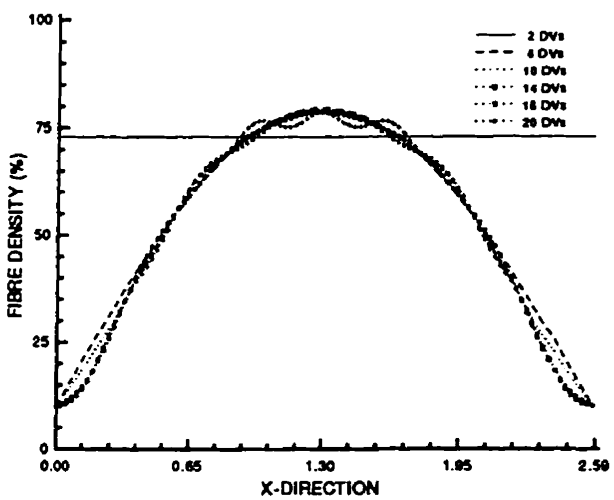

Figure 6.55: Change of Material Distribution Along the X-Direction for the Solar Array Support as the Number of Design Variables Increases: Approach 2A.

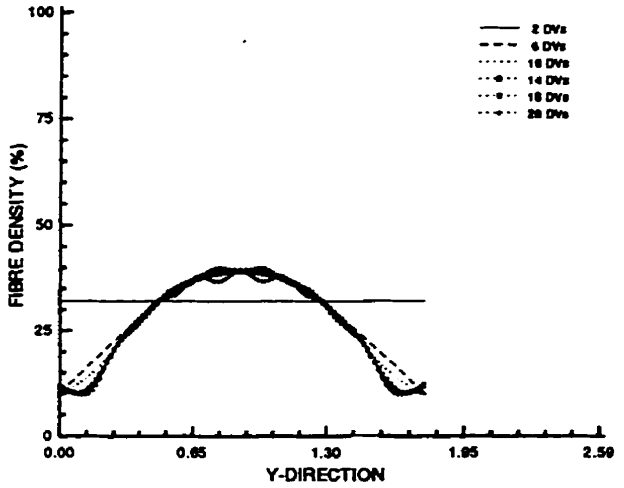

Figure 6.56: Change of Material Distribution Along the Y-Direction for the Solar Array Support as the Number of Design Variables Increases: Approach 2A.

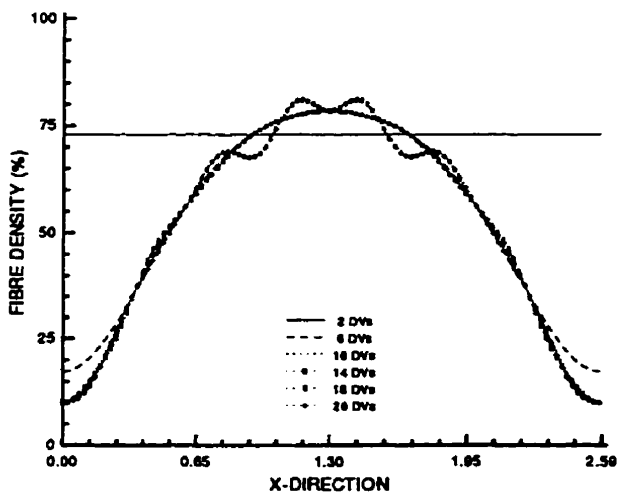

Figure 6.57: Change of Material Distribution Along the X-Direction for the Solar Array Support as the Number of Design Variables Increases: Approach 2B.

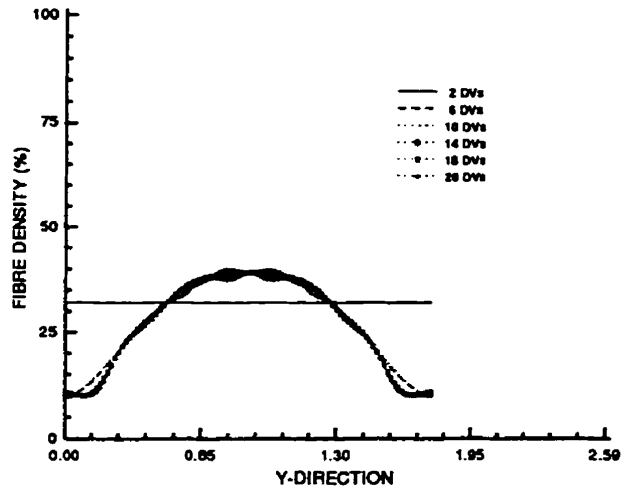

Figure 6.58: Change of Material Distribution Along the Y-Direction for the Solar Array Support as the Number of Design Variables Increases: Approach 2B.

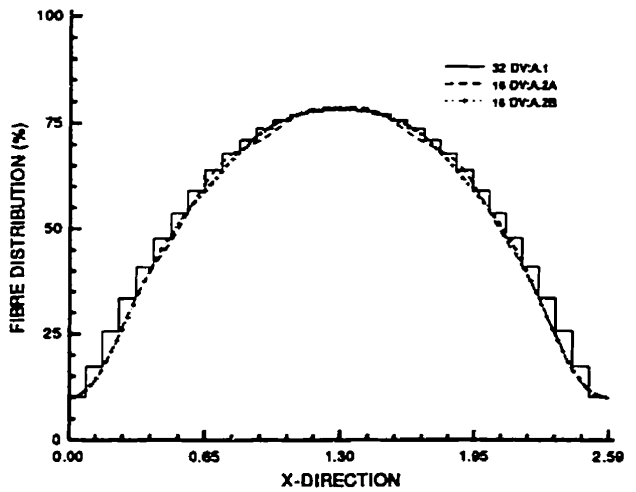

Figure 6.59: Material Distribution Along X-Direction Given by the Three Approaches for the Solar Array Support.

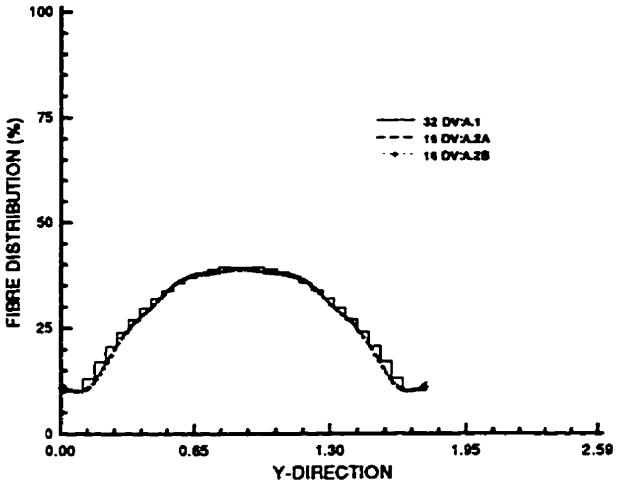

Figure 6.60: Material Distribution Along Y-Direction Given by the Three Approaches for the Solar Array Support.

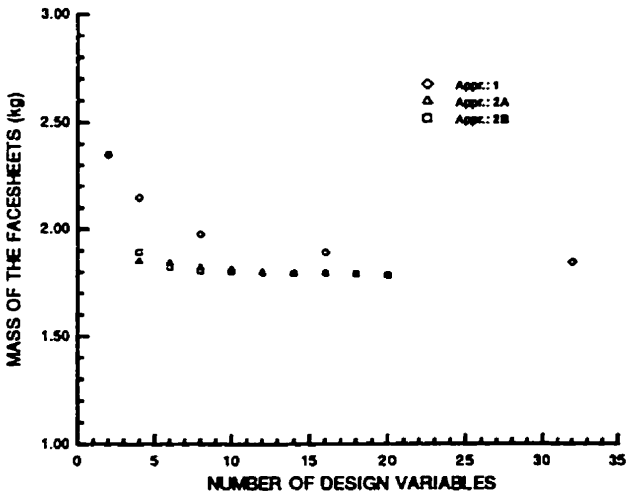

Figure 6.61: Convergence of the Objective Function using the Three Approaches for the Solar Array Support.

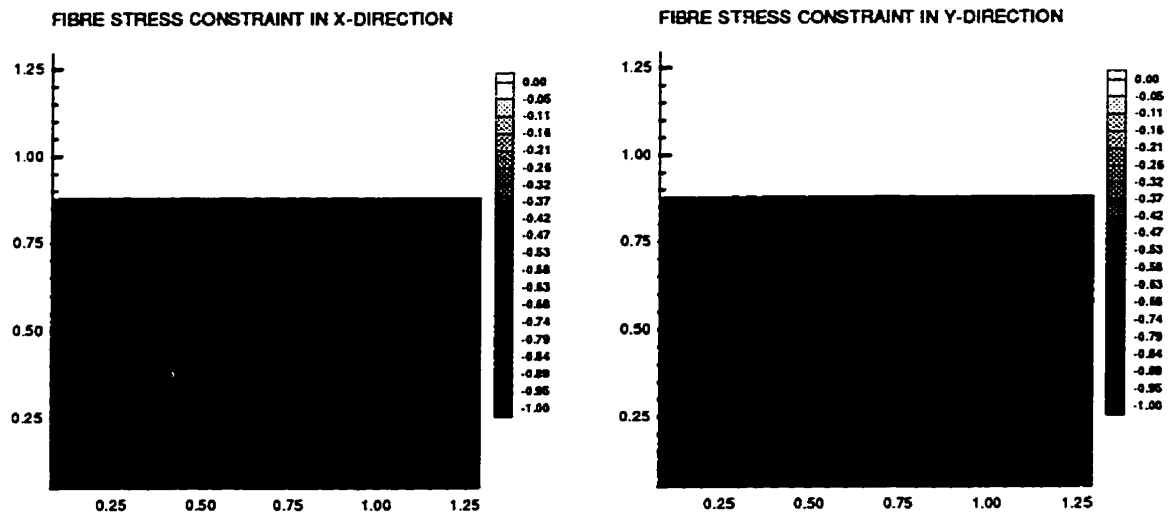

Figure 6.62: Fibre Stress Constraint for Optimal Design with 32 Design Variables of the Solar Array Support: Approach 1.

using the three methods. From these figures, it is clear that intercell buckling is the failure mode that drives the optimal design.

From the results presented, three points should be mentioned. First, all results follow the same pattern as those of the previous problem. Second, the optimal design with uniform material distribution (two design variables) is heavier than the initial design of the CBERS solar array support, Figure 1.3. The reason for this is that CBERS has been designed to be launched by liquid fuel rocket, so the design load is smaller, around 12 g acceleration. Third, the facesheet mass decreased from 2.35 kg to 1.78 kg as the number of design variables increases, this represents a 24% mass saving, which gives a 12% saving in the overall mass of the sandwich panel.

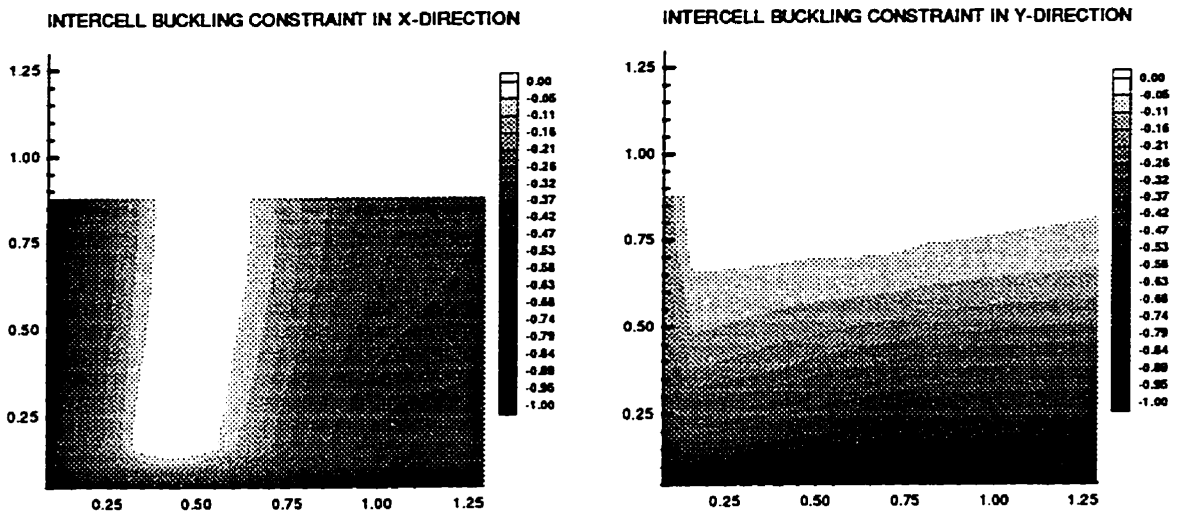

Figure 6.63: Intercell Buckling Constraint for Optimal Design with 32 Design Variables of the Solar Array Support: Approach 1.

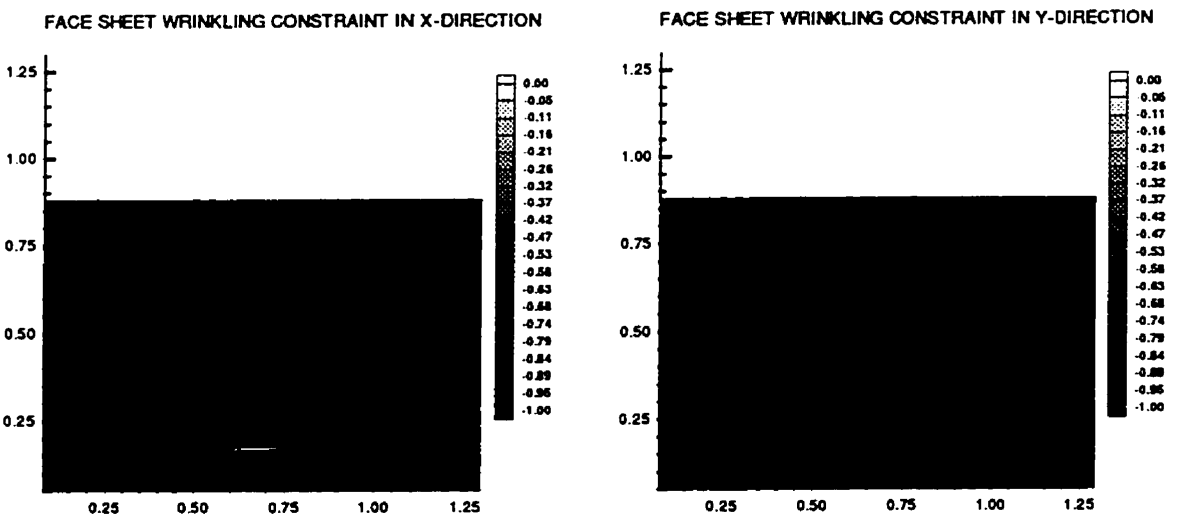

Figure 6.64: Facesheet Wrinkling Constraint for Optimal Design with 32 Design Variables of the Solar Array Support: Approach 1.

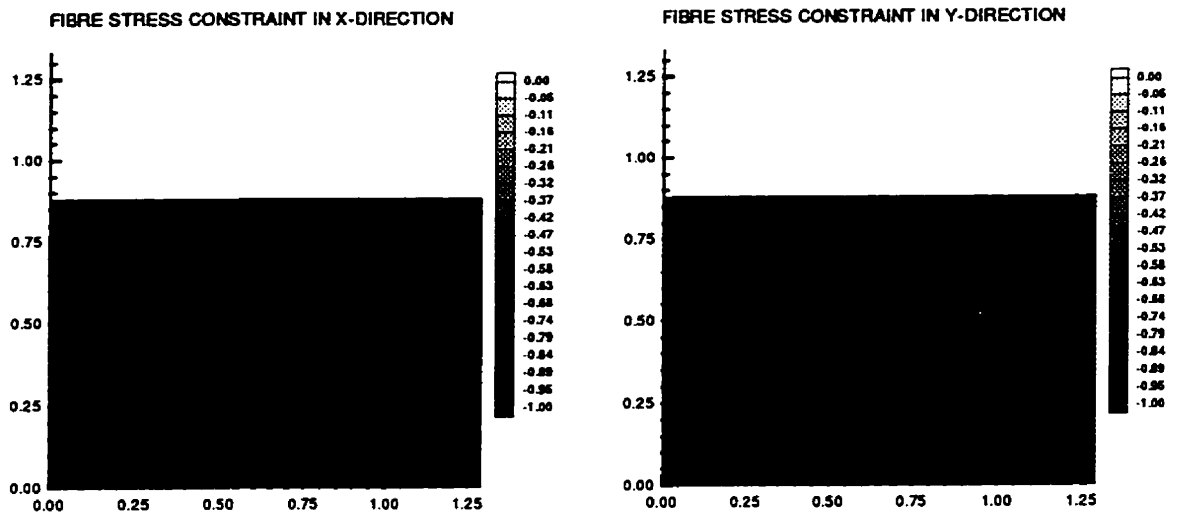

Figure 6.65: Fibre Stress Constraint for Optimal Design with 20 Design Variables of the Solar Array Support: Approach 2A.

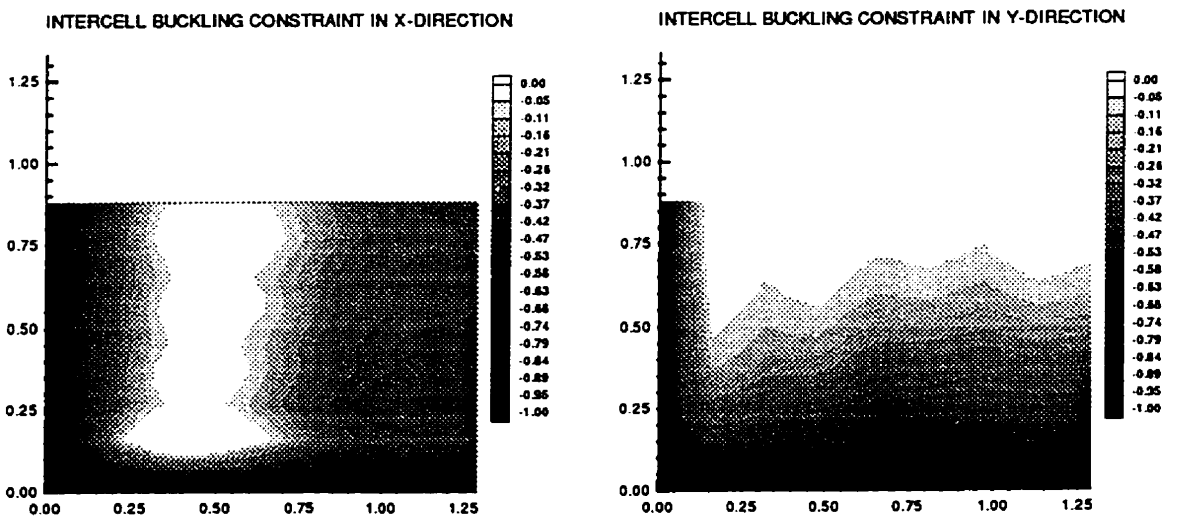

Figure 6.66: Intercell Buckling Constraint for Optimal Design with 20 Design Variables of the Solar Array Support: Approach 2A.

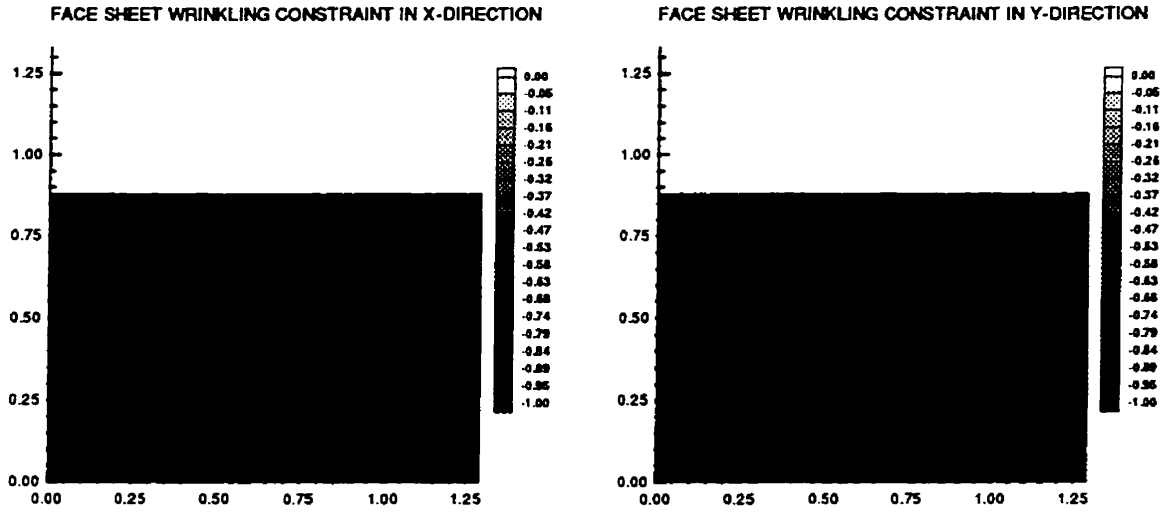

Figure 6.67: Facesheet Wrinkling Constraint for Optimal Design with 20 Design Variables of the Solar Array Support: Approach 2A.

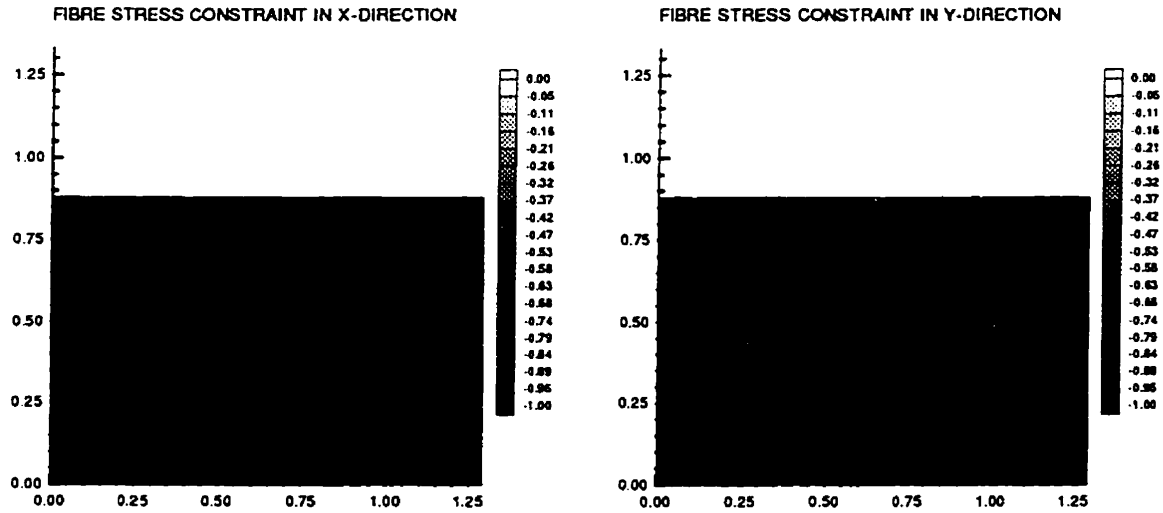

Figure 6.68: Fibre Stress Constraint for Optimal Design with 20 Design Variables of the Solar Array Support: Approach 2B.

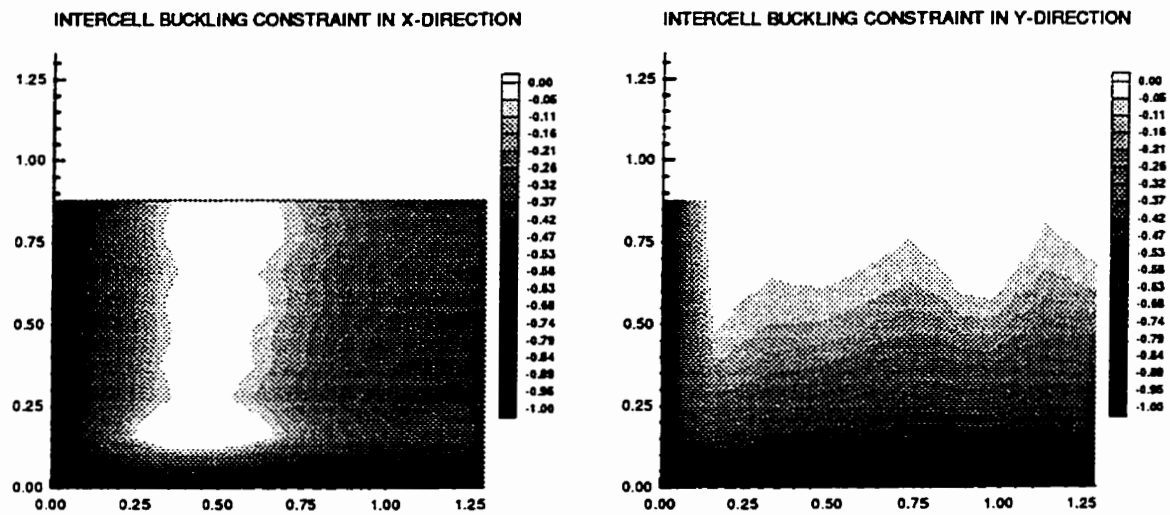

Figure 6.69: Intercell Buckling Constraint for Optimal Design with 20 Design Variables of the Solar Array Support: Approach 2B.

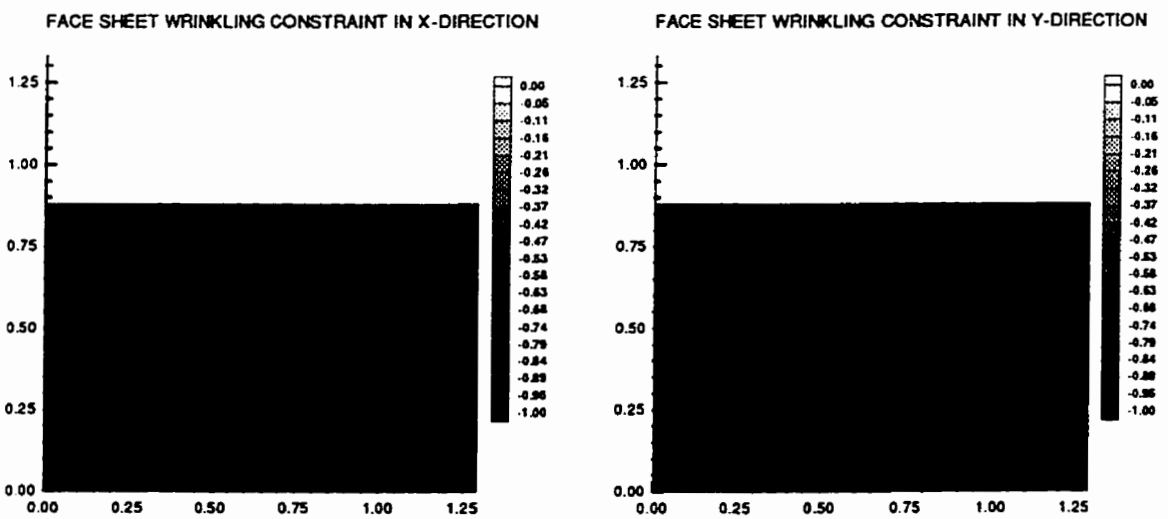

Figure 6.70: Facesheet Wrinkling Constraint for Optimal Design with 20 Design Variables of the Solar Array Support: Approach 2B.

Chapter 7

Summary and Conclusions

This thesis has examined the optimal design of sandwich plates with spatially heterogeneous composite facesheets. The essential idea in the work has been to determine the optimal, spatially varying stiffness of the composite facesheets which yields a minimum weight design. The work is primarily oriented toward the design of aeronautical and aerospace structures in which weight saving results in significant advantages either in the form an increased pay-load or improved vehicle performance. The current work represents an advance over previous sandwich plate optimization as previous work was restricted to designs with a homogeneous stiffness distribution of the facesheets.

The specific design considered was the minimization of the facesheet mass while satisfying constraints on the plate first natural frequency and certain facesheet stress levels. The stress constraints were based on actual design failure criteria for honeycomb–core composite–facesheet sandwich plates used in typical spacecraft. In the work, the facesheets are assumed to be composed of an orthotropic net of unidirectional composite fibre strips; the optimal design (the least mass design) is obtained by changing the strip widths and the spacing between them over the domain of the plate.

This chapter presents a summary of what was developed in this dissertation and highlights the results and contributions.

7.1 Summary

This work first presents an overview of the research in the field of structural optimization. This is followed by a review of the analysis and optimization of sandwich plates.

In Chapter 2 a summary and description of commonly used numerical methods applied to structural optimization was given. The chapter ends with the description of a computer code and the corresponding flow chart which was developed as part of this work and which is based on the numerical methods described in the beginning of the chapter. Chapter 3 presents the background necessary to develop a computer code for the evaluation of facesheet stresses and natural frequencies of composite sandwich plates with heterogeneous composite facesheets. The developed code was verified by comparison to numerical and experimental results published in the literature as well as finite element results from a MSC/NASTRAN.

Since the sandwich plates considered have facesheets manufactured from a carbon fibre/epoxy composite net, it was necessary to approximate the nets as a heterogeneous orthotropic continuum. Two procedures were developed to achieve this approximation. In the first, a single basic cell of the net was modelled using the finite element method. Boundary conditions for the cell were determined to represent the periodicity of the structural response under simple load conditions. By determining the strain energy of the model and equating this energy to the strain energy of a continuum cell (referred to as a homogenised cell) under the same boundary conditions, it was possible to evaluate the homogenised engineering constants of this equivalent continuum. In the second procedure, a *large* segment of the facesheet net is modelled by a finite element mesh, and then boundary conditions and loads are applied to this model in order to simulate the boundary conditions and loads of an equivalent laboratory test. The work done by the nodal forces acting on a basic cell closest to the centre of the model is calculated and set equal to the strain energy of a homogenised cell under the same boundary conditions; the homogenised engineering constants were thereby determined. The second approach was then used to generate tables of homogenised engineering constants for different material densities in both the x and y directions. In order to validate the concept of homogenised elastic constants a sandwich plate with facesheets made of an aluminium nets was designed and manufactured. This plate was tested in the laboratory and the first three natural frequencies determined; these results were compared to the numerical results predicted using the homogenised based numerical model. An excellent comparison was obtained between the experimental results and numerical prediction.

Chapter 5 addresses a number of issues related to the implementation of the numerical optimization. During the optimization, two techniques were used to represent the material

density in terms of useful numerical design variables. In the first, an independent design approach, the face sheets are discretized into regions with uniform design parameters. In the second, a reduced basis formulation, the material density is specified as a linear combination of orthogonal, complete, basis functions. The next issue dealt with three failures loads (fibre failure, intercell buckling and wrinkling) which were included as constraints. Among all the design requirements that a composite sandwich plate should meet, these failure loads are the ones affected by changes in the distribution of material in the face sheets. That is, these failure constraints are the only aspect altered during the optimization process. This lead to the next issue of the sensitivity analysis. In order to accelerate the optimization process, a semi-analytical approach was applied to determine the sensitivity of the constraints, since no simple analytical expressions can be obtained. The final issue discussed involves the choice of optimization algorithm. Therefore, before proceeding, it was necessary to determine which combination of numerical optimization methods would best solve the specific problems of interest. The methods available in the optimization code previously developed were tested and a choice of algorithms was made.

The may results of this work are contained in Chapter 6. This involves two composite sandwich plate studies: in the first, a square one and then a series of rectangular plates with varying aspect ratios are considered while in the second a plate with the dimensions and material properties of an actual remote sensing satellite solar array support is analysed. In both studies the analysis proceeds as a two step process. In the first step, the optimization process was applied considering only the first natural frequency as a constraint and using the two techniques to define the design variables. Two important issues were examined: first, the effect of the number of design variables on the optimal solution; second, how the representation of the design variables affects the optimal solution. The second step included both natural frequency and failure load constraints and the same issues were investigated how the failure loads affect the optimal solution.

7.2 General Findings

The two models (for free-free and simply-supported composite sandwich plates) developed to determine the natural frequencies and failure loads of composite sandwich plates performed well. They were verified in comparison to experimental results, results from the literature

and numerical results from MSC/NASTRAN a commercial finite element code

The two approaches used to evaluate the homogenised engineering constants gave excellent results. The calculated values were found to be in close agreement with values data in the literature and with experimental results. Since the approach using only one basic cell is easier to implement and numerically less demanding it should be used rather than the approach that models part of facesheet net.

Among all the combinations of numerical optimization methods used, the set composed of sequential linear programming, the method of feasible directions and the golden section method gave the best performance. The combination of these methods was found to reach the optimal design with the least number of objective function and constraint evaluations. It should also be noted that the golden section method is one of the simplest one-dimensional search technique available and in addition, it was the most stable for the solution of the current problem.

An important by-product of this thesis is the idea of machining aluminium sheet to be used as facesheets of sandwich plates. It is possible to manufacture almost any design defined by a optimization package using a numerically controlled milling machine. To our knowledge this technology has never been employed in this context and seems most promising.

When the two approaches proposed to define the design variables were applied to solve the optimization problem, it was found that Approach 1 (an independent design approach) usually gives the least mass design. However, it requires more design variables and its solution has sharp changes in the material density from one region to the other. Approaches 2A and 2B (reduced basis formulation) give similar solutions; however, since the basis functions used in Approach 2B are more complex (it uses hyperbolic functions) and demand more computer time to be evaluated numerically, Approach 2A is preferred over Approach 2B.

From the aspect ratio studies and when using Approach 1 with only the first natural frequency as a constraint, it may be concluded that a small variation on the aspect ratio ($a/b \leq 0.90$) causes a rapid change in the optimal design. Furthermore, the material density oriented in the longer plate dimension drops to the minimum allowed. When failure loads are included in the constraint, this transition is smoothed out. In general, the optimal designs obtained when the failure loads are considered as constraints present a much smoother material density distribution than the solution with only the first natural frequency as

constraint. It is interesting that the only failure load constraint that is active in determining the optimal design is intercell buckling; this result is of course only valid for the honeycomb cell dimensions considered here and should not be generalised indiscriminately. An addition point and one that may be considered as a bit of an aside, is that the inclusion of the failure constraints seems to bring some stability to the numerical aspects of problem.

7.3 Significance of the Present Study

A number of studies have been completed concerning the optimization of composite sandwich plates; these works considered the thicknesses of the facesheet layers and the core and/or the direction of fibres in the facesheet laminate as design variables. The present study extends the research by considering variation of material density in different parts of the plate. This dissertation developed an approach for the optimization of light-weight composite sandwich plates. The plate facesheets are constructed using a net of composite fibre-strip in which the strip widths and spacing are variable; this variability defines the nonuniform material density distribution in the facesheets. The specification and solution of this problem has been not addressed before.

In order to solve this problem many questions had to be asked and answered. These include: among the numerical optimization methods used in structural optimization, which one best solve this problem? What is a suitable procedure to represent the composite-strip net as a smoothed heterogeneous orthotropic continuum? What is a reasonable way to define the design variables for this problem? This study solved the problem proposed. The results of this work demonstrate clearly that a variation in material density leads to important design advantages. Furthermore, the optimal design shows significant changes in material density; typical optimal designs exhibit a factor of nine in density variations. That is over the full range permissible material densities from 10% to 90% is used in the design. The results obtained are also impressive from the point of view of the gains that are possible; typical calculations showed that the mass of the facesheets can be reduced 10 to 50% depending on plate aspect ratio. It is also worth adding that the solutions obtained are conceptually straightforward to manufacture and therefore could lead to significant performance improvements with little cost penalty.

7.4 Recommendations

As possible extensions of this work, it is of great interest to investigate the effect of other boundary conditions on the optimal design; the current study is limited to simply-supported plates. Also, it is important to consider the thickness and density of the core, and the orientation of the net as design variables. When the properties of the core are assumed as design variables, other failure modes such as shear crimping and interlaminar stress should also be considered in the problem specification. When only the first natural frequency was considered as constraint, the present work showed that the optimal solution concentrates material in well defined local areas of the plate; this suggests that the use of stiffeners can improve the design. In such a formulation, the shape, number and position of the stiffeners should be investigated.

Regarding optimization algorithms, heuristic methods, such as genetic algorithms and simulated annealing, seem to present some advantages when compared to gradient-based methods. These claims should be investigated by using these methods to solve the problems presented here and their performance compared with the performance of gradient-based methods presented in this work.

Finally it is important to build and test the optimal designs obtained. It seems clear that the present optimization results fit very naturally with computer controlled milling of metallic facesheets or computer controlled weaving of fibre reinforced composites. These designs present interesting challenges from a manufacturing point of view; however, the challenge seems to be an extremely worthwhile undertaking. For, the potential weight savings are truly significant and therefore the gamble in the undertaken could pay significant dividends.

References

[1] Abrate, S., "Design of Multispan Composite Plates to Maximize the Fundamental Natural Frequency", *Composites*, Vol. 26, 1995, pp. 691-697.

[2] Adelman, H. M. & Haftka, R. T., "Sensitivity Analysis for Discrete Structural Systems", *AIAA J.*, Vol. 24, No. 5, 1986, pp. 823-832.

[3] Argyris, J. & Tenek, L. T., "A Natural Triangular Layered Element for Bending Analysis of Isotropic, Sandwich, Laminated Composite and Hybrid Plates", *Computer Methods in Applied Mechanics and Engineering*, Vol. 109, 1993, pp. 197-218.

[4] Arora, J. S. & Lee, T. H., "Design Sensitivity Analysis of Nonlinear Structures III: Shape Variation of Viscoplastic Structures", *Structural Optimization: Status and Promise*, edited by M. P. Kamat, Progress in Astronautics and Aeronautics, Vol. 150, AIAA, Inc., 1993, pp. 447-486.

[5] Bacon, M. D. & Bert, C. W., "Unsymmetric Free Vibrations of Orthotropic Sandwich Shells of Revolution", *AIAA J.*, Vol. 5, No. 3, March 1967, pp. 413-417.

[6] Bakhvalov, N. & Panasenko, G., "Homogenisation: Averaging, Processes in Periodic Media", Kluwer Academic Publisher, Dordrecht, 1984.

[7] Baldur, R., "Structural Optimization by Inscribed Hypersheres", *J. Engin. Mech.*, ASCE, Vol. 98, No. EM3, June 1972, pp. 503-508.

[8] Bendsøe, M. P., *Optimization of Structural Topology, Shape, and Material*, Spriger-Verlag, Heidelberg, 1995.

[9] Bendsøe, M. P. & Kikuchi, N., "Generating Optimal Topologies in Structural Design Using a Homogenization Method", *Computer Methods in Applied Mechanics and Engineering*, Vol. 71, 1988, pp. 197-224.

[10] Broydon, C. G., "The Convergence of a Class of Double Rank Minimization Algorithms - Part I and II", *J. Inst. Math. Appl.*, Vol. 6, 1970, pp. 76-90 & pp. 222-231.

[11] Bruhn, E. F., *Analysis and Design of Flight Vehicle Structures*, Jacobs Publishing, Philadelphia, PA, 1973.

[12] Brush, D. O. & Almroth, B. O., *Buckling of Bars, Plates and Shells*, McGraw Hill, 1975.

[13] Butler, R.; Tyler, A. A. & Cao, W.,"Optimum Design and Evaluation of Stiffned Panels with Practical Loading", *Computers & Structures*, Vol. 52, No. 6, 1994, pp. 1107-1118.

[14] Cauchy, A., "Methode Generale Pour Resolution des Systemes d'Equations Simultanees", *Comp. Rend. l'Academie des Sciences Paris*, Vol. 5, 1847, pp. 536-538.

[15] Cerny, V., "Thermodynamical Approach to the Travelling Salesman Problem: an Efficient Simulation Algorithm", *J. of Optimization Theory and Applications*, Vol. 45, 1985, pp. 41-52.

[16] Chan, H. C. & Cheung, Y. K., "Static and Dynamic Analysis of Multi-Layered Sandwich Plates", *Int. J. Mech. Sci.*, Vol. 14, 1972, pp. 399-406.

[17] Chen, H.-J. & Tsai, S. W., "Analysis and Optimum Design of Composite Grid Structures", *J. of Composite Materials*, Vol. 30, No. 4, 1996, pp. 503-534.

[18] Choi, K. K., "Design Sensitivity Analysis of Nonlinear Structures II", *Structural Optimization: Status and Promise*, edited by M. P. Kamat, Progress in Astronautics and Aeronautics, Vol. 150, AIAA, Inc., 1993, pp. 407-446.

[19] Dantzig, G. B., "Programming in a Linear Structure", *Comptroller*, USAF, Washington, D.C., February 1948.

[20] Davidon, N. C., "Variable Metric Method for Minimization", Argone National Laboratory, ANL-5990 Rev., University of Chicago, 1959.

[21] Dennis, J. E., Jr. & More, J. J., "Quasi-Newton Methods, Motivation and Theory", *SIAM Rev.*, Vol. 19, No. 1, 1977.

[22] Ding, Y., "Optimum Design of Sandwich Constructions", *Computers & Structures*, Vol. 25, No. 1, 1987, pp. 51-68.

[23] Ding, Y. "Optimum Design of Honeycomb Sandwich Constructions with Buckling Constraints", *Computers & Structures*, Vol. 33, No. 6, 1989, pp. 1355-1364.

[24] Duysinx, P. & Fleury, C., "Optimization Software: View from Europe", *Structural Optimizaiton: Status and Promise*, edited by M. P. Kamat, Progress in Astronautics and Aeronautics, Vol. 150, AIAA, Inc., 1993, pp. 807-849.

[25] Eschenauner, H. A. & Schuhmacher, A., "Simultaneous Shape and Topology Optimization of Structures", *WCSMO-1, Proc. on First World Congress of Structural and Multidisciplinary Optimization* (Ed. N. Olhoff, G. I. N. Rozvany), Pergamon, 1995, pp. 177-184.

[26] Fletcher, R. & Powell, M. J. D., "A Rapidly Convergent Method for Minimization", *Computer J.*, Vol. 6, No. 2, 1963, pp. 163-168.

[27] Fletcher, R. & Reeves, C. M., "Function Minimization by Conjugate Gradients", *Computer J.*, Vol. 7, No. 2, 1964, pp. 149-154.

[28] Fletcher, R., "A New Approach to Variable Metric Algorithms", *Computer J.*, Vol. 13, 1970, pp. 317-322.

[29] Forstig, Y. & Baruch, M., "Localized Load Effects in High-Order Bending of Sandwich Panels with Flexible Core", *J. of Engineering Mechanics*, Vol. 122, No. 11, November 1996.

[30] Gass, S. I., *Linear Programming, Methods and Applications*, 3rd ed., McGraw-Hill, New York, 1969.

[31] Glover, F., "Heuristics for Integer Programming Using Surrogate Constraints", *Decision Sciences*, Vol. 8, 1977, pp. 156-166.

[32] Glover, F., "Future Paths for Integer Programming and Links to Artificial Intelligence", *Computers and Operations Research*, Vol. 13, 1986, pp. 533-549.

[33] Goldfarb, D., "A Family of Variable Metric Methods Derived by Variational Means", *Math. Comput.*, Vol. 24, 1970, pp. 23-36.

[34] Grandhi, R., "Structural Optimization with Frequency Constraints - A Review", *AIAA J.*, Vol. 31, No. 12, December 1993, pp. 2296-2303.

[35] Haber, R. B.; Tortorelli, D. A. & Vidal, C. A., "Design Sensitivity Analysis of Nonlinear Structures I: Large-Deformation Hyperelastic and History-Dependent Material response", *Structural Optimization: Status and Promise*, edited by M. P. Kamat, Progress in Astronautics and Aeronautics, Vol. 150, AIAA, Inc., 1993, pp. 369-406.

[36] Habip, L. M., "A Survey of Modern Developments in the Analysis of Sandwich Structures", *Applied Mechanics Reviews*, Vol. 18, No. 2, February 1965, pp. 93-98.

[37] Haftka, R. T. & Grandhi, R. V., "Structural Shape Optimization - A Survey", *Computer Methods in Applied Mechanics and Engineering*, Vol. 57, No. 1, 1986, pp. 91-106.

[38] Haftka, R. T.; Gürdal, Z. & Kamat, M. P., *Elements of Structural Optimization*, Kluwer Academic Publishers, Dordrecht, 1990.

[39] Haftka, R. T. & Starnes, J. H., "Applications of a Quadratic Extended Interior Penalty Function for Structural Optimization", *AIAA J.*, Vol. 14, No. 6, June 1976, pp. 718-724.

[40] *TSB-124 Bonded Honeycomb Sandwich Construction*, Hexcel, 1989.

[41] Holland, J. H., "Adaptation in Natural and Artificial System", University of Michigan Press, Ann Arbor, MI, 1975.

[42] Ibrahim, I. M.; Farah, A. & Rizk, M. N. F., "Dynamic Analysis of Unbalanced Anisotropic Sandwich Plates", *J. of the Engineering Mechanics Division*, Vol. 107, No. EM2, April 1981, pp. 405-418.

[43] Johnson, E. H., "Tools for Structural Optimization", *Structural Optimization: Status and Promise*, edited by M. P. Kamat, Progress in Astronautics and Aeronautics, Vol. 150, AIAA, Inc., 1993, pp. 851-863.

[44] Jones, R. M., *Mechanics of Composite Materials*, Hemisphere Publishing Corp., New York, 1975.

[45] Kavlie, D. & Moe, J., "Automated Design of Frame Structures", *J. Struct. Div.*, ASCE, Vol. 97, No. ST1, January 1971, pp. 33-62.

[46] Kelley, J. E., "The Cutting Plane Method for Solving Convex Programs", *J. SIAM*, Vol. 8, 1960, pp. 702-712.

[47] Khatua, T. P. & Cheung, Y. K., "Bending and Vibration of Multilayer Sandwich Beams and Plates", International J. for Numerical Methods in Engineering, Vol. 6, 1973, p. 11-24.

[48] Kirkpatrick, S., Gelatt, Jr., C. D. & Vecchi, M. P., "Optimization by Simulated Annealing", *Science*, Vol. 220, 1983, pp. 671-680.

[49] Kirsch, U., *Structural Optimization - Fundamentals and Applications*, Springer-Verlag, Berlin, 1993.

[50] Kodiyalam, S.; Nagendra, S. & DeStefano, J., "Composite Sandwich Structure Optimization with Application to Satellite Components", *AIAA J.*, Vol. 34, No. 3, March 1996, pp. 614-621.

[51] Kuhn, H. W. & Tucker, A. W., "Nonlinear Programming", *Proc. 2d Berkeley Symp. Math. Stat. Probab.*, Berkeley, California, 1950, pp. 481-492.

[52] Kulkarni, A. M.; Banerjee, J. R. & Sinha, P. K., "Response of Randomly Excited Orthotropic Sandwich Plates", J. of Sound and Vibration", Vol. 41, No. 2, 1975, pp. 197-205.

[53] Langhaar, H. L., *Energy Methods in Applied Mechanics*, John Wiley and Sons, Inc., New York, 1962.

[54] Liaw, B.-D. & Little, R. W., "Theory of Bending Multilayer Sandwich Plates", *AIAA J.*, Vol. 5, No. 2, February 1967.

[55] Luus, R. & Jaakola, T. H. I., "Optimization by Direct Search and Systematic Reduction of the Size of Search Region", *AIChE J.*, Vol. 19, No. 4, 1973, pp. 760-766.

[56] MacNeal, R. H., "The NASTRAN Theoretical Manual", NASA SP-221(01), April 1971

[57] Malott, B.; Averill, R. C.; Goodman, E. D.; Ding, Y. & Punch, W. F., "Use of Genetic Algorithms for Optimal Design of Laminated Composite Sandwich Panels

with Bending-Twisting Couplig", Paper 96-1538-CP, *Proc. of* 37^{th} *AIAA/ASME/-ASCE/AHS Structures, Structural Dynamics and Materials Conference*, Salt Lake City, Utah, April 1996.

[58] Martin, P. M. J. W., "Optimum Design of Anisotropic Sandwich Panels with Thin Faces", *Eng. Opt.*, Vol. 11, 1987, pp. 3-12.

[59] McCulloch, W. S. & Pitts, W., "A Logical Calculus of the Ideas Immanent in Nervousactivity", *Bulletin of Mathematical Biophysics*, Vol. 5, 1943, pp. 115-133.

[60] Meirovitch, L., *Elements of Vibration Analysis*, McGraw-Hill, New York, 1975.

[61] Metropolis, N.; Rosenbluth, A. W.; Rosenbluth, M. N.; & Teller, A. H, "Equation of State Calculations by Fast Computing Machines", *The Journal of Chemical Physics*, Vol. 21, No. 6, June 1953, pp. 1087-1092.

[62] Min, K. T. & de Charentenay, F. X., "Optimum Weight Design of Sandwich Cylinders with Orthotropic Facings and Core Under Combined Loads", *Computers & Structures*, Vol. 24, No. 2, 1986, pp. 313-322.

[63] Monforton, G. R. & Ibrahim, I. M., "Analysis of Sandwich Plates with Unbalanced Cross-Ply Faces", *Int. J. Mech. Sci.*, Vol. 17, 1975, pp. 227-238.

[64] Noor, A. K. & Whitworth, S. L., "Model-Size Reduction for Buckling and Vibration Analyses of Anisotropic Panels", *J. of Engineering Mechanics*, Vol. 113, No. 2, February 1987, pp. 170-185.

[65] Olhoff, N. & Taylor, J. E., "On Structural Optimization", *J. of Applied Mechanics*, Vol. 50, Dec. 1993, pp. 1139-1151.

[66] Olhoff, N.; Thomsen, J. & Rasmussen, J., "Topology Optimization of Bi-Material Structures", *Optimal Design with Advanced Materials*, editor P. Pedersen, Elsevier Science Publisher B. V., Amsterdam, 1993, pp. 207-219.

[67] Oren, S. S. & Luenberger, D., "Self-Scaling Variable Metric Algorithms - Part I", *Manage. Sci.*, Vol. 20, 1974, pp. 845-874.

[68] Ostwald, M., "Optimum Weight Design of Sandwich Cylindrical Shells Under Combined Loads", *Computers & Structures*, Vol. 37, No. 3, 1990, pp. 247-257.

[69] Pagano, N. J., "Exact Solutions for Rectangular Bidirectional Composites and Sandwich Plates", *J. Composite Materials*, Vol. 4, January 1970, pp. 20-34.

[70] Park, W. J., "An Optimal Design of Simple Symmetric Laminates Under the First Ply Failure Criterion", *J. Com. Matls.*, Vol. 16, 1982, pp. 341-355.

[71] Park, Y. K., *Extensions of Optimal Desing Using the Homogenization Method*, Ph.D. thesis, Department of Mechanical Engineering, The University of Michigan, 1995.

[72] Paydar, N. & Park, G.-J., "Optimal Design of Sandwich Beams", *Computers & Structures*, Vol. 34, No. 4, 1990, pp. 523-526.

[73] Pearce, T. R. A. & Webber, J. P. H., "Buckling of Sandwich Panels with Laminated Face Plates", *Aeronautical Quartely*, Vol. 23, May 1972.

[74] Pearce, T. R. A. & Webber, J. P. H., "Experimental Buckling Loads of Sandwich Panels with Carbon Fibre Faceplates", *Aeronautical Quartely*, Vol. 23, November 1973.

[75] Pedersen, P. & Laursen, C. L., "Design for Minimum Stress Concentration by Finite Elements and Linear Programming", *J. Struct. Mech.*, Vol. 10, No. 4, 1982-83, pp. 375-391.

[76] Pedersen, P., "Design for Minimum Stress Concentration - Some Practical Aspects", in *Structural Optimization* (Rozvany and Karihaloo, eds.), Kluwer, Dordrecht, The Netherlands, 1988, pp. 225-232.

[77] Pedersen, P.; Tobiesen, L. & Jensen, S. H.; "Shapes of Orthotropic Plate for Minimum Energy Concentration", *Mech. Struct. & Mach.*, Vol. 20, No. 4, 1992, pp. 499-514.

[78] Pierson, B. L., "A Survey of Optimal Structural Design Under Dynamic Constraints", *International J. for Numerical Methods in Engineering*, Vol. 4, 1972, pp. 491-499.

[79] Plantema, F. J., "Sandwich Construction", John Wiley & Sons, Inc., New York, 1966.

[80] Powell, M. J. D., "A Fast Algorithm for Nonlinearly Constrained Optimization Calculations", No. DAMPTP77/NA2, University of Cambridge, England, 1977.

[81] Powell, M. J. D., "Optimization Algorithms in 1979", *Committee on Algorithms Newsletter*, No. 5, Mathematical Programming Society, February 1981, pp. 2-16.

[82] Rangacharyulu, M. A. V. & Done, G. T. S., "A Survey of Structural Optimization Under Dynamic Constraints", *Shock and Vibration Digest*, Vol. 11, No. 12, 1979, pp. 15-25.

[83] Rao, J. R. J. & Mistree, F., "Recent Applications of Bilevel Models in Multidisciplinary Optimization", *WCSMO-1: First World Congress of Structural and Multidisciplinary Optimization* (Ed. by N. Olhoff and G. I. N. Rozvany), Pergamon, 1995, pp. 17-23.

[84] Rao, K. M. & Meyer-Piening, H.-R., "Analysis of Sandwich Plates Using a Hybrid-Stress Finite Element", *AIAA J.*, Vol. 29, No. 9, September 1991, pp. 1498-1506.

[85] Rao, K. P. & Tripathy, B., "Composite Cylindrical Panels-Optimum Lay-Up for Buckling by Ranking", *Computers & Structures*, Vol. 38, No. 2, 1991, pp. 217-225.

[86] Raville, M. E. & Ueng, C. E. S., "Determination of Natural Frequencies of Vibration of a Sandwich Plate", *Exp. Mech.*, Vol. 7, Nov. 1967, pp. 490-493.

[87] Reissner, E., "Finite Deflections of Sandwich Plates", *J. of Aerospace Sciences*, Vol. 15, No. 7, July 1948, pp. 435-440.

[88] Reissner, E., "Reflections on the Theory of Elastic Plates", *Appl. Mech. Rev.*, Vol. 38, No. 11, Nov. 1985, pp. 1453-1464.

[89] Reymond, M. & Miller, M., *MCS/NASTRAN - Quick Reference Guide - version 68*, The MacNeal-Schwendler Corporation, Los Angeles, CA, 1994.

[90] Rockafellar, R. T., "The Multiplier Method of Hestenes and Powell Applied to Convex Programming", *J. Optim. Theory Appl.*, Vol. 12, No. 6, 1973, pp. 555-562.

[91] Rosemblatt, F., *Principles of Neurodynamics*, Spartan, Washington, DC., 1962.

[92] Rosen, J. B., "The Gradient Projection Method for Nonlinear Programming - Part II: Nonlinear Constraints", *SIAM J.*, Vol. 9, 1961, pp. 555-562.

[93] Schmit, L. A., "Structural Design by Systematic Synthesis", *Proc. Second Conference on Electronic Computation*, ASCE, New York, 1960, pp. 105-122.

[94] *Scout User's Manual*, Link Themko Vought (LTV) - Missiles Division, January 1989.

[95] Shames, I. H. & Dym, C. L., *Energy and Finite Element Methods in Structural Mechanics*, Hemisphere Publishing Corporation, New York, 1985.

[96] Shanno, D. F., "Conditioning of Quasi-Newton Methods for Function Minimization", *Math. Comput.*, Vol. 24, 1970, pp. 647-656.

[97] Shin, Y. S.; Haftka, R. T.; Watson, L. T. & Plaut, R. H., "Design of Laminated Plates for Maximum Buckling Load", J. of Composite Materials, Vol. 23, April 1989, pp. 348-369.

[98] Shivakumar, K. N. & Riddick, J. C., "Minimum-Mass Design of Sandwich Aerobrakes for a Lunar Transfer Vehicle", *J. of Spacecraft and Rockets*, Vol. 32, No. 1, January-February 1995, pp. 156-161.

[99] Sigmund, O., "Materials with Prescribed Constitutive Parameters: an Inverse Homogenization Problem", *International J. of Solids and Structures*, Vol. 31, No. 17, 1994, pp. 2313-2329.

[100] Sobieszczanski-Sobieski, J., "A Linear Decomposition Mathod for Large Optimization Problems - Blueprint for Development", NASA TM 83248, Feb 1982.

[101] Sobieszczanski-Sobieski, J., "Structural Optimization: Challenges and Opportunities", *International J. of Vehicle Design*, Vol. 17, 1986, pp. 242-263.

[102] Sullins, R. T.; Smith, G. W. & Spier, E. E., "Manual for Structural Stability Analysis of Sandwich Plates and Shells", NASA CR-1457, 1969.

[103] Tauchert, T. R. & Adibhatla, S., "Design of Laminated Plates for Maximum Stiffness", *J. of Composite Materials*, Vol. 18, January 1984, pp. 58-69.

[104] Tauchert, T. R. & Adibhatla, S., "Design of Laminated Plates for Maximum Bending Strength", *Eng. Opt.*, Vol. 8, 1995, pp. 253-263.

[105] Ueng, C. E. S. & Liu, T. L., "Minimum Weight of a Sandwich Panel", *J. of Aerospace Engineering*, Vol. 1, No. 4, March 1988, pp. 248-253.

[106] Vanderplaats, G. N. & Moses, F., "Structural Optimization by Method of Feasible Directions", J. Computers Struct., Vol. 3, July 1973, pp. 739-755.

[107] Vanderplaats, G. N., "CONMIN - A Fortran Program for Constrained Function Minimization, User's Manual", NASA TM X-62, 282, 1973. Nov. 1981.

[108] Vanderplaats, G. N., "Numerical Optimization Techniques for Engineering Design", McGraw-Hill, 1984.

[109] Vanderplaats, G. N., "ADS - A Fortran Program for Automated Design Synthesis - version 1.10", NASA CR 177965, Sep. 1985.

[110] Venkayya, V. B., "Introduction: Historical Perspective and Future Directions", *Structural Optimizaiton: Status and Promise*, edited by M. P. Kamat, Progress in Astronautics and Aeronautics, Vol. 150, AIAA, Inc., 1993, pp. 1-10.

[111] Vinson, J. R., "Optimum Design of Composite Honeycomb Sandwich Panels Subjected to Uniaxial Compression", *AIAA J.*, Vol. 24, No. 10, 1986, pp. 1690-1696.

[112] Vinson, J. R. & Handel, P. I., "Optimal Stacking Sequences of Composite Faces for Various Sandwich Panels and Loads to Attain Minimum Weight", 29^{th} *AIAA/-ASME/ASCE/AHS Structures, Structural Dynamics and Materials Conf.*, Williamsburg, April 1988, pp. 999-1006.

[113] Yu, Y.-Y., "Flexural Vibrations of Elastic Sandwich Plates", *J. of the Aero/Space Science*, April 1960, pp. 272-290.

IMAGE EVALUATION
TEST TARGET (QA-3)

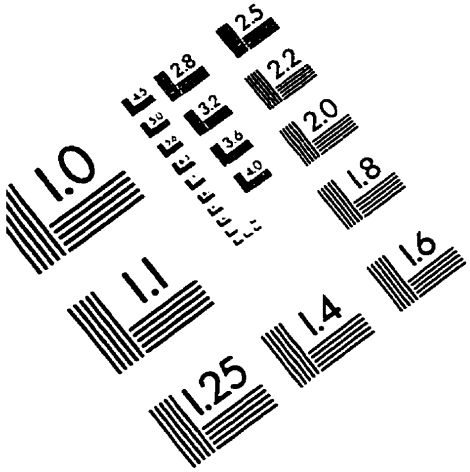

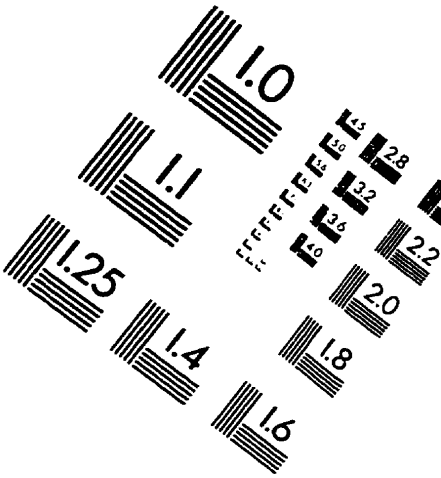

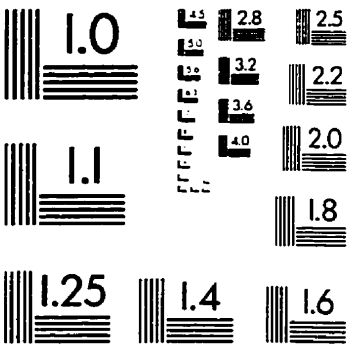

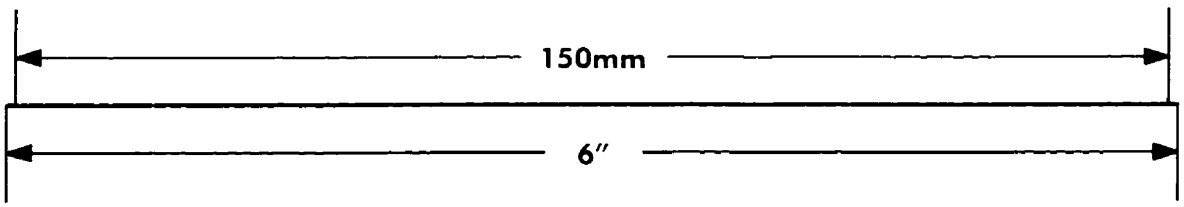

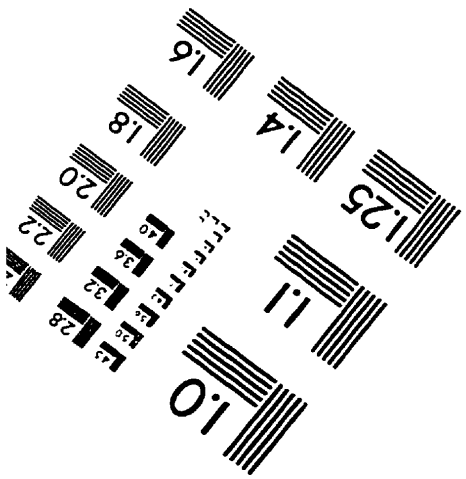

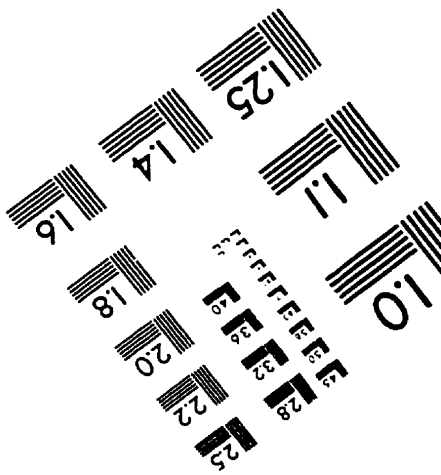

APPLIED IMAGE, Inc
1653 East Main Street
Rochester, NY 14609 USA
Phone: 716/482-0300
Fax: 716/288-5989